EFFECT OF MAGNETIC FIELD ON WEAR

A Thesis Submitted
in partial Fulfilment of the Requirements
for the Degree of

DOCTOR OF PHILOSOPHY

By

MOHAN KRISHAN MUJU

to the

DEPARTMENT OF MECHANICAL ENGINEERING

INDIAN INSTITUTE OF TECHNOLOGY KANPUR

SEPTEMBER 1975

Thesis
621.81
M896

I.I.T. KANPUR
CENTRAL LIBRARY
Acc. No. A 46347

14 MAY 1976

ME-1975-D-MAJ-EFF

Dedicated

to

Sumeet, Sandeep and Krishna

POST GRADUATE OFFICE
Submitted on 12/1/05

CERTIFICATE

Certified that this work entitled "Effect of Magnetic Field on Wear" has been done by Shri Mohan Krishan Muju under my supervision and has not been submitted elsewhere for a degree.

Amitabha Ghosh
Professor
Department of Mechanical Engineering

Dated: 8/5/06

ACKNOWLEDGEMENT

The author is indebted to Professor Amitabha Ghosh who suggested the problem and also guided the work at all stages of the progress.

The author also wishes to express his sincere gratitude to Professors, A.S. Parasnis, P.T. Narasimhan, T.V. Ramakrishnan, K.P. Gupta, M.N. Shetty, M.L. Vaidya, A.K. Majumdar, T.R. Ramachandran and Shri Subrata Ray with whom the author had some discussions of general nature. The much needed encouragement provided by Professor V.K. Stokes, Head, Mechanical Engineering Department is also gratefully acknowledged.

In course of this work considerable assistance was received from many members of technical staff. It is not possible to mention all the names here. However, the author would like to express his deep sense of gratitude to :

- Mr. D.P. Vishwakarma and Mr. R.M. Jha for their excellent cooperation during the experimental work,
- Mr. K.P. Mukherjee and Mr. D.K. Sarkar who provided the quality photographs,

- Dr. K.N. Swamy Rao who made large number of indentations on diffusion samples,
- Mr. S.R. Chaurasia who took pains to carry out careful chemical analysis of the wear particles,
- Mr. B.L. Arora for his excellent drawings,
- Mr. M.H. Rahman for assisting me in conducting tests on the Instron testing machine, and
- Mr. J.D. Verma for doing a very good job of typing from the manuscript.

The author is 'aware' of having neglected his family during the years of current research, and hopes that the future days will compensate for the loss.

TABLE OF CONTENTS

LIST OF IMPORTANT SYMBOLS

A_r = Real area of contact.

a = Width of asperity junction.

a_1 = Radius of wear particle.

$\bar{b}$ = Burgers vector.

b_o^3 = Atomic volume.

β = Apex angle of asperity.

$\bar{\beta}, \beta_1$ = Constants.

C = Concentration of diffusing material.

C_o = Concentration of the diffusing material at the interface.

C_j = Concentration of jogs.

D = Diffusion coefficient (or diffusivity).

D_o = Frequency factor.

D_u^H , D_u^o = Diffusivity in unstrained condition with and without the presence of the external magnetic field, respectively.

D_s^H , D_s^o = Diffusivity in strained condition with and without the presence of the external magnetic field, respectively.

D_g = Diameter of a single grain.

$\acute{D}$ = Diameter of the cylinder (= 2 r_c).

d = Maximum depth of fracture zone in body II.

$\acute{d}$ = Diameter of the pin (= 2 r_p).

$d_{o,o}$ = Major diameter of the elliptical wear scar in the absence of the magnetic field.

$d_{o,H}$ = Major axis of the elliptical wear scar in presence of external magnetic field.

Δ = Distance between two neighbouring dislocations.

$E_{I,II}$ = Surface energy of adhesion between body I and body II.

E_{ex} = Exchange energy.

$\dot{\epsilon}_o$ = Creep strain rate without the application of magnetic field.

$\dot{\epsilon}_H$ = Creep strain in presence of magnetic field.

f = Coefficient of friction.

F = Force on a dislocation.

F_1, N_1 = Instantaneous tangential and normal forces, respectively, on an asperity junction.

$\bar{F}_1$, $\bar{N}_1$ = Average tangential and normal forces, respectively, on an asperity junction.

γ = Surface energy.

G, G_o = Gain factor.

G_I, G_{II} = Gain factor of body I and body II respectively.

G^* = Shear modulus.

h_o, h_m = Flank wear in the absence and presence of external magnetic field, respectively.

$H_{II}(x,t)$ = Hardness on the side of body II of an asperity junction, as a function of depth and time, during diffusion.

H_s = Magnetic field strength.

J = Diffusional mass transfer per unit area per unit time.

J_{ex} = Exchange integral.

K = Boltzmans constant.

K^o = Degree kelvin.

L = Distance of sliding.

l = Size of dislocation network.

λ^* = Longitudinal magnetostriction coefficients.

λ_t = Transverse magnetostriction coefficient.

λ_s = Average to magnetostriction coefficient.

λ = Mechanical interaction factor.

Λ = Load parameter.

M_s = Mass transfer due to diffusion in static contact.

M_d = Mass transfer due to diffusion in dynamic contact.

μ = Micron (10^{-3} mm.)

N = Contact load.

N_d = Number of lattice spacings in the domain wall.

n_r = Number of dislocations lying on a circle with radius.

$\simeq$ = Of the order of.

P_{fI}, P_{fII} = Probability of failure on side I and side II of the asperity junction, respectively.

ν = Poisson's ratio.

Q = Activation energy for bulk diffusion

Q_D = Activation energy for diffusion in a single domain.

Q_H = Activation energy for diffusion in presence of external magnetic field.

R = Universal gas constant.

ρ_o = Initial uniform dislocation density in an asperity.

ρ_{lim} = Limiting dislocation density at the notch of an asperity junction.

$\rho^{o}_{ri}(t)$, $\rho^{H}_{ri}(t)$ = Dislocation density at the notch as function of time (t), in the absence and presence of an external magnetic field respectively.

σ = Stress.

σ_i = Internal stress.

σ_a = Applied stress.

σ^* = Effective stress (= $\sigma_a - \sigma_i$).

σ^*_H, σ^*_o = Effective stress in the presence and absence of an external magnetic field, respectively.

σ_j = Stress needed to break an attractive junction.

σ_w = Internal stress due to the presence of domain wall.

σ_y = Yield strength of materials.

t = Time (measured from t_o onwards).

t_j = Junction life.

θ = Temperature in degree kelvin.

θ_c = Curie temperature in degree kelvin.

U_j = Energy of formation of jogs.

$V(\sigma, \theta)$ = Dislocation velocity due to the presence of an external stress and temperature θ.

V_o, V_H = Dislocation velocity in absence and presence of external magnetic field, respectively.

V_c = Dislocation velocity at zero stress.

V^o = Shear wave velocity.

V_j = Velocity of jogs.

V_s = Sliding velocity.

v^* = Activation volume.

W^o, W^H = Volume of wear in the absence and presence of an external magnetic field respectively.

W = Volume of wear.

Z = Wear coefficient.

SYNOPSIS

Wearing action of Solid Sliding Surfaces plays an extremely important role in determining the life of mechanical systems with moving members. It also determines the life of cutting tools and ultimately the productivity of a machining system. It is realised that wear is a very complex phenomena, involving interaction of several physical processes simultaneously. Thus, while several empirical approaches have been used to improve the wear characteristics of rubbing solids, scientific analysis of the basic mechanisms involved are extremely necessary. It has been confirmed by a large number of experiments, conducted recently, that the application of external magnetic field affects the wear rate of cutting tools to a considerable extent. Till now, no scientific study has been made of the phenomenon and no explanation for the effect has been found out.

The objective of this work is to look into the basic problem of wear of Solid Surfaces with sliding contact in the presence of an externally applied steady magnetic field. It has been shown that internal stresses, developed during deformation in a ferromagnetic body, are reduced when an external magnetic field is applied. This results in increased mobility

of dislocations. It is postulated from this result that creep rate of a ferromagnetic body should get enhanced under the influence of an external magnetic field. This has been corroborated by experimental results. An asperity junction model for wearing of metalic surfaces has been proposed and it has been shown that the application of external magnetic field causes faster agglomeration of dislocations at the notches. This fact has been used to explain the enhancement of wear of the body having higher magnetic permeability.

A large number of experiments have been conducted with different combinations of ferromagnetic and non-magnetic metals, for instance, iron, nickel, mild steel, high speed steel, brass, aluminium etc. Experimental results are in good agreement with the theoretical predictions. It is found that when the velocity of rubbing is increased the effect of magneticfield increases in magnitude first and then drops after reaching an optimum value.

When a sufficiently strong magnetic field is applied to H.S.S. tools cutting mild steel workpiece the increase in the tool life can go upto 40% depending upon the machining speed. The question of enhancement of diffusion also has been discussed and its effects have been postulated which agree with the experimental observations satisfactorily.

CHAPTER I

INTRODUCTION

1.1 Introduction

It is a well established fact that when two solid bodies, in contact, are in relative sliding motion, surface deterioration invariably occurs. The surface deterioration ultimately leads to the wear of these bodies. As there is hardly any mechanical system which does not comprise of members with relative sliding motion, the 'process capability' and the 'productivity' obtainable from such a system are very much governed by the wear characteristics of its surfaces. This makes the wear of sliding surfaces an extremely important aspect of manufacturing sciences and engineering.

Wear has been recognized to be a complex phenomenon in which several processes act simultaneously. Depending upon the nature of the surfaces, the environment and the demands of the particular situation wear may be considered to be tolerable or devastating. The complexity of the problem has not rendered it easy to arrive at a comprehensive analytical solution of general nature. Most of the effort of research workers has gone in providing empirical solutions to meet the needs of a specific situation. These empirical solutions may be considered to be based on two approaches.

First approach is to improve the bulk properties of the material. The second approach is to improve the surface characteristics and nature of contact.

An important class of the wear problems is the tool wear, specifically the cutting tool wear. Cutting tool wear directly determines the process capability as well as productivity of the machining operations. As such, the problem has assumed a significant position among the problems facing the manufacturing industry. The distinctive features of cutting tool wear are,

i) cutting tool wear occurs at relatively high speeds and temperatures,

ii) in cutting tool wear, the wearing of the work material is not considered as disadvantageous. In fact, excellent wear characteristics of the work piece are considered to be desirable from practical point of view, as it reduces the wear of cutting tools.

Thus, in attempting to reduce the tool wear, in addition to the two approaches mentioned above, a third approach is also practicable and is widely practiced. This approach may be outlined as, the

i) reduction in the strength of the work piece by localised heating or by adding suitable additives to the material, and

ii) the application of suitable lubricants and gaseous atmosphere to reduce the accumulation of heat at the cutting edge.

Ever since Taylor's classical paper (1) large number of workers have investigated the problem of cutting tool wear, using various approaches. Considerable evidence exists that adhesion and diffusion wear have been found to be predominant under metal cutting conditions.

It is to be noticed (2 - 9) that during the last several years wear problem has been tackled on the basis of interdisciplinary approach by many workers, as the problem is really so in its nature. In the present work also such an approach is attempted to a limited extent.

In the present work, wear has been studied as a general problem of interaction between two idealised asperities. These idealised asperities are expected to represent the microscopic behaviour of their respective bodies. An external magnetic field is expected to affect the dislocation mobility which governs the fracture characteristics and plastic deformation. Extension of these concepts to the wear of bodies results in certain postulates. It is seen that, under normal conditions prevailing at sliding surfaces, the external magnetic field will improve the wear

characteristics of one of the bodies resulting in longer useful life for that body.

It is possible to envisage that wear of bearings and other rotating parts in electrical machines can be better understood in the light of the present work.

1.2 Review of Previous Work

Effect of magnetic field on surface deterioration seems to have been first reported by Simpson and Russell (10). In these observations the inner races of ball bearings used in electrical generators, are reported to have suffered excessive surface deterioration due to the linking of magnetic flux. Possible cause for such deterioration has been given as the early breakdown of film of lubricant, due to the rise in temperature caused by the magnetic field.

It is apparent that Ghosh (11) also did similar work independently and he was the first to report the effect of magnetic field on the wear of cutting tools. He, by means of repeated experiments established that magnetisation of a H.S.S. tool rubbing against a mild steel job considerably reduced the wear rate of the tool. Possible increase in coherence or improvement in bonding affinity were explained as the possible reasons.

Bagchi and Ghosh (12, 13) repeated the experiments and showed that both during cutting and rubbing of mild steel job by H.S.S. tools presence of magnetic field during the operation improved the tool life.

They applied a constant magnetic field of 100 - 200 Oe to a turning tool and measured the change in the wear characteristics of the tool (care was taken that the tool always rubbed against a fresh surface). The general nature of their results is shown in Figures 1.1 and 1.2. Gain factor, G_o shown in these figures was defined as

$$G_o = \frac{h_o - h_m}{h_o} \qquad (1.1)$$

where h_o = flank wear without magnetic field,

h_m = flank wear in presence of magnetic field.

These curves depict some interesting features as follows :

i) At first the decrease in the wear rate obtained in presence of the magnetic field, increases with the cutting velocity or the rubbing velocity.

ii) The increase in the gain has an optimum value beyond which it decreases.

The authors explained their experimental results by means of the following theoretical model (13).

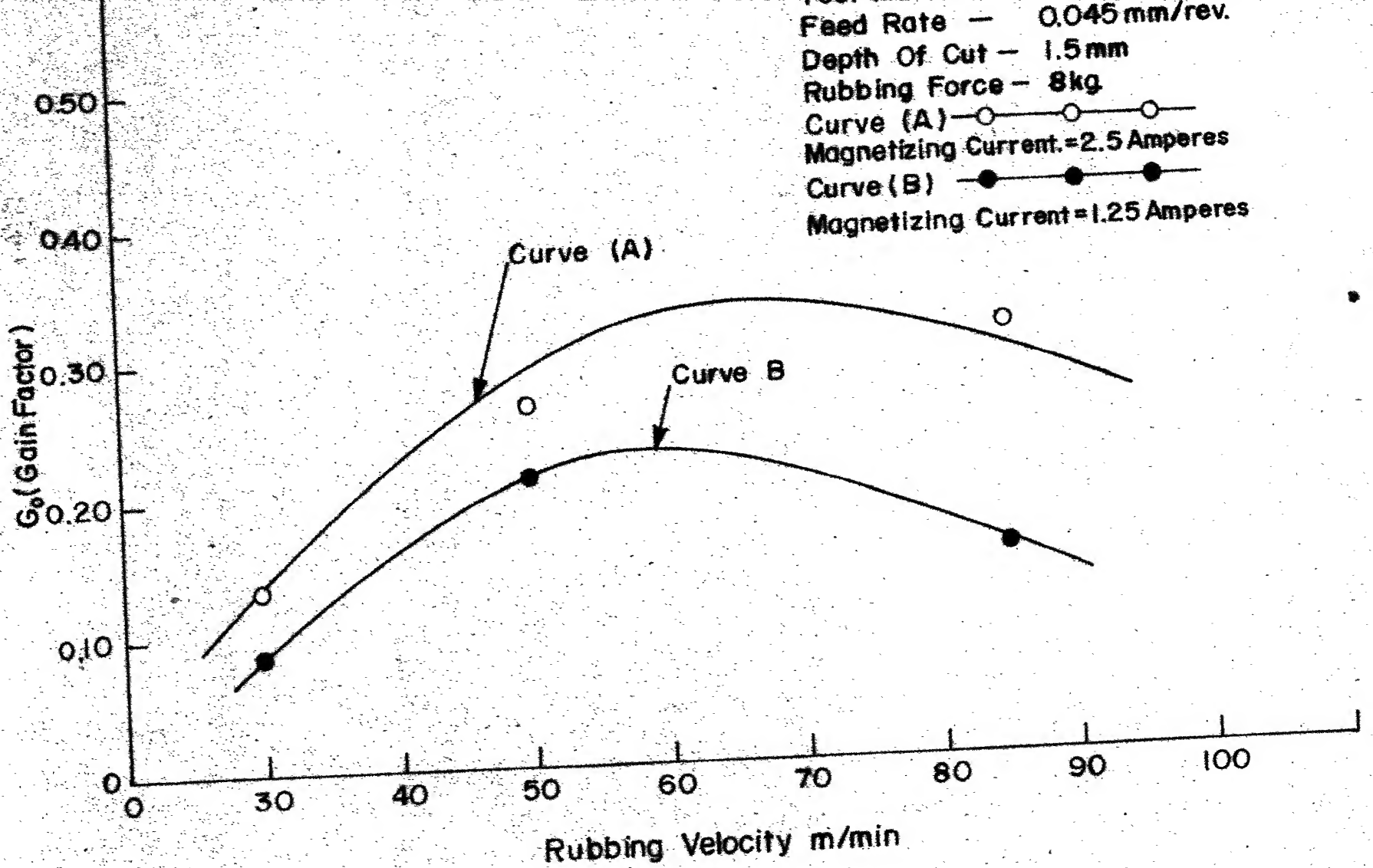

Fig.1.1 Variation Of Gain Factor With Rubbing Velocity (experimental)

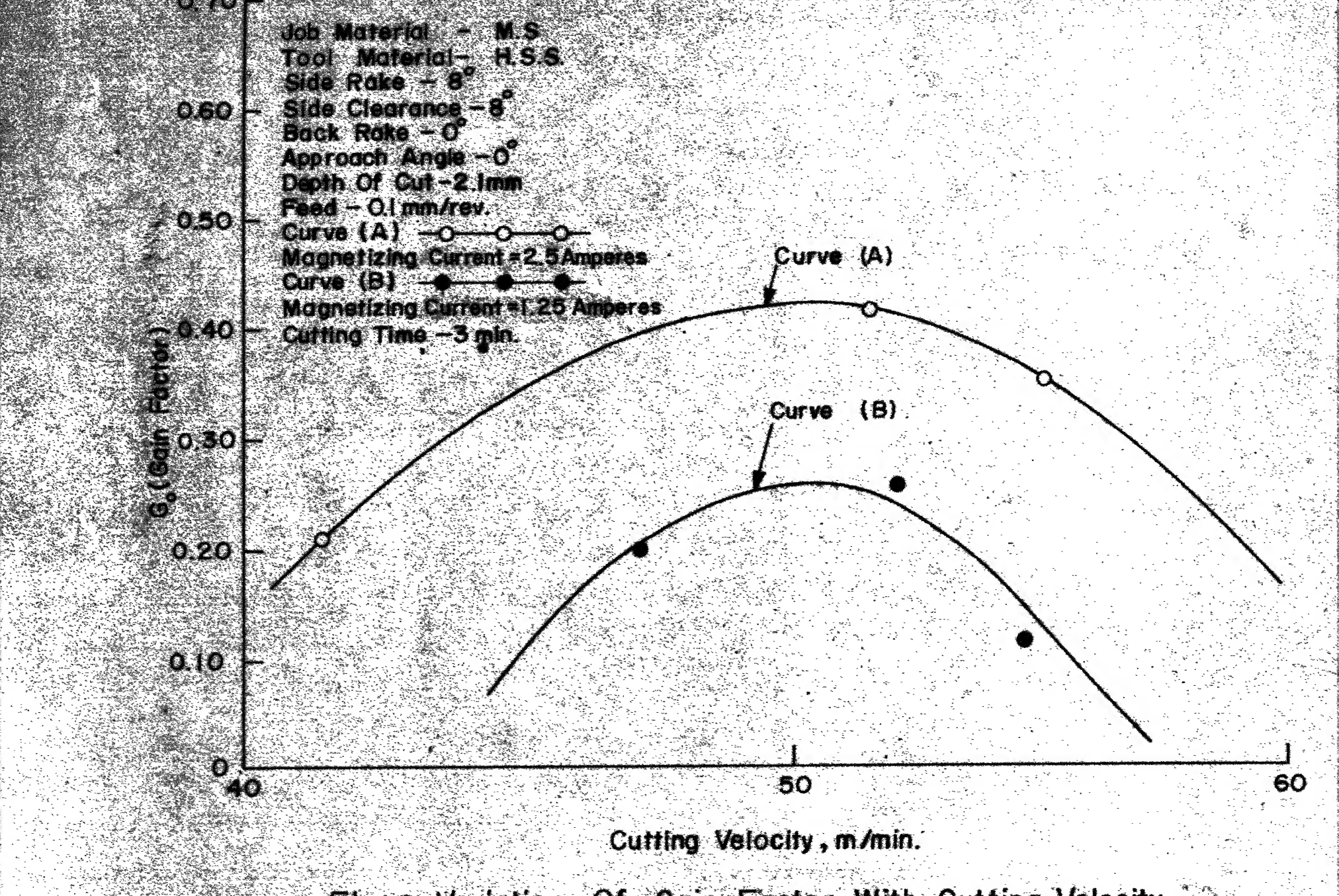
Job Material - M.S
Tool Material - H.S.S.
Side Rake - 8°
Side Clearance - 8°
Back Rake - 0°
Approach Angle - 0°
Depth Of Cut - 2.1mm
Feed - 0.1 mm/rev.
Curve (A)
Magnetizing Current = 2.5 Amperes
Curve (B)
Magnetizing Current = 1.25 Amperes
Cutting Time - 3 min.
Curve (A)
Curve (B)
G (Gain Factor)
0.60
0.50
0.40
0.30
0.20
0.10
0
40
50
60
Cutting Velocity, m/min.

They considered a hemispherical particle of radius a_1 to get extracted from the tool and rotated through 180° as shown in Figure 1.3, before being removed as a wear particle. The total energy E_T needed to produce such a wear particle has been considered to be composed of two parts, such that

$$E_T = E_s + E_m \qquad (1.2)$$

where, E_s ($= 4\pi a_1^2 \gamma$) is the work required to 'form' the wear particle, and E_m ($= 2 m_s H_s \cdot \frac{2}{3} \pi a_1^3 d_t$) is the extra energy needed to rotate the particle in presence of an external magnetic field. Various parameters used in these expressions are defined as follows :

γ = surface energy of the tool material,

m_s = magnetic moment per unit volume,

H_s = saturating magnetisation,

d_t = density of the tool material.

Obviously, no change in the 'energy of formation' of the article was envisaged. Gain factor G_o was shown to be reducible to the form

$$G_o = \frac{E_m}{E_m + E_s} \qquad (1.3)$$

Thus, it is seen that the gain G_o is controlled by the extra energy needed to remove the particle in presence of magnetic field.

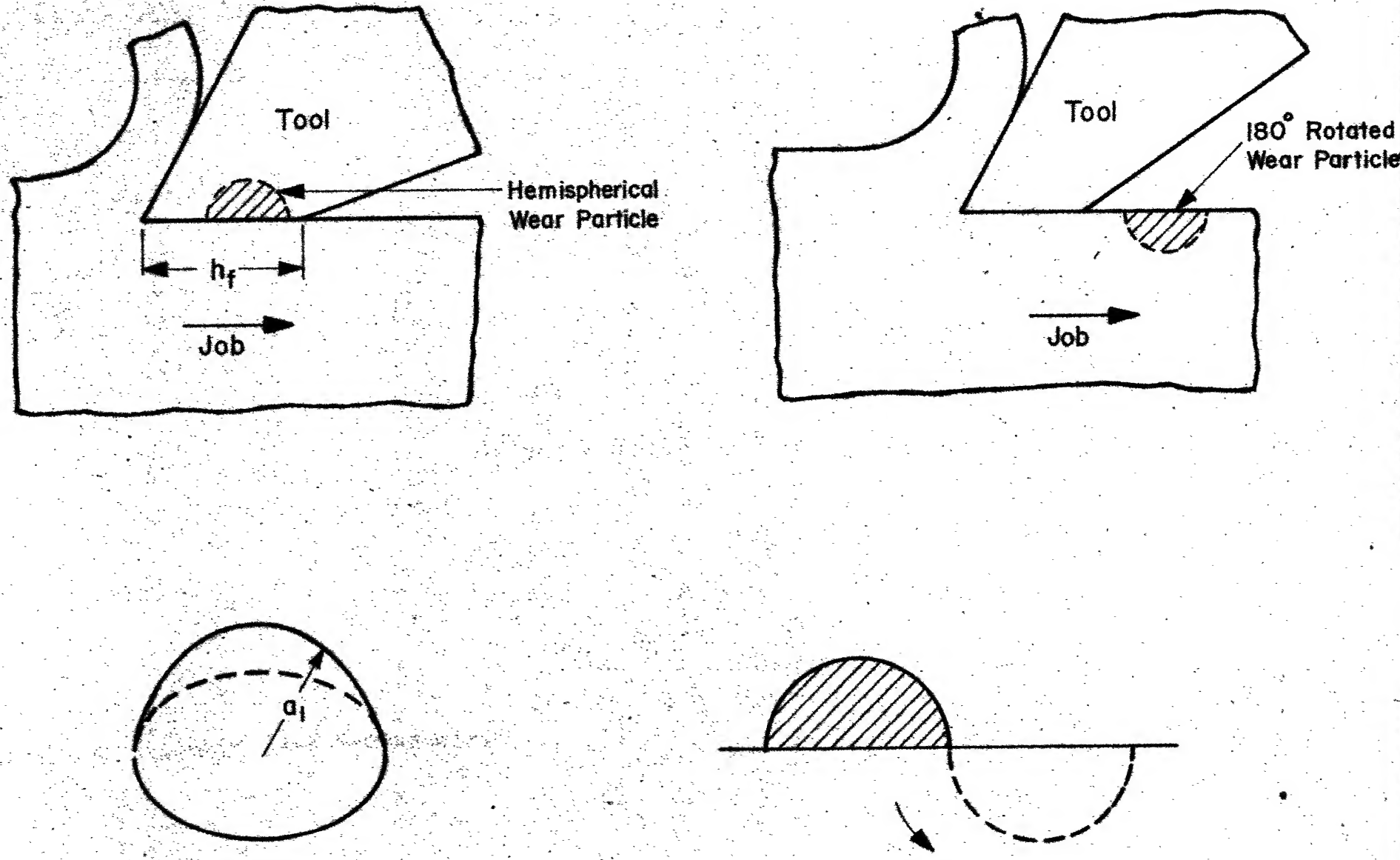

Fig. I.3 Mechanism Of The Wear Process

As seen from Figures 1.1 and 1.2, within the speed range investigated, Bagchi and Ghosh always found G_o to be a positive quantity. If the above model proposed by them were true G_o should always turn out to be positive, irrespective of the material of the job involved. This, however, does not tally with the results obtained in the present work when a non-magnetic job is machined by a ferromagnetic tool. Thus, further investigations in this direction are called for.

Following the work of Bagchi and Ghosh few other research workers (14,15) have performed experiments on wear of H.S.S. drills while drilling steel and cast iron. Essentially, similar results as those obtained by Ghosh and Bagchi have been reported.

No sound explanation of the observed behaviour has been provided so far, by any of the workers. The present work meets that objective to a large extent.

1.3 Objective and Scope of Present Work

The major objective of the present work is to investigate the basic physical phenomenae involved in the effects of magnetic field on wear. Though the work is most relevant to the problem of cutting tool wear, the author has looked into the general mechanism of wear of bodies sliding against each other. Dry conditions have been considered to simplify the work.

Of the two bodies sliding against each other at least one has been considered to be of ferromagnetic material. Various kinds of tests were conducted to find out the influence of magnetic field on a deforming body. Material property tests like tensile strength test and impact strength test were performed to see if magnetic field affects the bulk properties. Apart from these, the influence of magnetic field on cutting force in turning operation was also studied. The results of these tests indicated that magnetic field has insignificant effect on the bulk properties of ferromagnetic materials. This important observation necessitated the author to put in most of his efforts in investigating the mechanisms involved at microscopic level.

As the process of wear is an extremely complicated physical phenomenon, it is not possible to present an exact mathematical analysis. Consequently, the present work is based on a simplified asperity junction model and the entire wear has been considered to be resulting from failure of such junctions. The possibility of the enhancement of diffusion due to the application of a magnetic field has also been studied.

To verify the various conclusions drawn from the physical model author has conducted appropriate

experiments. Various combinations amongst the materials Iron, Nickel, Steel, Brass and Aluminium were used for the purpose. It would be extremely desirable to perform detailed experiments of specialised nature like wear particle formation, measurement of dislocation velocity etc. These experiments can throw much light on the nature of basic mechanisms involved. But, due to the limited facilities available, these aspects could not be covered and, inferences wherever relevant were drawn from the published works of other workers.

Since sophisticated methods of wear measurements were not readily available, measurements were mostly based on microscopic observations. Enough cares were taken to reduce the scatter of readings and to maintain fairly uniform accuracy limits of the readings at various speeds. Each reading was repeated five times both for the magnetised state and the non-magnetised state to ensure a reasonably reliable mean value of the wear.

CHAPTER II

THEORIES AND MECHANISMS OF WEAR

2.1 Nature of Solid Surfaces and their Contact

No matter how plane the surface of a solid body appears to be, when examined at microscopic level it is always wavy and rough. Even the surface formed by the cleavage of mica contains irregularities of the order of 20 Å in size. The irregularities on the surface of an ideally smooth crystal have been found to be of the order of 100 Å in height. The smoothest surfaces encountered in mechanical engineering practice have been seen to have projections of about 0.05 to 0.1 μ. Apart from being rough these surfaces are also accompanied by waviness. The length of the waves varies from 1 mm - 10 mm and their heights range from 20 to 40 μ. A profile of an actual surface is shown in Figure 2.1; (16). Due to the distortions in shape of the bodies as a result of direct stress and temperature effects the surface unevenness is likely to aggravate further. As a result, therefore, actual surfaces are in a position to develop contact only over small discrete areas, located in well defined regions. The total surface area which can be associated with these discrete regions is usually defined as the apparent area of contact, while the overall surface area of

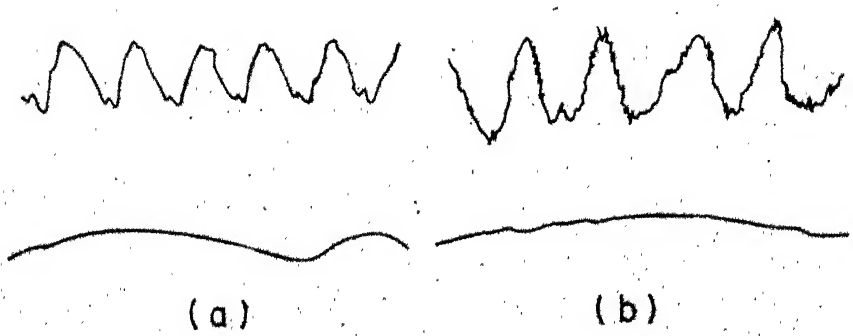

Fig 2.1 Roughness And Waviness Of Surfaces

(a) Profile Of a Turned Copper Surface (Top) On a Distorted Scale. Magnification, Horizontal, X 50; Vertical X 500; Below, Profile With Equal Horizontal And Vertical Magnifications.

(b) Waviness Diagram Of a Turned Surface, Transverse Pitch Of The Roughness Of The Irregularities = 240 μ; Magnification, Horizontal X 8; Vertical X 294; Below, Part Of Waviness Diagram With Equal Horizontal And Vertical Magnifications. (16)

contacting bodies iscalled the design area of contact.

A closer examination of these discrete regions of contact has revealed further that the actual contact between bodies occurs at certain high points located within these regions. These points are called contact points or, more commonly as asperities. The number of these asperities depends upon both, the load and the roughness of surfaces. When a load is applied to two bodies in contact the interacting regions of the bodies are deformed elastically at first. But, as the load is increased the deformation eventually becomes plastic. As a result, the two bodies come closer to each other.

To understand any physical phenomenon occuring between the two contacting bodies, the behaviour of these asperities is to be clearly understood. It is, therefore, to be observed that problems connected with passage of flux of any kind (like electrical, magnetic, thermal or even sound and light) cannot be fully studied unless the characteristics of these contact points are taken into consideration. In particular, the problems connected with metal transfer and wear during sliding processes are very much dependent on the nature of phenomenae taking place at these contact points or asperities.

The asperities are subjected to extremely high stresses even at ordinary loads, because of their very small dimensions. Due to the high stresses contact of the two bodies at the asperities generally results in formation of junctions, which have been the subject of investigations for many research workers. Various experimental techniques like electrical resistance measurements (17, 18), optical (19) and electron microscopy (20) have been employed to study these asperity junctions. It is generally accepted that the junctions formed by the asperity interactions are of roughly of the order of 10 to 20 μ (21). These junctions are expected to be in a state of incipient flow even under normal loads and much of friction and wear phenomenon has been analysed in light of these junctions. Rabinowitz (21, 22) used an auto-correlation analysis to determine the average junction size for sliding metals. The size distribution of the junctions is given in Figure 2.2. Ling (23), Greenwood and Williamson (24), Whitehouse and Archard (25), Tsakada(26), Gupta and Cook (27) and many others have also analysed surface profiles using statistical approaches. It is generally accepted on the basis of these works that the distribution of peak heights is closely given by Gaussian distribution, whereas the junction size varies from 5 - 20 μ .

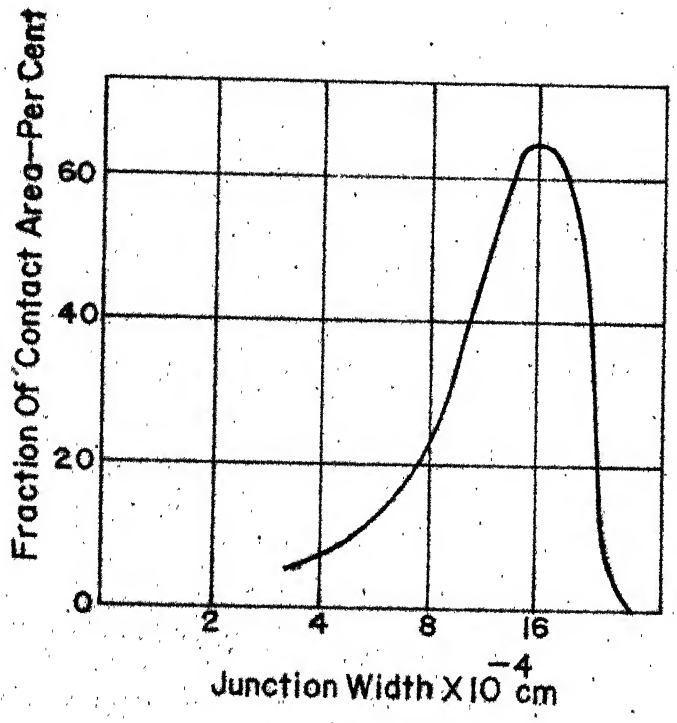

Fig2.2 Fraction Of Contact Area As a Function Of Junction Width.(21)

2.2 Types and Theories of Wear

In the previous section it was briefly discussed that the nature of contact between two solids is dependant on the type of surfaces. Rougher surfaces will generally result in larger asperity junctions, while well finished surfaces will result in fine asperity junctions. Adhesive wear occurs as a result of interaction of the asperities and subsequent failure of asperity junctions. Therefore, rougher surfaces result in more wear and larger wear fragments than obtainable in fine surfaces. Other parameters like, presence of lubricant, high temperatures, metallurgical treatments all affect the surface characteristics. Consequently, wear of sliding bodies is seriously affected by the overall interfacial conditions between them.

Wear is defined as the material which finally leaves the contact zone between the two rubbing bodies. The classical equation for wear is written as

$$W = \frac{ZNL}{3H} \qquad (2.1)$$

where W = volume of wear,

N = contact load,

L = distance of sliding,

H = bulk hardness (of the softer material),

Z = wear coefficient.

Equation 2.1 is due to Burwell and Strang (28) and is essentially an extension of Holm's (17) idea of atomic wear. Archard and Hirst (29) and other have found the magnitude of Z to vary within the limits of 10^{-2} to 10^{-7}. Author has also conducted experiments for the measurements of Z, Tungsten carbide bits were rubbed against mild steel. Values for $Z \simeq 10^{-6}$ were obtained. This value agrees with that provided by Kragelskii (16).

While the classical equation on wear relates the important parameters like load, velocity of sliding and the material property it cannot explain wear under all circumstances. This is so because no single mechanism is involved in wear phenomenon. When speeds are low, wear is mostly due to abrasion of the softer body by the asperities of the harder one unlike at higher speeds.

Considerable number of investigations conducted by many research workers have led to the identification of the following basic mechanisms responsible for wear.

(i) Abrasion
(ii) Adhesion
(iii) Chemical and Electrolytic action
(iv) Diffusion
(v) Fatigue

A short description of these mechanisms is given below.

(i) Abrasive Wear

In this kind of wear blunt particles or asperities plough grooves in the wearing surface without the creation of debris, while sharp edges behave as cutting tools to create debris or chips.

(ii) Adhesive Wear

When the metallic surfaces are pressed into intimate contact under moderate loads, a metallic bond between the two surfaces is produced. This phenomenon is known as adhesion. Under favourable equilibrium conditions if A type of atoms prefer to have B type of atoms as their neighbours, then a compatibility of B in A results in a solid solution of B in A. In the case of atomic bond formation across the interface during ideal adhesion, a negative free energy of the bond formation must exist. The strength of the bonding at the points of adhesion is often so great that while attempting to free the surfaces, separation takes place not along the interface but in one of the bodies itself resulting in metal transfer and subsequent removal. Archard has developed a model of transfer under such conditions considering the metal removal in the form of lumps. It is seen that metal removed is mainly proportional to actual area of contact and hardness ratio of the mating bodies.

iii) Chemical and Electrolytic Wear

Chemical wear may take place between two metals when a certain fluid is present between them which renders them to be active. Electrolytic wear is related to the chemical wear, because it arises due to possible galvanic corrosion between two bodies. For instance, high speed steel has been found to be anodic to 15-25-6 (65) stainless steel alloy and other high temperature alloys.

iv) Diffusion Wear

Solid state diffusion is the mechanism by which atoms diffuse from one lattice point to another thus leading to a net transfer of matter from one body to the other one in the direction of the concentration gradient. This is possible, however, only when temperature conditions are favourable for atomic movement.

Thus, if in the adhesion process localized temperature increases to a considerable level interfacial diffusion can occur.

Diffusion wear has been seen to be of particular significance in the high speed machining process.

v) Fatigue Wear

As a consequence of interpenetration of surface asperities sub-surface deformation occurs. This results in a wave of deformation, associated with each

asperity. For some distance, in front of an asperity the material is compressed and behind the asperity the material is elongated because of the frictional force. Thus each cross-section of the rubbing member is subjected to cyclic compressive and tensile stresses. This can lead to the removal of the surface material due to fatigue. Radchik and Radchik (30) have investigated this effect both theoretically and analytically.

Adhesion wear and diffusion wear were found to be most relevant to the present work and therefore major emphasis has been put on these. These two mechanisms are discussed in more details in the following sections.

2.3 Interaction of Surface Asperities and Adhesion Wear

2.3.1 Nature of adhesion wear

Archard (31) using Hertz solution for elastic contact of spherical bodies, showed that for a single elastic junction the contact area is proportional to $N^{2/3}$ (N = normal load). But for actual surfaces where contact occurs at many places the contact area is proportional to N. Archard (32) also modified the friction and wear theory of Barwell and Strang (33), based on asperity encounter. He showed that metal removal from the sliding surfaces could be of two types,

Though originally derived for rake face wear this model can be applied to wear between any two clean surfaces at high speeds. In terms of sliding velocity V_s between the two bodies, the wear rate $\dot{W}$ is given by

$$\dot{W} = \frac{Z_o V_s N}{H} \cdot \exp (- E / R \theta) \qquad (2.5)$$

$$\text{Or} \quad \dot{W} = \frac{V_s N}{H} Z \qquad (2.6)$$

where, $Z = Z_o \exp (- E / R \theta)$ (2.7)

Thus the wear coefficient Z used in Archards equation (2.1) is actually not a constant quantity but a rate [redacted] parameter. Generally E is associated with activation energy for self diffusion. Equation 2.4 was used by Nayak and Cook (35) to investigate the thermal aspects of tool wear. They also considered wear coefficient Z to be given by Equation 2.7. They, however, preferred to call E as the wear activation energy. Using this approach both the flank and the rake face wear results were found to be well correlated with the model.

.2.3.2 Junction Failure and Wear

It is realised that extremely high stresses exist at the contact points between two bodies. These high stresses cause plastic deformation of asperities leading to a finite area of contact between them. The magnitude of this area of contact is given by

$$A_r = \frac{N}{H} \qquad (2.8)$$

where, N = normal load,

and H = indentation hardness of softer material.

Due to the large stresses at these asperities strong adhesion occurs. The strong adhesion leads to the formation of a welded junction between the asperities. When the contacting members try to slide past each other a force of friction arises from the need to break these junctions in shear. If the stress required to shear such a junction is assumed to be dependent on just the shear strength 's' of the softer material, the coefficient of friction arising from such motion is

$$f = \frac{\text{tangential force}}{\text{Normal force}} = \frac{s\,A_r}{H\,A_r} = \frac{s}{H} \qquad (2.9)$$

Thus, if the shear strength of the softer material is the only controlling factor in shearing of junctions, the coefficient of friction is seen to be independent of load, surface roughness and other parameters. Almost for all materials $\frac{s}{H}$ is constant, leading to the conclusion that f is constant for a pair of materials, though experimental evidence does not support this (18, 22, 36).

Rabinowitz (36) visualised that shearing of junctions should also depend upon the surface energy.

This is because of the fact that the junction size is not only controlled by plastic deformation caused by the load but also by the surface attractive forces which are assumed to exist in adhesion but not accounted for in Equation 2.8. The surface energy acts so as to increase the size of the real area of contact over the value given by Equation 2.8. On this basis occurrence of high coefficient of friction can be explained when the ratio of surface energy of adhesion $E_{I,II}$ to hardness H is high (36). Rabinowitz (36) has shown that coefficient of friction is indeed directly related to $\frac{E_{I,II}}{H}$.

The existence of adhesion wear has also been experimentally established by autoradiographic tests (32, 36 - 39). Besides suggesting a constant value of coefficient of friction for a pair of materials, equation 2.8 results in $f \simeq 1/6$ which is a very small value. Experimental results under various conditions provided by whitehead (40), Rabinowitz (36), Bowden and Tabor (18) and others give values between 0.4 to 1.0, while for Indium on Indium it is very high $\simeq 1.7$. Also, the experimental results of several workers (41, 42, 43) indicate that the relation between f, H and s is not so simple as given by Equation 2.9. Thus, while Bowden and Tabor model (Equation 2.9) explains the essential nature of friction between unlubricated metals,

it cannot explain the friction between solids in a complete manner.

Green (44) elaborated the Bowden and Tabor theory in order to present a clearer picture of the determination of stresses and deformations during steady sliding. The interaction between metal surfaces is discussed in the following manner.

When clean metal surfaces are pressed together by a load N, the tips of the asperities are deformed plastically to a magnitude which can support the load. If strain hardening is ignored these junctions formed by mutual asperity deformations are in a state of perfectly plastic one. In this state even a minute force can lead to an increase in the size of the junction. This initial microscopic increase or growth in the size of the junction preceeds the macroscopic steady sliding. An important observation due to Green (44) is that junction growth must be associated with the movement of the surfaces closer together, as shown in Figure 2.3 (a). Green (45, 45) has shown theoretically that the approach angle ϕ' is initially about 45° but decreases as the frictional stress over the area of contact increases. Thus as the two surfaces approach each other area of contact increases rapidly and this is due to (i) the growth of original junctions, and (ii) the new regions coming into contact.

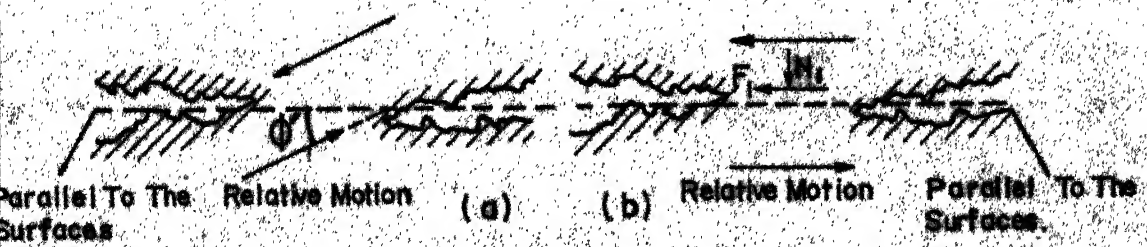

Fig. 2.3 Diagram Of a Junction. (a) During The Initiation Of Sliding, (b) During Steady Sliding.(44)

When sliding settles down to steady state, the growth of junctions stops which results in a constant area of contact thereafter. In steady state, the distance apart of the surfaces remains steady, and they no longer move closer i.e. $\phi' = 0$.

As the relative motion between the surfaces continues old asperity junctions get sheared while new junctions are produced. The process is a continuous one, so that the normal load N is continuously supported and, F, the friction force is nearly constant. In this process each junction passes through a cycle of formation, deformation and fracture. At any instant when a junction is just formed, force acting through the junction has a normal component N_1 (compressive) and a tangential force F_1 (shear) as shown in Figure 2.4. During the life cycle of a junction its shape and corresponding values of N_1 and F_1 are constantly changing. Thus at any instant the coefficient of friction is

$$f = \bar{F}_1 / \bar{N}_1 \qquad (2.10)$$

where $\bar{F}_1$ and $\bar{N}_1$ represent the average instantaneous values of shear force and normal force over the surface, respectively. It is logical to imagine that at any instant there are many junctions at different stages of development and thus averaging over all the junctions at a single instant is equivalent to averaging over the life cycle of a single typical junction

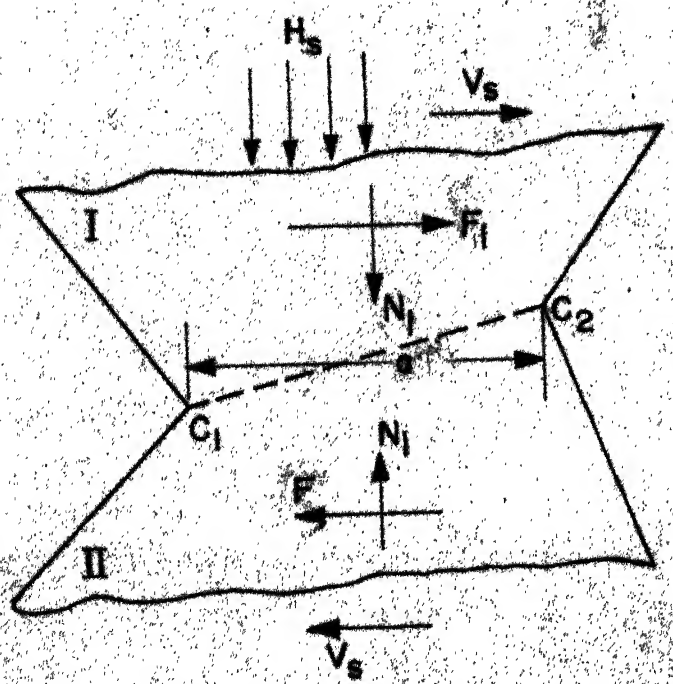

Fig2.4 Model Of An Asperity Junction

with respect to the relative displacement x of the two surfaces. On this basis $\bar{F}_1$ and $\bar{N}_1$ are defined as

$$\bar{F}_1 = \frac{\int F_1 \, dx}{\int dx} \qquad (2.11)$$

and $$\bar{N}_1 = \frac{\int N_1 \, dx}{\int dx} \qquad (2.12)$$

Thus, f can be evaluated as

$$f = \frac{\int F_1 \, dx}{\int N_1 \, dx} \qquad (2.13)$$

The integration is to be carried over the life - cycle of a typical junction. Hence, to investigate frictional behaviour theoretically, it is sufficient to examine in detail a typical junction throughout its life cycle.

Now, at any instant during steady sliding ratio F_1/N_1 is given by the junction shape, strength of adhesion and the condition that the two bodies are moving parallel to each other. Since the changing shape of a deforming body cannot be determined theoretically, theoretical estimation of f is not possible. As such recourse has been taken to model experiments to simulate the actual situation. Green (44), Greenwood and Tabor (47, 48) have done extensive experimentation on plasticine models under conditions of plane stress as well as plain strain.

The stages through which junctions have been observed to be passing can be understood with the aid of Figure 2.5. The figure illustrates the deformation of asperities I and II of similar hardnesses. After initial adhesion most of the centre of the junction is sheared uniformly; Figure 2.5 c. Due to this shearing the interface gets stretched. This would help to break any surface films present and thereby strengthen adhesion. As the tendency for the asperities to pass each other continues an intermediate stage shown in Figure 2.5 d is reached, when the junction has acquired a symmetric shape. Since the adhesion is assumed to be fairly strong the junction deforms as a single body and thus necking and fracture occurs in the most critically stressed region of the junction. In this manner a small particle is transferred from one asperity to the other one. In a subsequent encounter this transferred material may become a loose wear fragment. Experiments have shown that most of the times the softer asperity looses material to the harder one but the probability of harder body loosing material is also finite. The reason for this is the presence of weak spots within the harder asperity as well as its fatigue caused by the interactions. In general, therefore, the fracture occurs more often on the side of the softer asperity as against that of the harder asperity. The

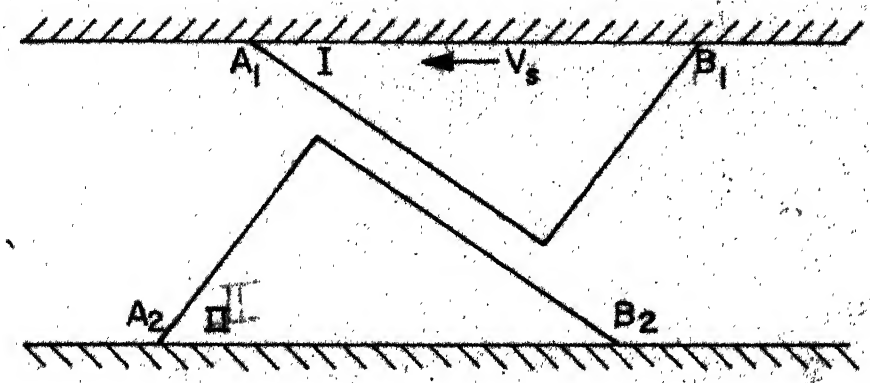
A1
I
Vs
B1
A2
II
B2

(a)

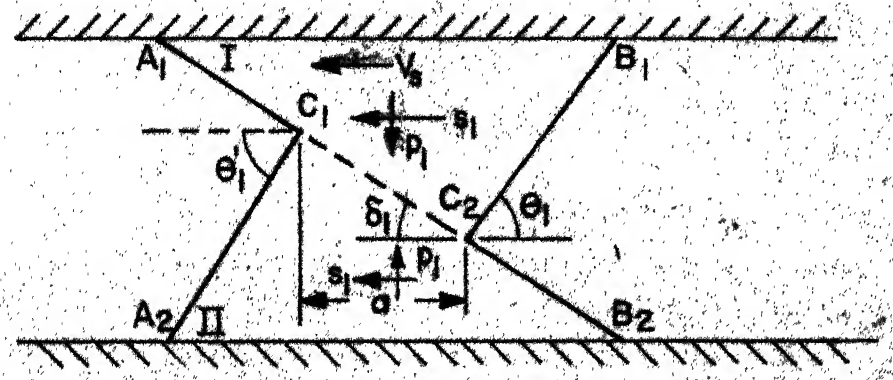
A1
I
Vs
B1
C1
s1
p1
θ'1
δ1
C2
θ1
s1
p1
a
A2
II
B2

(b)

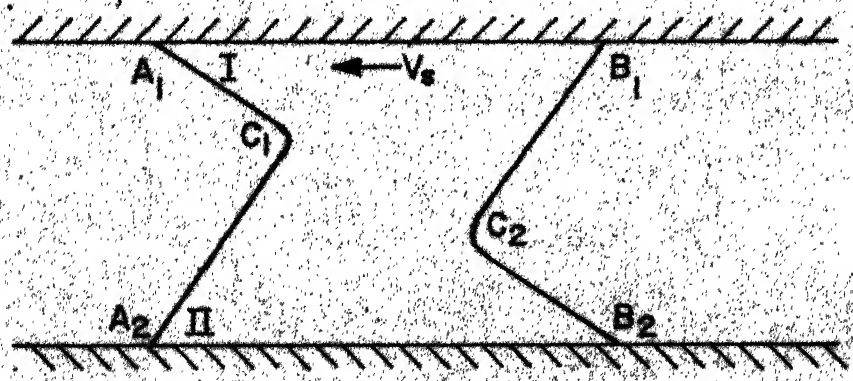
A1
I
Vs
B1
C1
C2
A2
II
B2

(c)

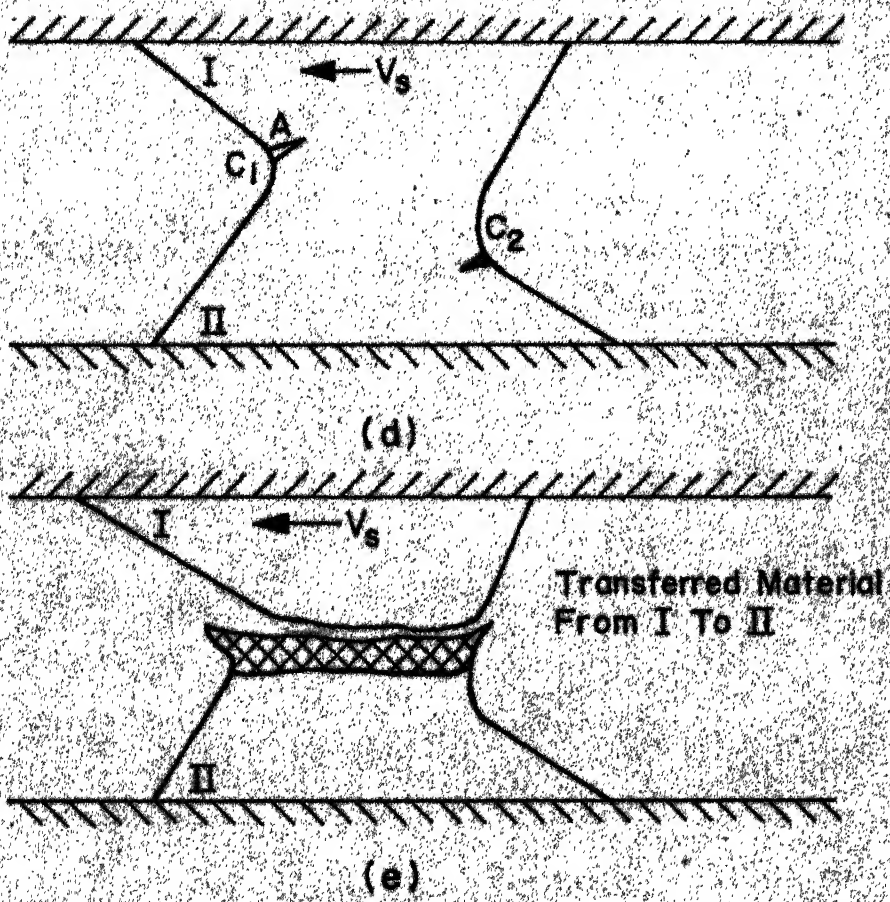

Fig 2.5 Fracture Of a Sliding Asperity Junction

ratio of probabilities also increases as the ratio of hardnesses increases. Mathematically, it can be put as,

$$\frac{P_{fI}}{P_{fII}} \propto \frac{H_{II}}{H_I} \qquad (2.14)$$

where,

P_{fI} , P_{fII} define the probability of junction fracture on the side of asperity I and II respectively, during time T.

H_I , H_{II} represent the indentation hardness on the side of asperity I and II respectively.

Equation 2.14 is generally borne out in practice. For instance, when lead or sulphur are added to steels wear of the H.S.S. tools has been observed to be generally reduced (49), compared to the case where no such additives have been added. Also wear rate of tools against steels is in general higher than that against metals like Brass and Aluminium.

Brockley and Fleming (50) conducted the experiments on copper metallic junctions cut from one piece. These single piece junctions were made to shear by applying a load from a motor. Failure of these junctions is shown in Figure 2.6. The figure illustrates that a junction formed by two identical materials has

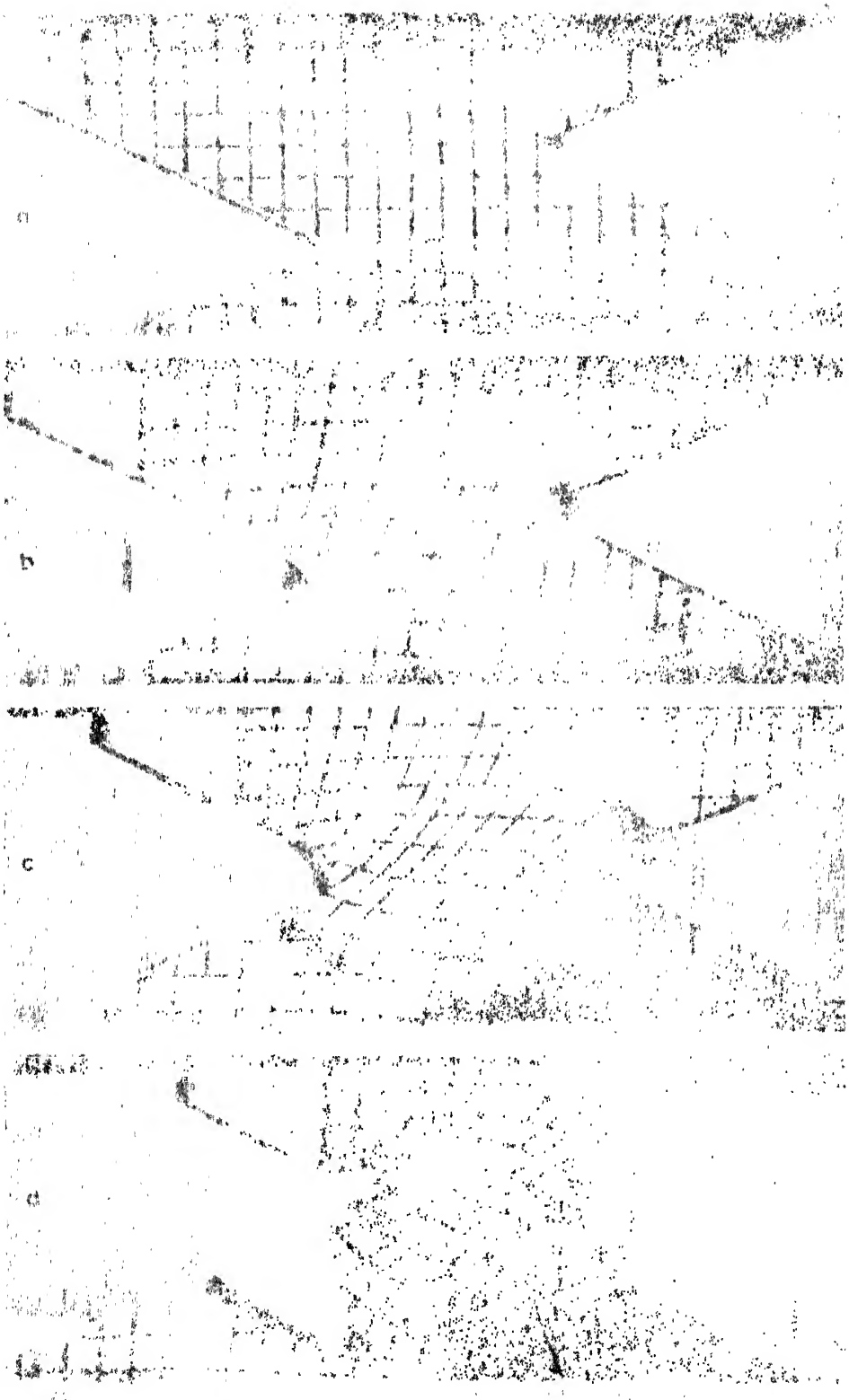

Fig. 2·6 Stages in the deformation and folding of a competent bed.

equal probability of failure on either side of the interface. This figure also indicates that compression, rotation, tension and shearing at the ends of the junctions are apparently involved in the process. Thus the mechanism of a wear fragment formation is quite complex and does not render itself to convenient analytical solution. However, rough estimates of the forces exerted through such junctions have been attempted by Green (44), Edward and Halling (51) and Gupta and Cook (52). It will now be seen how friction between two asperities depends upon the kind of junction formed between the asperities.

Let the Figure 2.5b where the asperities have just met be considered. A mean normal stress (compressive) p_1 and a tangential (shear) stress s_1 act through the junction. Due to these stresses the junction is deformed so that the two surfaces move parallel to one another. These stresses calculated by Green (44) are shown in Figure 2.7. For normal values of surface roughness, angles δ_1 and θ_1 shown in Figure 2.5 are less than 10°, when a junction is formed. For such values of δ_1 and θ_1 it can be seen from Figure 2.7 that $s_1 \simeq 1.25\ k_1$ and $p_1 \simeq 2\ k_1$, where k_1 represents the yield stress in shear of the softer body. Further deformation, as shown in Figure 2.5 c and d, causes changes of shape such that θ_1 increases, δ_1 decreases. It is also seen from Figure 2.7 that as δ_1

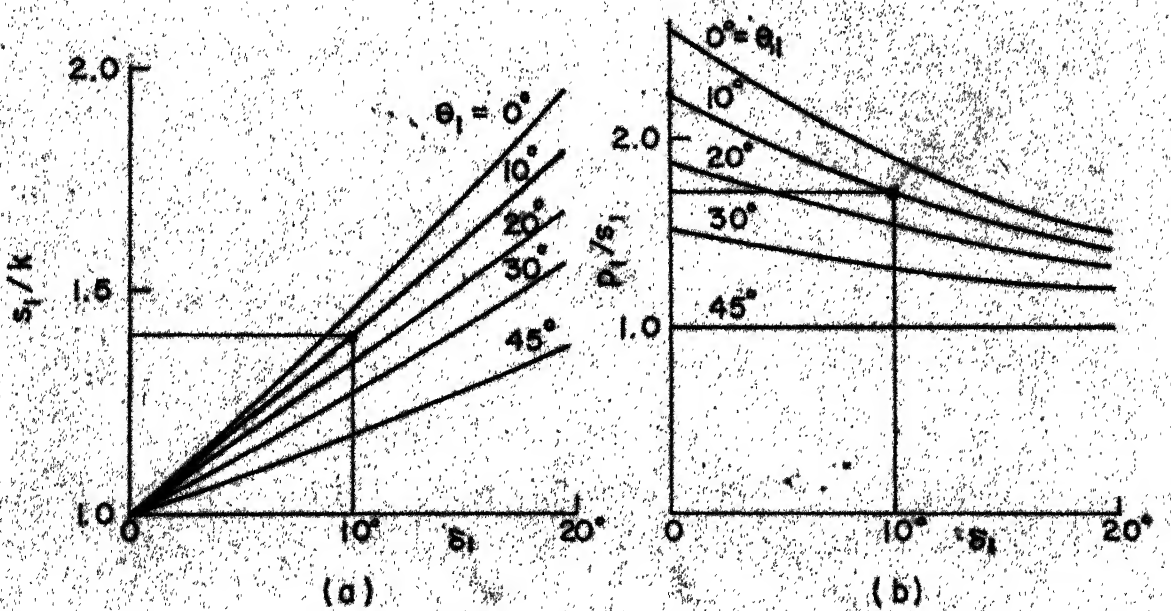

Fig.2.7 Theoretical Relations For Strong Junctions Between (a) s_1/k And δ, (b) p_1/s_1 And δ, For Various Values Of θ Under Conditions Of Plane Strain. (44).

decreases and θ_1 increases s_1 tends to k_1 and p_1 decreases continuously. Also as the junction tends to become roughly symmetrical p_1 continues to decrease. Thus when the junction has been deformed to the symmetrical state the normal stress on it is zero and the tangential stress is nearly equal to its initial value. After the symmetrical shape has been achieved the cycle gets reversed i.e. s_1 increases slightly while p_1 becomes tensile and remains so until the junction eventually breaks under combined shearing and tensile forces. Thus, after the asperities have matched up and firmly welded the cross-section 'a' remains approximately constant until necking and fracture commence. (The time that elapses between the formation of the junction and the ultimate fracture shall be defined as junction life). During this part of deformation N_1 and F_1 bear a constant ratio to p_1 and s_1 respectively. The variation of N_1 and F_1 for a strong junction as discussed is shown in Figure 2.8 a. The areas under these curves between the beginning and end of life cycle are proportional to $\bar{F}_1$ and $\bar{N}_1$ and f is obtained from their ratios as shown in Equation 2.13. It is not possible to calculate 'f' precisely because neither the point of fracture nor the shape of the curves can be defined quantitatively. However, to have an idea of the limits of 'f' certain cases can be considered. These are

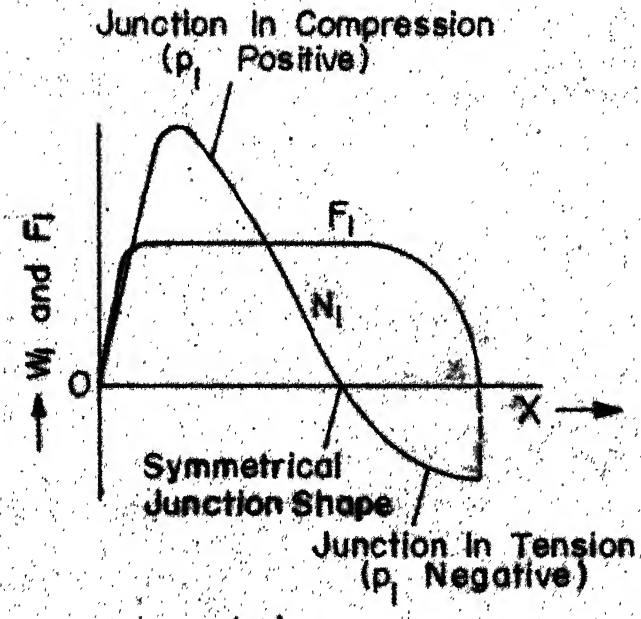

(a)

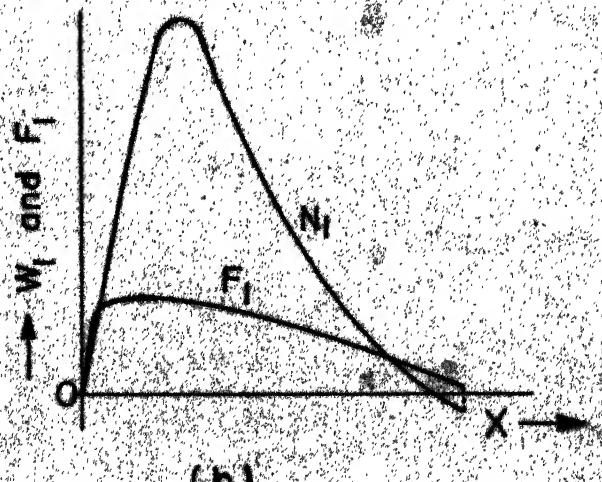

(b)

Fig. 2.8 Theoretical Estimate Of The Relations Between The Forces Exerted Through a Junction During Its Life Cycle And The Relative Displacement Of The Surfaces (Qualitative Only). (a) Strong Junction, (b) Weak Junction. The Broken Vertical Lines Indicate Fracture.(44)

(i) Strong adhesion or high friction.

(ii) Moderate adhesion or medium friction.

(iii) Weak adhesion or low friction.

(i) This occurs for junctions which survive till N_1 becomes tensile. In such a situation the area under F_1 curve is greater than the area under N_1 curve and so $f > 1$. Friction between Indium and Indium falls in this category.

(ii) If a junction survives till the symmetrical shape is reached the areas under N_1 and F_1 curves are roughly equal leading to $f \simeq 1$.

(iii) If the junction fractures as soon as the maximum normal load N_1 is reached

$$f \simeq \frac{F_1}{N_1} = \frac{s_1}{p_1} \qquad (2.15)$$

From Figure 2.7 $p_1 \simeq 1.75\ s_1$ and $s_1 \simeq 1.4\ k_1$ for asperity junctions with $\delta_1 \simeq 10^\circ$. So with these values $f \simeq 0.4$. Besides the early fracture of a weak junction, there are two other reasons for lower value of f in this case.

a) Weak adhesion leads to reduction in s_1 and an increase in p_1 at all stages of its life cycle. This results in lowering of F_1 curve relative to N_1 curve and increase in $\bar{p}_1$ leads to decrease in area of contact.

b) In weak adhesion, relative sliding can also occur at the interface along with plastic deformation of the two halves of the junction, and hence the effective area of cross-section of the junction decreases as p_1 decreases.

The foregoing analysis demonstrates that friction and wear seem to be inter-related and the formation of a loose wear fragment can be understood to occurs as a result of the following possible stages.

a) Matching up of two asperities.
b) Adhesion of these asperities across the interface.
c) Fracture initiation at a critical point.
d) Transfer of material from one asperity to another, and
e) Subsequent disintegration and removal of this transferred material.

The relative strength of the surface layer and the bulk material also plays an important role in the process of material removal from an asperity. This is explained as follows..

Consider again two asperities having got firmly bonded together as in Figure 2.4. If the adhesion bond strength between the surfaces of I and II is lower than the strength of the underlying layer a

positive gradient in the mechanical strength exists. Mathematically, $\frac{d\,H(x)}{dx}$ is a positive quantity for this situation, where H (x) is the hardness in the direction normal to the interface. When a positive gradient in the mechanical strength exists the deformation is confined to the surface layer. When the junction fails the failure is confined to the surface layer. Thus, the friction and wear characteristics are controlled primarily by the characteristics of the surface layer, in this case.

However, when the strength of the bond is greater than that of the bulk material, $\frac{d\,H\,(x)}{dx}$ is negative. Deformation in this case will be extended to larger volume of material. In this case the failure of the asperity junction occurs at a considerable depth below the interface. Thus friction and wear characteristics in this case are controlled by the bulk properties of the materials rather than that of the surface layers.

Figure 2.9 illustrates how different hardness gradients result in different deformation zones at asperities. Figure 2.9 a illustrates the case of positive hardness gradient from interface to bulk. The zone of deformation is shown confined to the surface layer itself. Figure 2.9 b shows the case of negative hardness gradient. The deformation zone is considerably larger than in the first case.

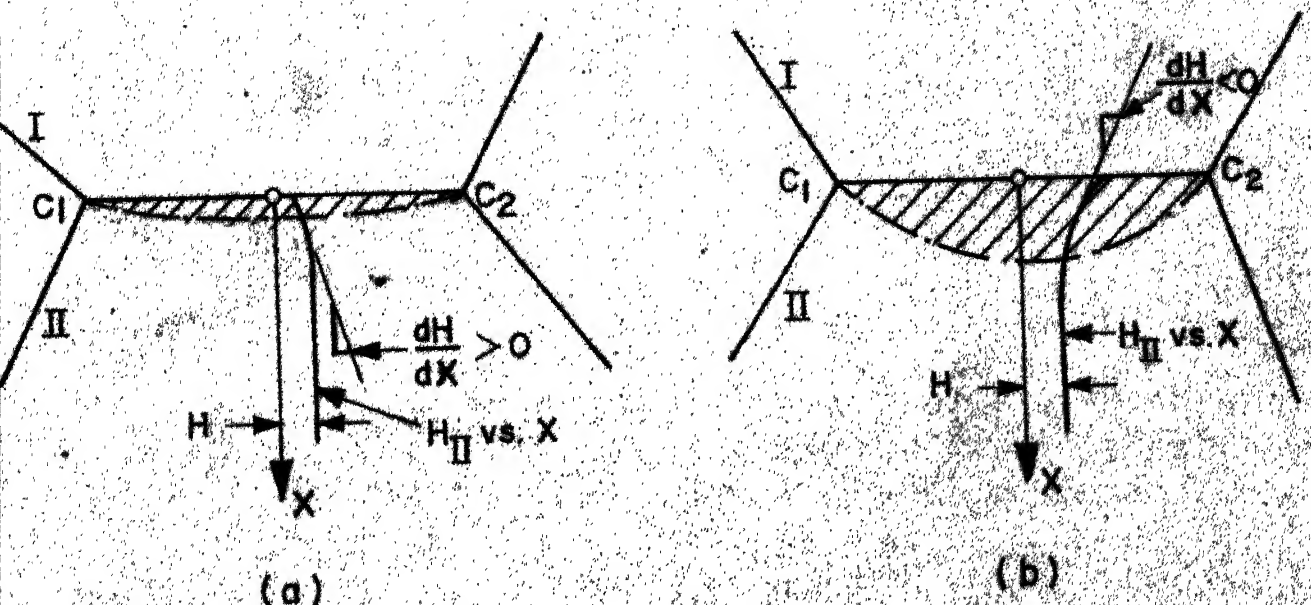

2.9 (a) Case Of a Positive Hardness Gradient. Deformation Is Confined To The Surface Layer.

(b) Case Of a Negative Hardness Gradient. Deformation Is Extended To a Larger Volume.

2.4 Diffusion Wear

2.4.1 Introduction

As mentioned in section 2.2, atoms may diffuse from one region of a body into another, or from one body into another in its intimate contact. This motion, over a sufficient period of time leads to a net transfer of matter in one direction. Essentially three possible mechanisms of diffusional mass transfer have been thought to be operative (53). These are as follows :

(i) Interstitial mechanism

This mechanism is considered to be operative in alloys for those solute atoms which normally occupy interstitial positions as does carbon in iron.

(ii) Ring mechanism

Groh and Hevesy and, Huntington (55) suggested that diffusion occurs merely by a simple exchange of two neighbouring atoms. Zener (56) suggested that instead of two atoms interchanging position three or four atoms could possibly exchange position with little lattice distortion. This method, however, has not been seen to be operative in metals and alloys.

(iii) Vacancy mechanism

If an atom moves from its position to a neighbouring vacancy, diffusion by vacancy mechanism

is said to occur. Also dislocations can offer easier paths for diffusion than a perfect lattice and thus assist the diffusion process. It is also widely known (57, 58) that vacancies can be generated by certain kinds of dislocation movements. Therefore, large dislocation movements are expected to lead to greater diffusion. At present there is considerable experimental evidence (53, 57 - 61) that diffusion occurs by vacancy mechanism.

In solid state diffusion, atoms of an element migrate in the direction of its concentration gradient. Since the thermal energy of an atom is given by $K\Theta$, atoms will vibrate with higher intensity at higher temperatures. Consequently, the rate of transport of matter by diffusion is temperature dependent. It is also to be observed that since diffusion involves atom by atom process of material transfer it is only after a sufficiently long time that observable metal transfer occurs. However, when large strains, strain rates and sharp concentration gradients exist, diffusion can be quite fast. Also in dynamic contact between two bodies the diffusion rate across the interface is very high (11). In both the static and the dynamic contact therefore, substantial material transfer is possible. The large scale diffusion therefore results

in diffusion wear of bodies in contact. There are two basic laws which are necessary for diffusion wear analysis. These laws are known as Fick's laws of diffusion.

(i) Fick's First Law

This law, in the mathematical form is written as,

$$J = -D \frac{\partial C}{\partial x} \qquad (2.16)$$

where, J = mass flow per unit area per unit time,

C = concentration at any point at a distance x from the origin, the distance being measured in the direction of J,

and D = diffusion coefficient or diffusivity and is very much sensitive to the variation of temperature.

Numerous experimental studies of diffusion over wide temperature ranges have confirmed that D is dependent upon temperature in the manner,

$$D = D_o \exp\left(-\frac{Q}{R\theta}\right) \qquad (2.17)$$

where, D_o = frequency factor

Q = activation energy for diffusion

R = universal gas constant,

θ = absolute temperature.

Activation energy Q, represents the energy spent for the atom to move from one equilibrium position to another. Measurements conducted have yielded a general relationship that Q is proportional to melting point Θ_m of a solid. Accordingly Bugakov (60) has calculated $Q \simeq 39\ \Theta_m$ while Askill (62) gives $Q \simeq 38\ \Theta_m$ for f.c.c. structure and $Q \simeq 33\ \Theta_m$ for b.c.c. structure. In these expressions Q is given in units of calories/mole and Θ in degrees kelvin.

(ii) Fick's Second Law

This law is expressed as,

$$\frac{\partial C}{\partial t} = \frac{\partial}{\partial x}\left(D \frac{\partial C}{\partial x} \right) \qquad (2.18)$$

$$= \frac{\partial D}{\partial x} \cdot \frac{\partial C}{\partial x} + D \frac{\partial^2 C}{\partial x^2}$$

Generally, D is considered to be independent of concentration and therefore of x also. This law therefore reduces to the following form :

$$\frac{\partial C}{\partial t} = D \frac{\partial^2 C}{\partial x^2} \qquad (2.19)$$

It is apparent from the very nature of the phenomenon that situations which involve large deformations and high temperatures are most amenable to diffusion studies. It is not surprising therefore that most of the diffusional wear studies have been confined to the cutting tool wear where such conditions are prevalent. Mutual diffusion across tool

chip interface and tool-work interface has been investigated by Loladze (63), Venkatesh (64) and Ghosh and Bhattacharya (11, 65, 66). Ghosh and Bhattacharya have analysed the diffusion wear process theoretically and have shown a fair agreement between the mathematical model and the experimental results. Loladze (63), Kikuchi et. al. (67) and many others have found experimental evidences confirming the existence of diffusion process in machining operations. Even in static contact inter-diffusion of elements like W, Mo, Cr, Co, C and Fe has been established (68, 69).

Kikuchi et. al.(67) have analysed the wear mechanism of H.S.S. using Electron Probe Micro Analyser and found that the white layer which is usually found in the worn out surfaces of H.S.S. is formed by diffusion of Cr, C, Co, and W from H.S.S. to mild steel workpiece. This corresponds to the B type of diffusion described by Nayak and Cook (70) wherein diffusion of major strengthening constituent like W from tool to job is postulated. Zlatin and Merchant (71) and Loladze (63) have confirmed by means of micro-hardness tests, that diffusion from WC tools into the chip is of frequent occurance. The inter-diffusion has also been seen to lead to structural transformation which results in weakened surface layer. This contributes further to the loss of material from the tool.

Scheme of diffusion wear occuring between two bodies in contact may be understood with the aid of Figure 2.10. The figure shows bodies I and II in intimate contact. For simplicity mass transfer only due to diffusion from I to II is examined. Moreover, the mass flow is considered to be one dimensional and in the direction x. If the x dimension of body II is large compared to diffusion zone, it can be treated as a semi-infinite body for the purpose of diffusion analysis. From Fick's Second Law the concentration at any position x of the semi-infinite body at time t is given as (53),

$$C = C_o \operatorname{erfc} \left(\frac{x}{\sqrt{4\,Dt}} \right) \qquad (2.20)$$

where C_o = concentration of the diffusing element in the bulk of I.

Thus, as time of diffusion increases the concentration of the diffusing element in body II increases continuously. When the contact is static ($V_s = 0$) the rise in the concentration of the element in II is rather slow. On the other hand, Bhattacharya and Ghosh (66) have shown that if the contact between the bodies is dynamic ($V_s \neq 0$) material diffused is quite high. They have shown that

$$M_d = M_s \sqrt{\frac{T}{t_c}}$$

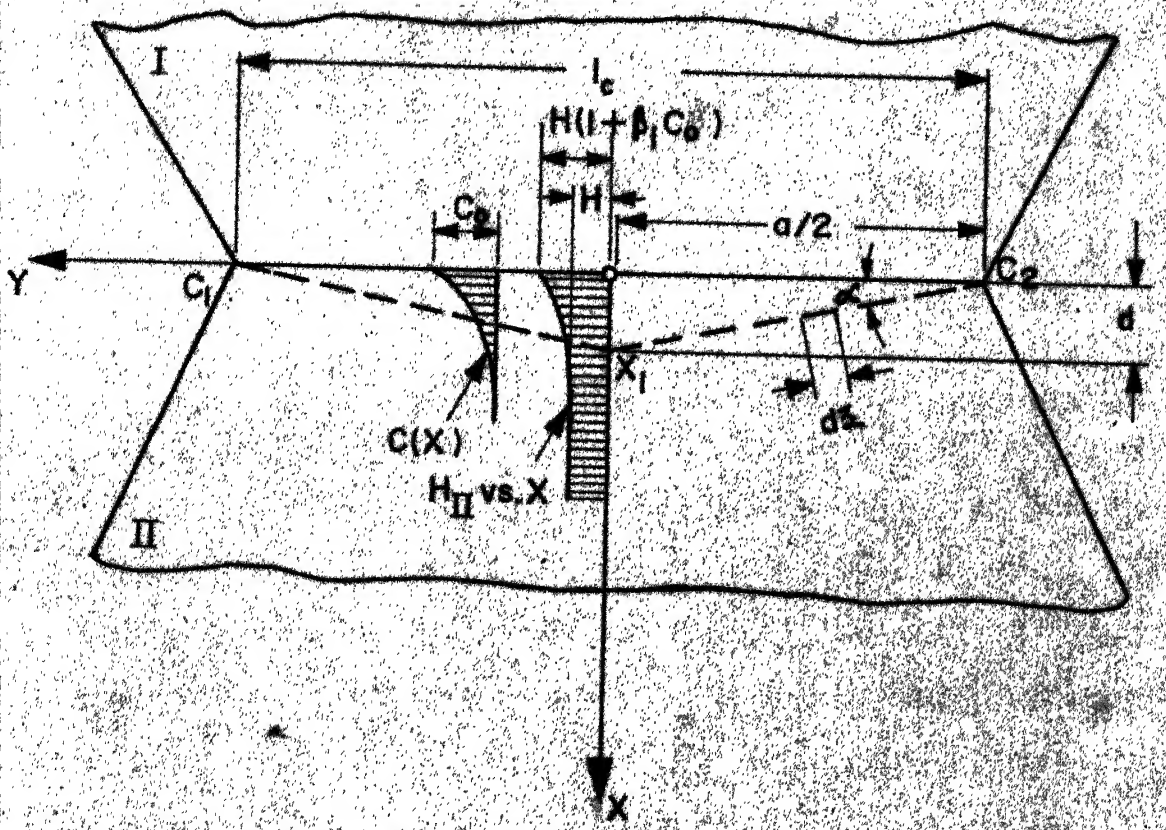

Fig. 2.10 Figure Showing Influence Of Diffusion On Hardness. Diffusion Of Element Of I Into II Is Considered. Diffusion Is Considered To Be Only In X Direction.

I. I. T. KANPUR
CENTRAL LIBRARY
Acc. No. A 16347

where, M_d = material diffused in time T from body I into II when there is relative sliding occuring between the bodies,

M_s = material diffused in time T from I into II when there is no relative sliding,

t_c = time during which an element of II is in contact with I. It is equal to l_c/V_s, where, l_c is the length of contact of the two bodies in Figure 2.10.

It is therefore clear, that if V_s and l_c are such that t_c is very small compared to T, M_d will be much larger than M_s. For instance, if V_s = 60 m/min and l_c = 1 mm and T = 2 min, $M_d \simeq 400\ M_s$. The magnification factor will further increase as the relative velocity is increased. The enhancement of diffusional mass transfer in this case is only due to the characteristic magnitude of the parameters and is not a result of any change in the diffusional property of the material as such. The enhancement due to the atomic rearrangement etc. is to be separately examined.

Several workers have investigated the influence of plastic deformation on diffusion in situations like torsion, creep and compression. It has been reported by these workers (72 - 75) that enhancement of diffusion occurs during plastic deformation. Hirano et al.(61) and Watanabe and Karashima (76) have

confirmed that a significant enhancement of diffusivity of α - iron occurs during plastic deformation. Usually, the ratio of diffusivity during deformation D_s, to diffusivity in undeformed condition D_u, varies linearly with strain rate. Values of $\frac{D_s}{D_u}$ of the order of 100 have been reported (72, 73, 77). Most of the current explanations for these observations is that excess vacancies are generated by deformation. Watanabe & Karashima (76) have concluded that strain-enhanced diffusion in α - iron can be explained in terms of excess vacancies generated by non-conservative motion of jogs on screw dislocations.

Hirano et. al. (61) have experimentally established that diffusivity of polycrystalline iron during compression, D_s, is related to D_u as,

$$\left(\frac{D_s - 1}{D_u} \right) = B \dot{\epsilon}$$

where, $\dot{\epsilon}$ is the strain rate and, B is a constant.

The constant of proportionality B has been established, by these authors, to be a strong function of temperature only, and is given by

$$B = 3 \times 10^{-3} \exp (39{,}200 / R \Theta)$$

It will now be examined how such an enhancement in diffusivity can affect the wear characteristics of a sliding pair.

2.4.2 Influence of Diffusion on Hardness Gradient and Wear

It is important to observe that the enhanced diffusivity is expected to lead to greater mass transfer across an interface. This should influence the diffusion wear of the mating surfaces in a significant manner. In this connection the variation of hardness in the direction normal to the interface seems to be of much significance. Author has analysed the problem of the influence of hardness gradient on wear in the following manner.

Referring again to Figure 2.10 in which the mass flow from I into II is considered, let the diffusion of the harder constituent from I into II be examined. (In actual practice diffusion of Iron from mild steel body I into body II of copper could simulate such a situation). Further, it is assumed that diffusion is only one dimensional and in the direction of x. In such a case the diffusion of material from I into II will result in increased hardness of II. And, with the passage of time the hardness at a certain depth of body II will go on increasing somewhat in the manner same as that of the concentration of the diffusing element. For a particular time T after the diffusion has started, the situation is shown in Figure 2.10. In the figure the hardness gradient has been assumed to

follow the concentration gradient in the diffusion zone. Also, hardness at any depth is assumed to be related to concentration of the harder diffusing material in the manner shown below :

$$H_{II}(x, t) = H (1 + \beta_1 C) \qquad (2.21)$$

where $H_{II}(x, t)$ = hardness of body II at any x and t,

H = hardness of body II in the bulk,

β_1 = constant of proportionality,

and C = concentration of the diffusing element in II.

It was shown in Equation 2.20 that C is given by

$$C = C_o \operatorname{erfc} \left(\frac{x}{\sqrt{4 Dt}} \right) . \qquad (2.22)$$

Thus, after the diffusion from I into II has commenced, hardness at any distance x at time t is given by,

$$H_{II}(x, t) = H \left\{ 1 + \beta_1 C_o \operatorname{erfc} \left(\frac{x}{\sqrt{4 Dt}} \right) \right\} . \qquad (2.23)$$

At x = 0, at any finite time therefore,

$$H_{II}(0, t) = H (1 + \beta_1 C_o) \qquad (2.24)$$

Now, since the diffusion of material from I (harder) into II is expected to lead to increased surface hardness of II, $H_{II}(0, t) > H$. Consequently $\beta_1 C_o$ has to be a positive quantity. (On the other hand, if

diffusion of softer material II into I is being investigated $\beta_1 C_o < 0$.) However, since the diffusion of element of I into II can raise the surface hardness of II only to a finite value,

$$0 < \beta_1 C_o \leq \text{upper limit.} \qquad (2.25)$$

If the above analysis is applied to an asperity junction, bodies I and II have to be considered as asperities with a junction of size 'a'. The asperities are sliding against each other at a velocity of V_s as shown in Figure 2.5. Now, during the junction life t_j (the time that elapses between the formation of the junction and its ultimate fracture)certain amount of material will diffuse across the interface. Both the soft and the hard elements will diffuse across the interface and this will influence the strength characteristics of the asperities.

It is apparent from the available literature on wear that the influence of the diffusing element on the hardness of the parent body has not been accounted for in analytical calculations. Author has proposed in the following paragraphs, that it is possible to take such effects into consideration.

When asperity I (harder) looses material to asperity II by diffusion and the junction failure occurs, the depth of the surface layer removed would be determined by the weakest path in II. This would be

controlled by the local hardness variations. When the diffusivity of the element from I has changed it is expected that the weakest path in II along which fracture occurs would also get changed. Consequently, the problem reduces to (i) recognizing a physical parameter which would have an optimum value along the fracture path, and (ii) establishing the fracture profile uniquely. To meet these requirements a load parameter Λ is defined, such that,

$$\Lambda = \int H_{II}(x)\, ds, \qquad (2.26)$$

where, $H_{II}(x)$ is the hardness at any depth x, and is given by Equation 2.23 and ds is segmental area of the fracture surface. The integration is to be carried over the entire fracture path. If the asperities are considered to be of unit thickness normal to the plane of the figure ds can be replaced by $d\xi$ a line segment of the fracture profile (in the plane of the figure).

The fracture surface in actual practice is not a well defined geometrical surface. Rather a hemispherical surface is generally considered to be appropriate one. The calculation of the load parameter Λ for such a profile is complex and therefore, for the present analysis the fracture profile has been assumed to be triangular in shape. Thus as shown in Figure 2.10, the fracture of body II is assumed to take place along the path $C_1 X_1 C_2$.

Now, the load parameter Λ will have a minimum value for the given profile, provided it satisfies the conditions for the existence of minima which are :

$$\frac{\partial \Lambda}{\partial d} = 0 \qquad (2.31)$$

and $$\frac{\partial \Lambda}{\partial d^2} \geqslant 0 \qquad (2.32)$$

Therefore differentiating Λ w.r.t. d the first condition reduces to,

$$\frac{\partial \Lambda}{\partial d} = \frac{1}{\beta_1 C_o} + \operatorname{erfc}\left(\frac{d}{\sqrt{4 Dt_j}}\right) + \frac{\sqrt{4 Dt_j}}{\sqrt{\pi}} \left(\frac{a^2}{4 d^3}\right) \times \left\{\exp\left(-\frac{d^2}{4 Dt_j}\right) - 1\right\} = 0 \qquad (2.33)$$

Thus the value of d which satisfies the given requirements has to satisfy the equation,

$$\frac{1}{\beta_1 C_o} + \operatorname{erfc}\left(\frac{d}{\sqrt{4 Dt_j}}\right) + \frac{\sqrt{4 Dt_j}}{\sqrt{\pi}} \left(\frac{a^2}{4 d^3}\right) \exp\left\{\left(-\frac{d^2}{4 Dt_j}\right) - 1\right\} = 0 \qquad (2.34)$$

It is easy to judge that with the usual values of diffusion coefficient (D), junction life (t_j) the quantity $\frac{d^2}{4 Dt_j}$ is fairly large. Also, for large values of z

$$\operatorname{erf}(z) \simeq 1 - \frac{\exp(-z^2)}{z\sqrt{\pi}} . \qquad (2.35)$$

These two approximations reduce Equation 2.33 to

$$\frac{\partial \Lambda}{\partial d} = \frac{d^3}{\beta_1 C_o} \frac{\sqrt{\pi}}{\sqrt{4 Dt_j}} - \frac{a^2}{4} = 0 , \qquad (2.36)$$

or, $$\frac{d^3}{\beta_1 C_o} \frac{\sqrt{\pi}}{\sqrt{4 Dt_j}} = \frac{a^2}{4} . \qquad (2.37)$$

As indicated in inequality 2.25 $\beta_1 C_o$ has an upper limit which would essentially be dependent on the increase in hardness of II due to the diffusion of the harder element from I. If the case of iron (harder) diffusing into copper (softer) is considered, the upper limit for $\beta_1 C_o$ may be set at unity. This follows from Equation 2.24 on the basis that hardness of iron is roughly twice that of copper (78). In the absence of an exact analysis, however, a rough value of $\simeq 0.5$ may be assumed to be valid for $\beta_1 C_o$. Equation 2.37 shows clearly that for all real values of 'a', D, t_j, β_1 and C_o the parameter d will always have a real value. Also, D, t_j and 'a' are very small quantities and $\beta_1 C_o$ is likely to be comparable to one. It is obvious therefore, that $\frac{\partial^2 \Lambda^2}{\partial d^2}$ will be always positive. Therefore, it is seen that a value of 'd' exists which satisfies the conditions 2.31 and 2.32. An estimate of 'd' for the triangular fracture profile may now be made. Using the value of 0.5 for $\beta_1 C_o$ equation 2.37 reduces to,

$$2 d^3 \frac{\sqrt{\pi}}{\sqrt{4 Dt_j}} = \frac{a^2}{4} \qquad (2.38)$$

$$\text{Or} \quad d^3 = \frac{a^2}{8} \frac{\sqrt{4 Dt_j}}{\sqrt{\pi}} \qquad (2.39)$$

If in Equation 2.39 the usual values for D, t_j, and 'a' are introduced as,

$D \simeq 10^{-13}$ cm^2/sec,

$t_j \simeq 10^{-5}$ sec,

and, $a \simeq 20 \times 10^{-4}$ cm,

the magnitude of d turns out to be $\simeq 0.2 \times 10^{-4}$ cm. Thus, $d \simeq a/100$. This seems to be a physically realistic value. Apparently therefore, the load parameter Λ and the fracture path chosen seem to be appropriate to the situation.

From Equation 2.39 it is also seen that

$$d \propto D^{1/6} \qquad (2.40)$$

Thus, if the diffusivity of the element diffusing from I into II increases from D_1 to D_2, the depth d_2 of the fracture path is expected to be deeper and given by,

$$d_2 = d_1 \left(\frac{D_2}{D_1}\right)^{1/6} \qquad (2.41)$$

As an example, if $D_2 = 4\ D_1$, $d_2 = 1.127\ d_1$. This means that the wear of body II is enhanced by about 13%. It will be seen in a latter section how the changing wear characteristics of a sliding pair can be explained on the basis of these observations.

CHAPTER III

ROLE OF DISLOCATIONS IN DEFORMATION AND WEAR

3.1 Plastic Deformation and Dislocations

3.1.1 Introduction

The theoretical strength of a crystal free from defects is calculated to be $\simeq \frac{G^*}{30}$, where G^* is the Shear Modulus (79). However, it is found from experimental observations that plastic deformation in actual crystals is initiated at stress $\simeq 10^{-3} - 10^{-4}\ G^*$. This paradox was solved by Taylor, Orowon and Polanyi, almost simultaneously. These workers developed the idea that all real crystals contain defects, called dislocations and slip in crystals occurs as a result of the movement of these dislocations (79).

It is now well established through experimental observations, that all real crystals contain dislocations which are produced in the crystals during crystal growth as well as by the deformation of the crystal (80).

3.1.2 Features of Dislocations

In Figure 3.1 it is shown that slip has occurred over region I, but not over region II of a slip plane of the crystal. The direction of slip is given by $\bar{b}$. The boundary A B C D is thus the dislocation line. Vector $\bar{b}$ describes the state of slip in I,

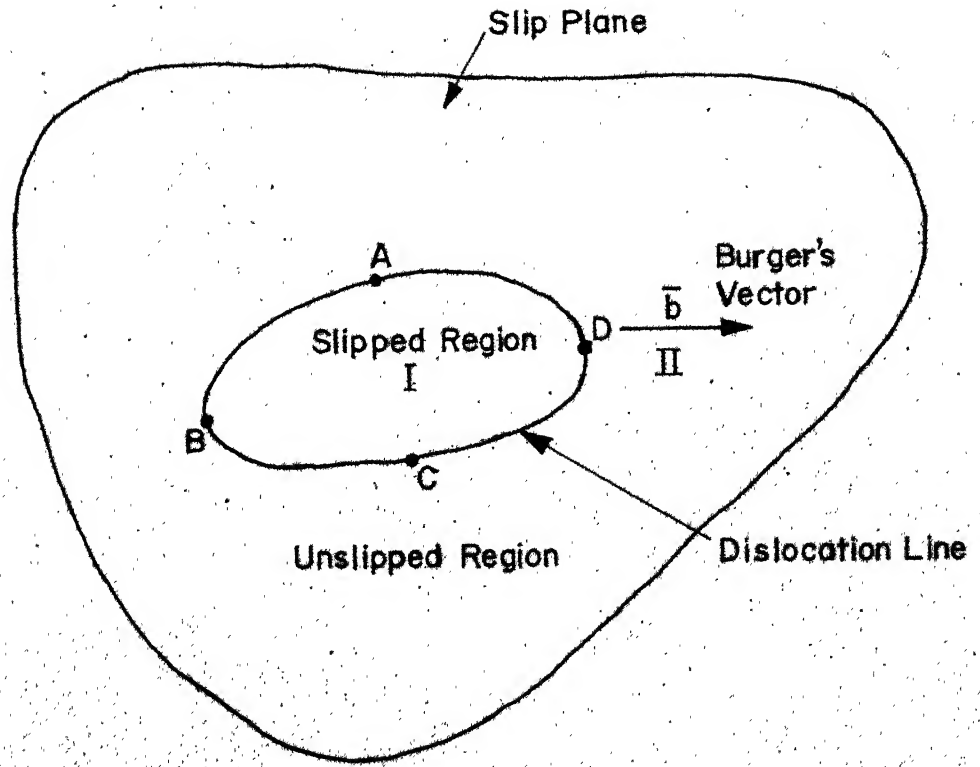

Fig3.1 Schematic Diagram Showing a Dislocation Line Lying In a Slip-Plane.

which specifies the direction and distance by which atoms in the region I on the upper side of the slip plane have moved with respect to those on the lower side. This vector $\bar{b}$ is called the Burgers vector of the dislocation. Burgers vector determines the nature of dislocation and is its most important invarient characteristic. Dislocations with $\bar{b}$ equal to one lattice spacing are called unit dislocations.

Though the Burgers vector is constant along a dislocation line the structure of the dislocation changes with the inclination of line to the slip direction. It is convenient to regard an arbitrary Burgers vector $\bar{b}$ as sum of two rectangular components $\bar{b}_1$ and $\bar{b}_2$ such that $\bar{b}_1$ is normal and $\bar{b}_2$ is parallel to the given dislocation line. Thus, the given dislocation line is studied as the sum of an edge dislocation which is characterized by $\bar{b}_1$ and a screw dislocation which is characterized by $\bar{b}_2$ (79). Therefore, $\bar{b}_1 + \bar{b}_2 = \bar{b}$, and $\bar{b}_1 \perp \bar{b}_2$. In actual crystals dislocations do not always exist as pure edge or screw dislocations, rather dislocations of mixed character are the most common. In Figure 3.1, it can be seen that the arbitrary dislocation line A B C D will have an edge character at B and D whereas at A and C will have a screw character.

When a dislocation of strength $\bar{b}$, sweeps over an entire slip plane the two half crystals which meet on this plane become displaced relative to each other by the magnitude $b = |\bar{b}|$ in the slip direction. But the total deformation of the crystal is a function of the number of dislocation lines present in it. This leads to the definition of density of dislocations ρ which is defined as the total length of dislocations per unit volume. In most cases, however, only those dislocations can be counted which emerge on the surface, and hence it is more suitable to consider the surface density (80). Thus ρ is also defined as number of dislocations intersecting a unit surface normal to dislocations. In metal crystals the density of dislocations after heat treatment and without any plastic deformation is $\simeq 10^7 - 10^8$ cm^{-2}, which may increase after a large plastic deformation, to a value $\simeq$ $10^{10} - 10^{11}$ cm.$^{-2}$. In carefully grown Si and Ge single crystals dislocation density may be reduced to a value $\simeq$ 1 - 100 cm.$^{-2}$ (81).

Dislocations, found in real crystals, usually build up characteristic networks depending upon the treatment to which the crystals have been submitted. A good crystal generally contains $10^4 - 10^6$ dislocations cm.$^{-2}$ distributed in a three-dimensional network. According to Mott (82) and Frank (83) such a network is

expected to be stable, since all the nodes can be near to their equilibrium configurations. Etch pit techniques have shown (58) that well annealed crystals contain fairly regular networks in which dislocation lines are usually 10 - 100 μ long. Such a network is shown in Figure 3.2. Electron microscopy has also revealed that in most heavily cold worked materials, a three-dimensional and fairly isotropic network of dislocations is developed (58). This is analogous to Frank network of annealed metals but usually on a much smaller scale. Carrington et. al. (84) have done extensive study of deformation on iron and have revealed that dislocations form nicely distributed networks roughly all of the same size. Those dislocation lines of the networks which are free to move are called mobile dislocations. It is such dislocation lines of the networks which participate in slip and deformations. In order to investigate this further, it is necessary to study the important properties of various types of dislocations.

It is easy to visualise that displacement and distortion of material occurs around a dislocation. Such distortions are obviously absent in crystals free from dislocations. In the case of an edge dislocation, the region above the slip plane is in compression whereas the region below the slip plane is in tension. On the

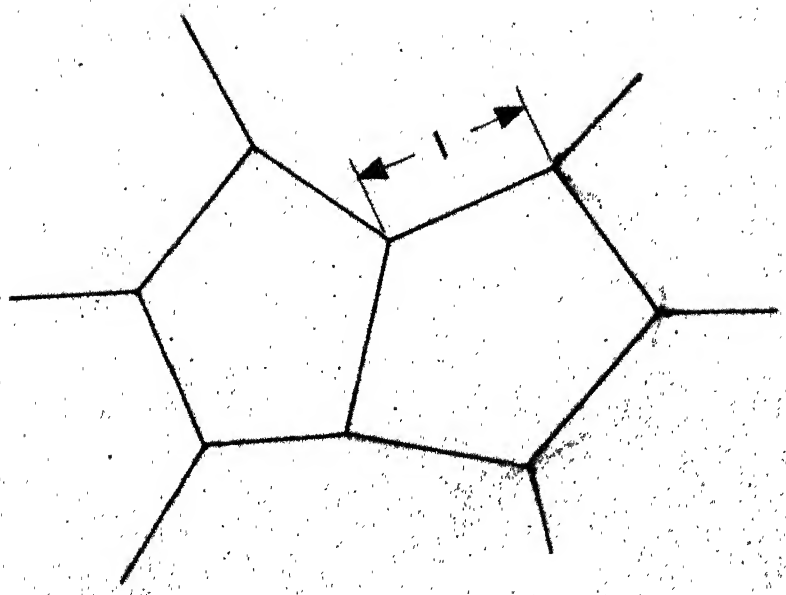

Fig.3.2 Frank Network

other hand, screw dislocation produces only pure shear. These stress fields decrease as the distance from the centre of dislocation increases (79). Thus, dislocations are said to be having stress fields of long range nature associated with them. For instance, the stress field of a screw dislocation shown in Figure 3.3 is simply given by,

$$\sigma_{\theta z} = \sigma_{z\theta} = \frac{G^* b}{2\pi r} , \qquad (3.1)$$

and all the other stress components being equal to zero. Obviously the stress field consists of two pure shears ($\sigma_{\theta z}$ and $\sigma_{z\theta}$) and these stresses decrease as the distance r from the centre of the dislocation increases. It is also evident that extremely high stresses must be existing at the centre of the dislocation.

Another very important characteristic of a dislocation is that it acts as a source for generation of new dislocations in a crystal. Thus, the large plastic strains occurring in practice have been explained on the basis that large dislocation densities are developed during plastic deformation. Mechanisms which have been suggested to account for the production of such large dislocation densities fall under three categories (81) :

(i) Frank - Read type source,

(ii) multiple cross glide,

(iii) multiplication by climb.

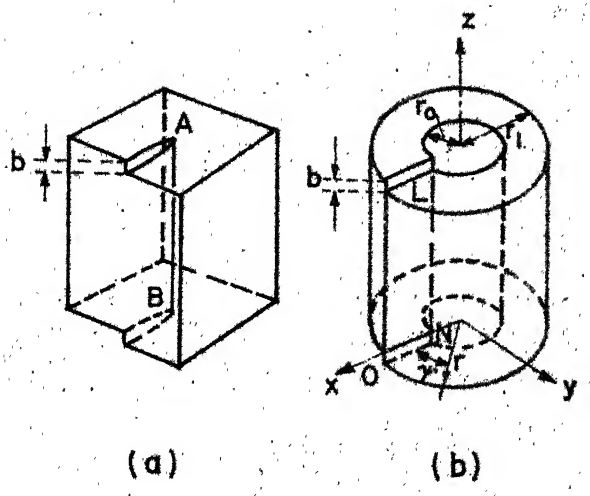

Fig. 3.3 (a) Screw Dislocation AB Formed In a Crystal. (b) Elastic Distortion Of a Cylindrical Ring Simulating The Distortion Produced By The Screw Dislocation AB

Also, like a physical entity a dislocation line has an associated strain energy, line tension, velocity, kinetic energy etc. (79). These various mentioned features of dislocations have been found to be of great significance in explaining plastic deformation, creep, fracture, fatigue and many other physical phenomenae occuring in real materials. Also, it will be shown in the following chapters how the behaviour of dislocations at the asperity junctions can explain some phenomenae associated with the wear of sliding bodies.

Since large plastic strains realised in actual practice have been explained on the basis of large number of mobile dislocations, the strain rates are also explained on the basis of the rate of movement of such dislocations. The next section forms the subject matter of this topic.

3.1.3 Movement of Dislocations

Various experiments on etch pit observation, growth patterns of crystals and electron microscopic observations have proved conclusively that dislocations in a crystal can move. Two basic types of dislocation movement, have been identified. These are,

(i) glide or conservative motion in which the dislocation moves on the surface defined by its line and Burgers vector, and

(ii) climb or non-conservative motion in which the dislocation moves out of its glide surface.

Dislocations move by glide at velocities which depend upon stress and temperature. Johnston and Gilman (85) were one of the first to provide a direct method of measuring dislocation velocity. They observed the movement of dislocation etch pits in lithium fluoride at various stages of deformation. By repititive experiments they showed that

$$V(\sigma, \theta) \propto \left(\frac{\sigma_a}{\sigma_o}\right)^n \qquad (3.2)$$

where, $V(\sigma,\theta)$ = dislocation velocity under the influence of stress and temperature.

σ_a = applied shear stress resolved in the slip plane,

σ_o = shear stress when V = 1 cm/sec

and n = constant ($\simeq$ 25 for lithium fluoride).

Equation 3.2 was obtained on a purely empirical basis. It is, however, to be observed from the form of the equation that the velocity of dislocations is very sensitive to stress. This is so both for screw as well as edge dislocations. Stein and Low (86) studied dislocation velocity in Fe - 3.25% Si using the same method as used by Johnston and Gilman. Essentially same equation as the Equation 3.2 was obtained

with $n \simeq 35$ at room temperature. These authors also measured dislocation velocity at various temperatures. The influence of temperature was also like that of stress, seen to enhance the dislocation velocity.

As mentioned a dislocation line can also be moved by a process called climb. Climb is a process in which diffusion of atoms to or from a dislocation line occurs. This leads to the movement of the dislocation line. Since diffusion is a temperature dependent phenomenon, the movement of dislocations is restricted almost entirely to glide at low temperatures. But when diffusion is possible, as at high temperatures an edge dislocation can move out of its glide plane by loosing or gaining atoms. If the dislocation looses a row of atoms (or gains a row of vacancies) it is said to climb up. On the other hand if a row of atoms is added to it (or a row of vacancies is lost by it) the dislocation is said to have climbed down. It is clear that these processes require mass transport by diffusion and therefore climb is a thermally activated process. In practice, instead of loosing or gaining a complete row of vacancies (or atoms) only individual vacancies or small clusters of vacancies diffuse to the dislocation. In this manner only a short section of a dislocation climbs leading to formation of steps on the dislocation line.

These steps are called jogs. Figure 3.4 shows a single jog on an edge dislocation. Jogs are also produced in a deforming material by the intersection of dislocations (79). Further positive and negative climb of the dislocation occurs by motion of these jogs. It is believed that in practice, most of the deformations at high temperatures and high stresses occur by means of climb of jogs rather than of the entire dislocation line. This is because of the following reasons :

(i) An extremely high stress is necessary to make the edge dislocation line climb as a whole (58).

(ii) It is only at certain locations that conditions, favourable for diffusion, may be prevalent. On the other hand climbing of jogs by diffusion process is an easier one and has been found operative in practice.

Therefore, in actual practice the rate at which a dislocation can climb should be determined by the rate at which the jogs can climb. And, this depends upon the temperature which determines the diffusion rate and the stresses which assist the diffusion process. Therefore, the climb rate of edge dislocations reduces to finding out the concentration and diffusion rate of jogs.

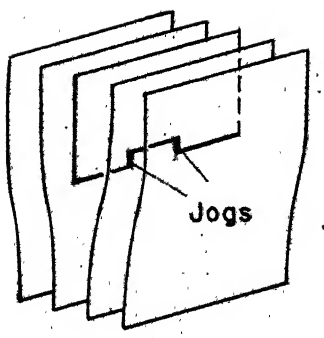

Fig.3.4 Single Jogs On Edge Dislocation.

For, if C_j is the concentration of jogs and V_j is the speed of jogs then the velocity at which the edge dislocation line climbs $= V_j C_j$. Friedel (58) has shown that for large stresses, the velocity of dislocation derived in this manner can be finally given in the form :

$$V(\sigma, \theta) = \frac{D C_j}{b} \times \exp\left(\frac{b_0^3 \sigma}{K \theta}\right) \qquad (3.3)$$

In this equation

D = diffusion coefficient,

b_0^3 = atomic volume,

σ = operating stress,

K = Boltzman's constant,

θ = operating temperature,

b = Burgers vector

and,

C_j = concentration of jogs

The quantity $\frac{D C_j}{b}$ may be considered as the velocity at zero stress. So it can be treated as a constant for a particular temperature and will be written as V_c It's value can be calculated as follows.

Diffusion coefficient D is given by

$$D = D_0 \exp\left(-\frac{Q}{R \theta}\right) \qquad (3.4)$$

and $C_j \simeq \exp\left(-\frac{U_j}{K \theta}\right) \qquad (3.5)$

where, U_j = Energy of jog formation. Friedel (58)

has given the value of U_j as $\simeq$ 2.5K θ_m, where θ_m is the melting point of the solid. Therefore $C_j \simeq \exp(-2.5\,\theta_m / \theta)$. The Equation 3.3 is specifically applicable when stress is very large as to that corresponding to the third stage of stress-strain curve or at the head of a dislocation pile-up (58).

It was mentioned in section 3.1.2 that dislocation regeneration can occur by Frank-Read type of source. Under a large enough stress the source, can produce large number of successive loops which explains the large strains achieved in practice. However, several effects provide obstacles to this process which may be summarised as follows :

(i) Difficulty of bending a dislocation line to the radius needed to create a ring.

(ii) The resistance to the movement of dislocations caused by lattice irregularities such as foreign atoms, precipitates and other dislocations.

As a moving dislocation approaches an obstacle its energy increases. The obstacle exerts a force F which acts as a resistance to the movement of the dislocation. Using Mott and Nabarro's relation (79),

$$F = \sigma \bar{b} \qquad (3.6)$$

the opposing force F is seen to be equivalent to an internal stress σ_i, the magnitude of which is given by

$$\sigma_i = \frac{F}{b} \qquad (3.7)$$

In some cases this internal stress actually exists, as for example, when the obstacle is the stress field of other dislocations. In other cases this internal stress is fictitious and is merely the stress which, if present, would have the same effect as the obstacle has on the dislocation. Thus, the stress σ in Equation 3.3 has actually to be replaced by an effective stress σ^* which would be defined as thedifference between the applied stress σ_a and the internal stress σ_i, or

$$\sigma^* = \sigma_a - \sigma_i \qquad (3.8)$$

Also, in Equation 3.3, the atomic volume = b_0^3 is involved in the exponential term. Author makes the observation that this term enters the equation because in the process of 'climbing up', of the jog by one lattice spacing an empty space of volume b_0^3 has been considered to be created (58), and the thermal disturbance is considered to be confined to this volume. In other words b_0^3 is the representative volume in which the activation process of diffusion has been considered to be affected. This is called the activation

volume. However, experimental works of various workers (87, 88, 89) have yielded that in actual deformations the activation volume varies between $10^2\ b_0^3$ to $10^3\ b_0^3$. Thus actually the small representative volume of matter (space) which participates in a thermally activated process is several times larger than the atomic volume. The activation volume is conventionally written as v*. Therefore, using v* in place of b_0^3 and σ^* in place of σ, Equation 3.3 is written as

$$V(\sigma, \theta) = V_c \exp\left(+\frac{v^* \sigma^*}{K\theta}\right) \qquad (3.9)$$

where, $V_c = \frac{D\ C_j}{b}$.

The rate of plastic deformation of a body depends directly upon the dislocation velocity and is given by

$$\dot{\epsilon} = V(\sigma, \theta)\ \rho_m\ b \qquad (3.10)$$

where, $\dot{\epsilon}$ = strain rate,

ρ_m = density of mobile dislocations,

and $V(\sigma,\theta)$= dislocation velocity under a stress σ and temperature θ.

It is seen from Equation 3.9 and 3.10 that the dislocation velocity and, therefore, the strain rate are sensitively dependent upon the effective stress σ^*

and not just on σ_a. The temperature does not play such a sensitive role since it has compensatory effects in the terms, $\exp\left(\frac{v^* \sigma^*}{K\theta}\right)$ and the diffusion coefficient D. Equation 3.9 may now be used to obtain an order of magnitude of the dislocation velocity at high stresses.

Assuming for iron an activation volume $v^* \simeq 200\ b_0^3 = 2 \times 10^{-21}\ cm^3$, and an effective stress $\sigma^* = 2000\ Kg/cm^2$,

$$\sigma^* v^* = 4 \times 10^{-18}\ Kg\ cm$$

$$= 392 \times 10^{-21}\ Joules.$$

Also, the values for D_o and Q may be taken as,

$$D_o = 0.14\ cm/sec., (59)$$

and $Q = 52000\ Cal/mole, (59).$

Using Equations 3.4 and 3.5 the value of V_c is calculated to be,

$$V_c = \frac{10^8}{2.8} \times 0.14 \times \exp\left(-\frac{52000}{R\theta}\right) \times \exp\left(-2.5\frac{\theta_m}{\theta}\right)$$

The value of R, the gas constant may be taken to be 2 Cal/mole degree K. Therefore at a temperature $\theta = 300\ ^oK$ (taking the melting point θ_m for iron as 1810 ^oK),

$$V_c \simeq 3 \times 10^{-36.75}$$

Also, at $\theta = 300\ ^{o}K$,

$$K\theta = 4.2 \times 10^{-21} \text{ Joules.}$$

Therefore, for these assumed values of θ, v* and σ^*

$$\exp\left(\frac{\sigma^* v^*}{K\theta}\right) \simeq 10^{40.1}$$

Therefore, at $\sigma^* = 20\ Kg/mm^2$ and $\theta = 300\ ^{o}K$

$$V(\sigma, \theta) \simeq 0.3 \times 10^{-36.75} \times 10^{40.1} \simeq 0.3 \times 10^{3.3} cm/sec$$

In the same manner at $\sigma^* = 20\ Kg/mm^2$ but $\theta = 373\ ^{o}K$, calculations yield,

$$V(\sigma, \theta)\ \ 0.3 \times 10^{4}\ cm/sec.$$

Again, at $\sigma^* = 20\ Kg/mm^2$, and $\theta = 1000\ ^{o}K$

$$V(\sigma, \theta) \simeq 10^{5}\ cm/sec.$$

The magnitude of velocities obtained in these calculations indicate that dislocation velocities approach that of the velocity of sound at high temperature and stress. In fact, in the metal forming processes where the stresses are close to flow stress, dislocations are expected to be moving with velocities $\simeq 0.8\ V^{o}$, where V^{o} is the shear wave velocity (79). Also, the experimental results of Gilman and Johnson (85) and Stein and Low (86) show that the velocity of dislocations has an upper limit which is of the order of the shear wave velocity. In actual practice, however, the dislocations attain velocities which are only a fraction

of the shear wave velocity. This is due to the damping within the lattice.

Since strain rate is directly proportional to the dislocation velocity, any effect on the dislocation velocity is expected to be manifested in the strain rate $\dot{\epsilon}$. This is an important observation and will be discussed further. Equation 3.4 for the strain rate is usually written in the form,

$$\dot{\epsilon} = A_1 \exp\left(-\frac{Q}{R\theta}\right) \exp\left(\frac{v^*(\sigma_a - \sigma_i)}{K\theta}\right) \qquad (3.11)$$

where A_1 = constant, generally called a structure factor.

Author notes with interest, that many workers (91, 92, 93) have also found this equation to be valid under hot working conditions for various materials. It has been shown by these workers that the activation energy Q involved in creep, hot extrusion, compression and torsion is of the same order of magnitude as that involved in the diffusion process. On the basis of these experimental findings it is therefore, concluded that the hot deformation processes are diffusion controlled thermally activated processes like creep at high temperatures.

In the discussion on asperity interaction in section 2.3 it was shown that large stresses and deformations exist in the junction. The formation of

wear particle occurs under conditions of large stresses and complex deformations. It is also probable that temperature of few hundred degrees is prevalent in the asperity junction zone. As such the author believes that conditions which normally prevail during hot compression and extrusion and other similar processes may also be existing at the asperity junctions. Accordingly it is quite probable that diffusion controlled thermally activated processes are also participating in the wear phenomenon.

Also, since the stresses and strains in the asperity junction are very high, the density of dislocations as well as their velocities are likely to be very high. This should lead to high rate of intersection of dislocations which in turn leads to an excessive vacancy generation. Thus diffusion in the junction zone is likely to be prominent. In fact the enhanced diffusion in strained materials has been confirmed by several workers (61, 89).

On the basis of these observations the author concludes that at the asperity junctions movement of dislocations is controlled by diffusion motion of jogs. Consequently, Equation 3.3 can be safely used in the evaluation of dislocation velocities in the vicinity of such junctions. Obviously, near the asperity junction, the dislocation velocities would be very large.

Large dislocation velocities should at any instant result in a significant concentration of dislocations at a point in the matrix. Besides, due to the high velocities the kinetic energy of dislocations is extremely high at high stresses. This large kinetic energy should enable the dislocations to overcome barriers like dislocation tangles, precipitate particles and even to generate cracks at a faster rate. This is because dislocations have an inherent capability of nucleating a crack in the matrix. In the present work fracture of an asperity junction has been considered to be due to such a property of dislocations.

In the following section it will be shown as to how the dislocation accumulation at a point can lead to the generation of a crack. Consequently, the wear of an asperity junction can be discussed in light of the dislocation accumulation at the notch.

3.2 Dislocations and Crack Initiation

In the central region of an edge dislocation overlapping of the atomic cores exists. This leads to high repulsive forces. Due to these excessive repulsive forces, large compressions are difficult. On the other hand, large dilatational strains will be produced relatively easily. This is so because the restoring forces do not increase indefinitely as the atoms are separated. It follows therefore, that near an edge dislocation deformation tends to be dilatational (94).

Now, if a dislocation with a large Burgers vector $n\bar{b}$ ($n > 1$) is considered, a considerable amount of deformation must be accommodated near the dislocation. This would lead to large dilatational strains. Some pairs of atoms will thus be displaced to positions far apart compared with their natural spacing. If the Burgers vector of a dislocation is large enough ($n > 1$) the separation of atoms near this dislocation will be so large that they no longer interact and an incipient crack will be formed. This is illustrated in Figure 3.5. Thus, it is possible that a crack would develop spontaneously from a dislocation with a sufficiently large Burgers vector (94).

It was mentioned earlier that the dislocation movement can be impeded by many kinds of

obstacles. In a crystalline material the grain boundaries have been seen to be acting as obstacles to the movement of dislocations. This leads to the piling up of dislocations on a barrier like a grain boundary. Such pile-ups are shown in Figure 3.6. Eshelby, Frank and Nabarro (95) have evaluated the distances between various dislocations in a pile-up of dislocation held up across a barrier and have shown that the distance between first two dislocations is $\simeq 0.3\,b$ and that between the 2nd and 3rd is $\simeq b$. Rigorous analysis shows that the actual distances should be further less. It can therefore, be concluded that the leading dislocations of the pile-up will coalesce to form a single dislocation of large Burgers vector, thus leading to the possibility of an incipient crack, as shown in Figure 3.5. Stroh (94) has shown, analytically that the incipient crack arises mainly due to the short-range interaction of a few dislocations at the head of a pile-up. He has considered the case of a dislocation approaching an incipient crack. It is assumed that a dislocation with Burgers vector $\bar{b}$ is brought near a large dislocation, with Burgers vector $n\,\bar{b}$ ($n > 1$). Also, an incipient crack is considered to be associated with this large dislocation. Stroh (94) has shown that the force F which the giant dislocation exerts on the unit dislocation is given by

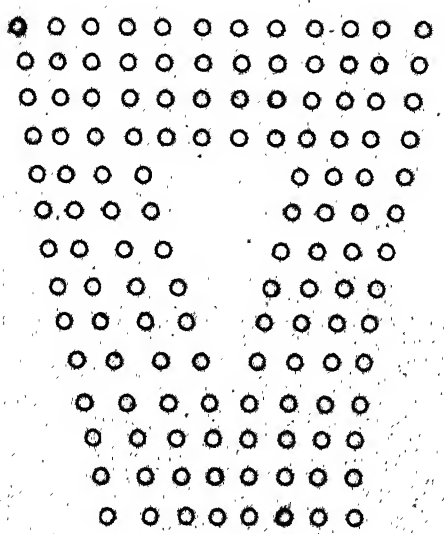

Fig.3.5 Dislocation With Burger's Vector 4b Showing An Incipient Crack.

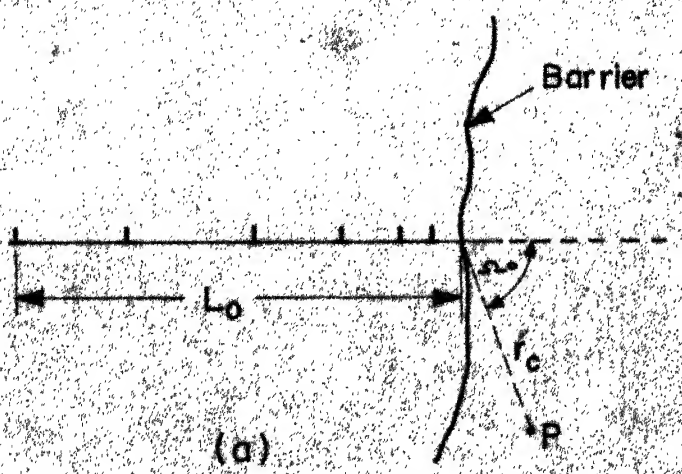

Dislocation Pile Up At a Barrier

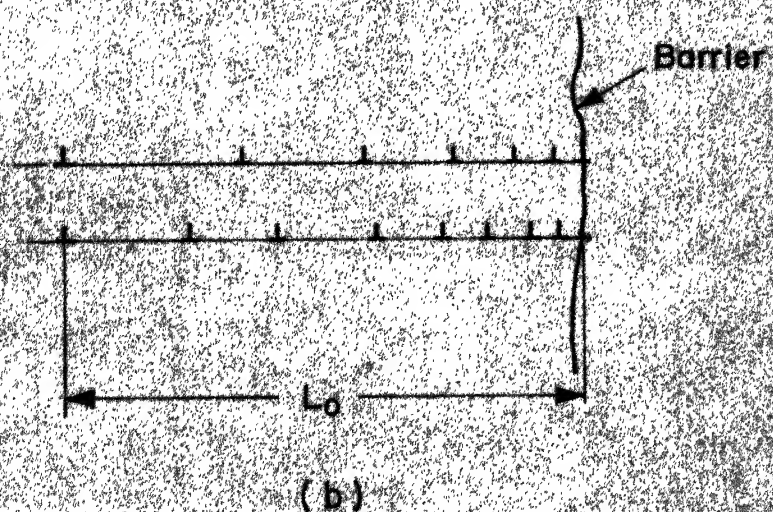

Fig. 3.6 (a) Dislocation Pile Up At a Barrier

(b) Piled Up Pair Of n Dislocations Each, Against a Common Barrier.

$$F = \frac{n\, b\, D_2}{x}, \text{ (for large x)} \qquad (3.12)$$

where, $$D_2 = \frac{G^* b}{2\pi(1-\nu)} \qquad (3.13)$$

and ν = Poisson's ratio.

This is the usual expression for force between two like dislocations. For very small values of x on the other hand,

$$F = -\frac{b\, D_2}{4\, x} \qquad (3.14)$$

This shows that for sufficiently small values of distance x the two like dislocations attract one another. This attraction arises because, when the distance between the dislocations is very small, the crack acts as a free surface and so gives rise to an image force attracting the other dislocation to it (94). The general relation between F and x is exhibited graphically in Figure 3.7. It is seen that the presence of the crack makes very little change in the force until the dislocations are within a few atomic spacings of each other. At short distances the repulsion attains a maximum and then drops quite steeply. The maximum stress σ_m opposing the addition of a further dislocation to the compound dislocation with Burger vector $n\bar{b}$ decreases very sharply as n increases. Figure 3.8 shows this effect and it leads to the conclusion that the most difficult stage in the crack initiation is in

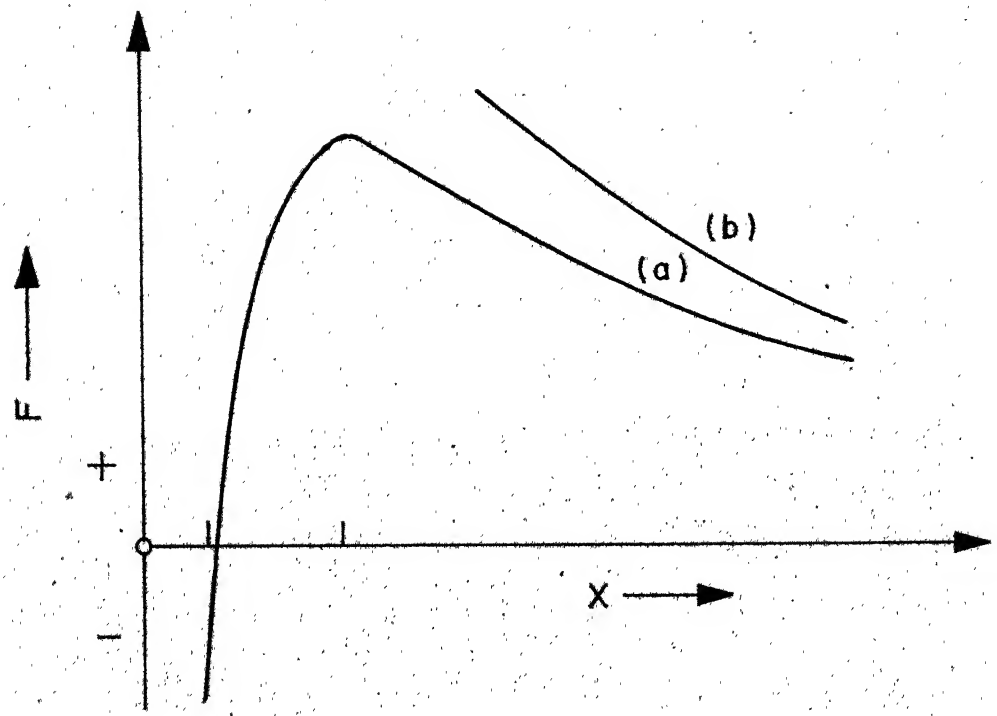

Fig. 3.7 Force Between Two Dislocations As a Function Of The Distance ,X Between Them.

(a) Crack Extending From One Dislocation.

(b) With No Crack (94)

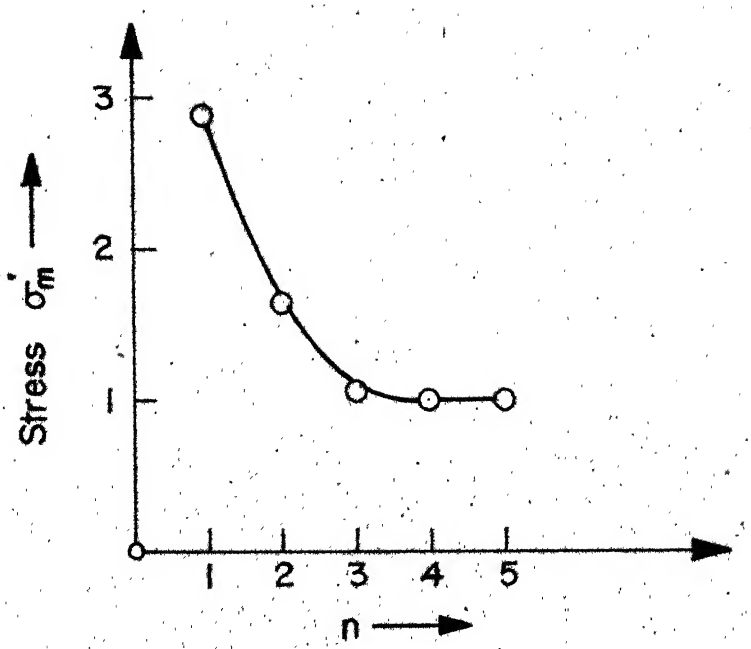

Fig.3.8 Maximum Stress Opposing Addition Of a Unit Dislocation To a Joint Dislocation ($n>1$), (94).

bringing the first two dislocations together. When this is achieved, further dislocations can be added more easily and so once the process has started, the crack should develop rapidly. Thus, while the initiation of a crack at the head of a pile-up is due to the interactions of few leading dislocations the rest of the dislocations serve to produce high stress concentration required to force the leading dislocations together. Author therefore makes the observation that the dislocation density has to reach a certain minimum in the region, before the proper stress concentration can be attained. In the present work also, this observation has been made use of, to explain the fracture and wear of an asperity junction.

It can be shown that a pile-up of dislocations can result in proper stress conditions to initiate a crack at the head of the pile-up. Figure 3.6a shows a pile-up of n positive edge dislocations. The leading dislocation is locked up in position and the remainder, which are free to move in the slip-plane, are held in equilibrium by an applied stress σ_a. The total stress round such a piled up group arises from two sources :

(i) Stresses due to the locked dislocation and the applied shear stress.

(ii) The stress due to (n - 1) free dislocations.

Mathematical treatment due to Stroh (96) of this case yields the maximum value of the total stress, to occur at $\theta_0 = 70.5^{\circ}$ and its magnitude is

$$\sigma_m = \left(\frac{2}{\sqrt{3}}\right)\left(\frac{L_o}{r_c'}\right)^{1/2}\sigma_a \qquad (3.15)$$

Also, the condition for the crack initiation reduces to

$$n\sigma_a \geq 12\alpha_1 G^* \; (= 12\gamma/b) \qquad (3.16)$$

Since length r_c' does not occur in Equation 3.16 it follows, that if this condition is satisfied for one length r_c' of crack, it will be satisfied for all lengths of the crack. Equation 3.16 is thus considered as the condition for the initiation of a crack at the head of the pile-up. For most of the metals $\alpha_1 \simeq .06$ (96). Therefore the condition for crack nucleation reduces to

$$n\sigma_a \geq 0.7\, G^* \qquad (3.17)$$

$$\text{or} \quad n b \sigma_a \geq 12\gamma \qquad (3.18)$$

Author observes that for a material like steel in work hardened state $\sigma_a \simeq 2 \times 10^9$ dynes cm^{-2} and $G^* \simeq 10^{12}$ dynes cm^{-2}. With these values, n turns out to be $\simeq 300$. Thus a crack should get formed around a dislocation pile-up of about 300 dislocations. With $b \simeq 2 \times 10^{-8}$ cm, motion of 300 dislocations gives a slip height of $\simeq 600$ A and some evidence exists (97) for steps of this height. This magnitude however,

is not very common. On the other hand, the experimental observations have often yielded existance of crack at the head of piled-up groups lying in several slip planes and against a common barrier. This situation is shown in Figure 3.6b. Each of these pile-ups may then be considered as being formed under a stress consisting of the applied stress together with the stress due to the other pile-ups. This situation is similar to the existence of slip band meeting on a grain boundary. Now, two piled-up groups, each of n dislocations in different slip planes as shown in Figure 3.6 are considered. The leading dislocations are locked in positions on the same normal to the slip planes. If the interaction between different dislocations in different slip lines is neglected, each pile-up is formed under the applied stress σ_a alone. However, when the shear stress due to the other pile-up is considered the analysis yields the effective shear stress on each pile-up to be $= 2\sigma_a$ (94). From this result and the condition $n b \sigma_a \geqslant 12\gamma$ it is seen that the number of dislocations required in each pile up to produce a crack is only half of that needed for an isolated pile-up. This result can be extended to more than two pile-ups. Therefore, when several piled-up groups are held up against a common barrier, it requires the

existence of fewer dislocations on each pile-up to satisfy the condition, $n\, b\, \sigma_a \geq 12\gamma$ to initiate a crack. Since there might be about 10 slip lines in one slip band, the number of dislocations required per slip line is reduced from about 300 to a less than a hundred. This value is often observed experimentally.

Thus, it is concluded by the author that obstacles where dislocations get piled-up offer possible nuclei for the initiation of a crack in a body. The obstacles can be grain boundaries, second phase particles or immobile groups of dislocations. The number of dislocations that can be supported by an obstacle depends upon the type of the barrier, structural features at the barrier, the material and the temperature. The breakdown of a barrier in general can occur by slip on a new plane, by climb of dislocations around the barriers or by generation of high enough stresses to produce a crack.

The initiation of a crack by dislocation accumulation can be of great significance in determining the fracture characteristics of a material. In the following section it is seen how this property of dislocation accumulation can be responsible for affecting the wear characteristics of a sliding pair.

3.3 Dislocations and Fracture of Asperities During Wear

3.3.1 Dislocation agglomeration at a notch

It has been revealed by many experimental and analytical investigations that the interaction between dislocations and bimetallic interfaces or surface layers plays an important role in determining the surface properties of metals. The first analytical work on elastic interaction of dislocations with a surface layer is due to Head (98). He gave a condition for the stable equilibrium of dislocations near a surface. Conners (99) studied the interaction between a surface layer and an edge dislocation. Tamate and Kurihara also studied the behaviour of screw and edge dislocations near an interface with geometric irregularities. The main objective in these works has been to investigate how the surfaces with different relative elastic properties attract or repel dislocations lying in the bulk of the solids. These workers have shown that when the surface is nascent and there is no surface layer present, dislocations are attracted to the surface under the action of a force which varies inversely as the distance from the surface. But, when a surface layer is present as is generally the case with all exposed surfaces, dislocations close to the surface are repelled, while the

dislocations far from the surface are attracted. In this process an equilibrium position is established beneath the surface where these dislocations get piled up in an equilibrium state. Since the plastic behaviour of solids is governed by the behaviour of dislocations, such piling up can affect the mechanical behaviour near the surface layers. It is necessary therefore, that wear characteristics of surfaces be studied in relation to behaviour of dislocations near biometallic interfaces formed between two asperities as discussed in Section 2.3.

Warren (100) has investigated the possibility of clustering of dislocations beneath a surface irregularity. He has considered the particular case of a notch and protrusion on an elastic half-space, the surface of which is stress free. Force acting on a dislocation is calculated as the gradient of the elastic strain energy.

It is known that force of attraction F/unit length, exerted by a free surface on a dislocation at a distance r from the surface, is given by

$$F = \frac{G^* b^2}{4\pi(1-\nu)} \quad \frac{1}{r} \quad , \qquad (3.19)$$

for an edge dislocation and, for a screw dislocation.

$$F = \frac{G^* b^2}{4\pi} \quad \frac{1}{r} \qquad (3.20)$$

Warren has shown that the presence of the notch does not alter the order of this force singularity. However, an additional force term of the order of $\left(\frac{1}{\sqrt{r}}\right)$ is added to the force F. Thus, the notch creates a major effect of attracting the dislocations towards it. This, therefore, should lead to accumulation of dislocations at the notch or the crack tip. Figures 3.9 and 3.10 show two cases considered by Warren. In these figures the line segments show the magnetitude and the direction of the force acting on a dislocation located at the position of the directed line segment. It appears, therefore, that if these dislocations become mobile, say, when a large stress is applied these should agglomerate at the notch. Also, since the piling up of dislocations can initiate a crack at such a point in the matrix, such agglomeration would increase the probability of crack initiation at the notch. Author proposes that this agglomeration of dislocations at the notches may be utilized to explain the fracture and thus the wear characteristics at the asperity junctions. This is explained in the following section.

3.3.2 A simple model for the dislocation agglomeration at the notch.

It was explained in section 2.3 how the two independent asperities I and II match up and get

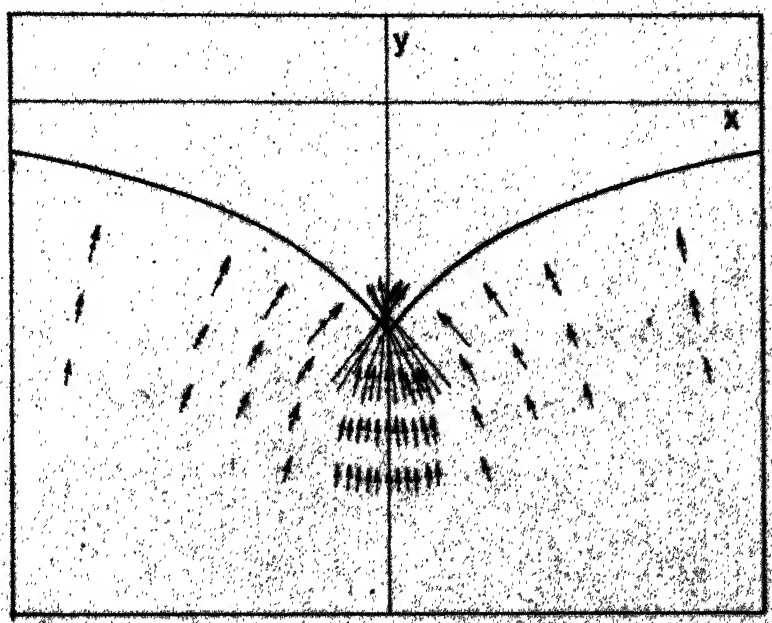

Fig.3.9 Screw Dislocation Force (100)

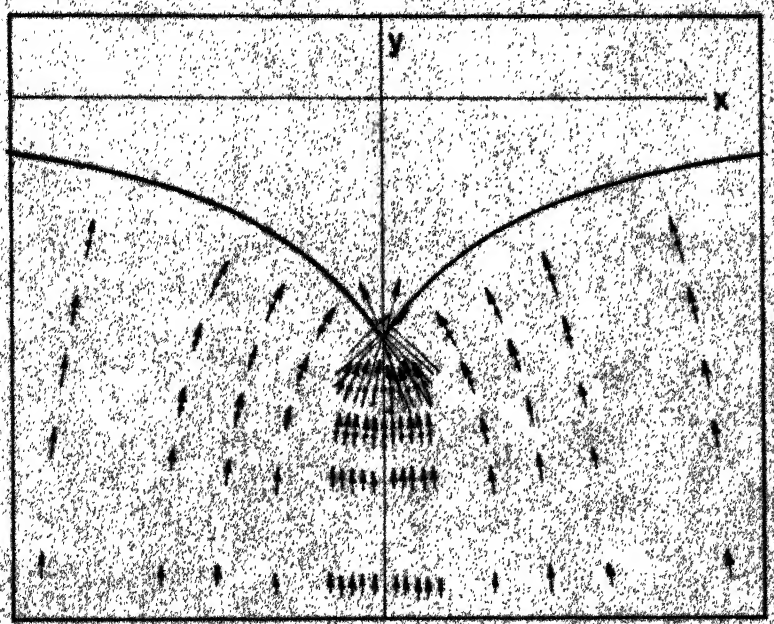

Fig.3.10 Edge Dislocation Force (100)

welded to form a single body which subsequently gets deformed and fractured. Thus the two body junction has essentially reduced to a single body with notches at C_1 and C_2 as shown in Figure 2.4. Under these conditions Warren's results on notches may be considered in evaluating the failure behaviour of such junctions.

Let t_j be the life of a typical asperity junction. Ideally, at the high value of stresses, involved in the deformation state, the dislocation velocity approaches shear wave velocity. In practice, however, the actual velocity attained would be a fraction of this velocity. Since the notch has been shown to be acting as a focal point towards which the dislocations get attracted, the high velocity of the dislocations will enhance such accumulation. Assuming typical values as,

a (junction width) $\simeq 15 \times 10^{-4}$ cm

V_s (sliding velocity) $\simeq 50$ m/min

and V_o (average dislocation velocity) $\simeq 10^2$ m/sec

the life of a typical junction results to be $\simeq 18 \times 10^{-6}$ sec. If the dislocations are expected to agglomerate at the notch from a distance $\simeq$ 'a' the time required for the dislocations to travel a distance of 'a' $\simeq 10 \times 10^{-8}$ sec. This time is much less than the junction life. These calculations show

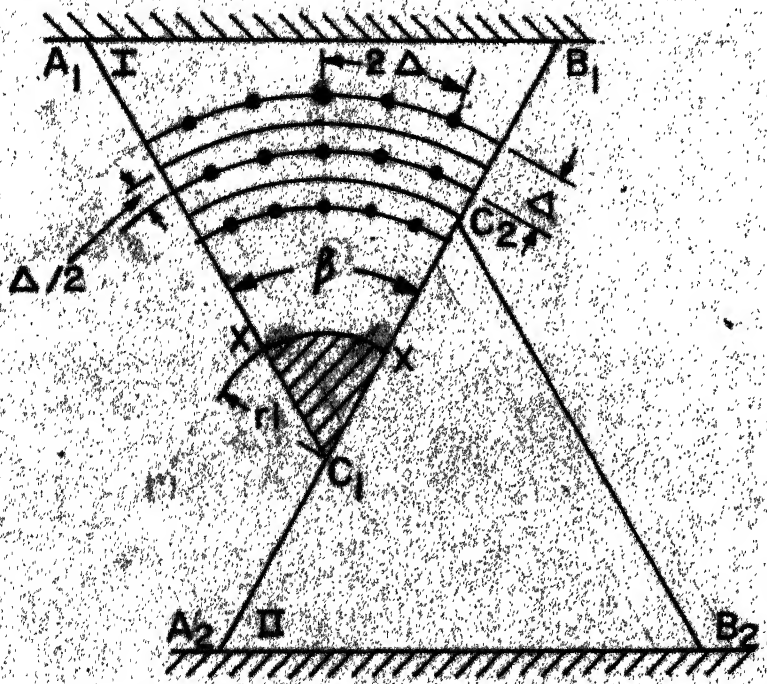

3.11 Idealised Junction Between Two Grain Size Asperities

(i) Initially the dislocations are uniformly distributed in the asperity.

(ii) Dislocation density in the bulk is uniform at all stages.

(iii) Velocity of dislocations is constant at all stages.

(iv) The forces between dislocations are neglected.

(v) Temperature effects on velocity dislocations are also neglected.

Referring to the Figure 3.11 let the number of dislocations in the circle with a radius r be n_r. If the apex angle of the asperity is β, the distance between two neighbouring dislocations on the same circle is $\Delta \simeq \beta r / n_r$. If dislocations are assumed to lie on radial arcs as shown in the figure, the distances between two consecutive circles is also Δ. Considering the asperities to be of unit thickness the volume δv associated with an element of radius δr can be calculated as :

$$\text{If,} \quad \delta r = (r + \frac{\Delta}{2}) - (r - \frac{\Delta}{2}) , \qquad (3.21)$$

$$\text{then,} \quad \delta v = \left\{(r + \frac{\beta r}{2 n_r})^2 - (r - \frac{\beta r}{2 n_r})^2\right\} \frac{\beta}{2}$$

$$= \frac{\beta^2 r^2}{n_r} \qquad (3.22)$$

Since, the number of dislocations in this volume $\delta v = n_r$ and density of dislocations is ρ_o given by the equation

$$\rho_o = \frac{n_r}{(\beta^2 r^2 / n_r)} = \frac{n_r^2}{\beta^2 r^2}, \qquad (3.23)$$

n_r is obtained as,

$$n_r = \beta r \sqrt{\rho_o} \qquad (3.24)$$

and $$\Delta = \frac{\beta r}{\beta r \sqrt{\rho_o}} = \frac{1}{\sqrt{\rho_o}} \qquad (3.25)$$

Now an infinitesimal area $C_1 x \; x$ bounded by radius ri and arc βri, at the apex of the asperity I may be considered. At the instant t_o the number of dislocations in this small volume is simply given by

$$N_{ri}(0) = \left(\frac{\beta ri^2}{2}\right) \rho_o \qquad (3.25a)$$

Now, since at time t_o the deformation of the asperity junctions has commenced, dislocations will start agglomerating near the notch as discussed in the previous section.

After time t total number of dislocations in area $C_1 x \; x$ is assumed to be equal to the initial dislocation quantity plus all those dislocations which can reach the apex C_1 during time t. If V_o is the dislocation velocity then the dislocations lying on the circular arcs of radii within $r_i + V_o t$ can reach the apex C_1 in time t.

Then the number of dislocations within the zone $C_1 \times x$ after time t will be given by

$$N_{ri}(t) = \frac{\beta\, ri^2}{2} \rho_o + \beta\sqrt{\rho_o}\,(ri + \Delta) + \beta\sqrt{\rho_o}\,(ri + 2\Delta) + \ldots + \beta\sqrt{\rho_o}\,(ri + V_o\, t) \tag{3.26}$$

$$= \frac{\beta\, ri^2}{2} \rho_o + \beta\sqrt{\rho_o}\left\{(ri + \Delta) + (ri + 2\Delta) + \ldots + (ri + V_o\, t)\right\} \tag{3.27}$$

The sum of the series within the brackets is calculated to be

$$= \frac{V_o\, t\sqrt{\rho_o}}{2}\left(2\, ri + \frac{1}{\sqrt{\rho_o}} + V_o\, t\right) \tag{3.28}$$

So, $$N_{ri}(t) = \frac{\rho_o \beta\, ri^2}{2} + \left(\frac{\beta \rho_o}{2}\right)\left\{V_o\, t\,(2\, ri + V_o\, t + \frac{1}{\sqrt{\rho_o}})\right\} \tag{3.29}$$

Thus, the density of dislocations after time t in the area $C_1 \times x$ of the asperity junction, is

$$\overset{\circ}{\rho}_{ri}(t) = \frac{N_{ri}(t)}{\beta\, ri^2/2} = \rho_o\left\{1 + \frac{V_o\, t}{ri^2} \times (2\, ri + V_o\, t + \frac{1}{\sqrt{\rho_o}})\right\} \tag{3.30}$$

Equation 3.30 shows that the density of dislocations at the notch of the asperity junction increases continuously with time. Also, for the same period of

of time t, dislocation density will be higher if the dislocation velocity is higher. When the density of dislocations ρ_{ri}^{o} (t) at the notch is plotted as a function of time for a constant dislocation velocity V_o, a curve of the form 0 - 3 as shown in Figure 4.14a is obtained. The curve clearly shows the fast increasing trend in ρ_{ri}^{o} (t) as time increases. However, it can be argued that such increasing trend cannot persist indefinitely and the dislocation density will attain an upper limit of ρ_{lim} after some time. Also, the curve for ρ_{ri}^{o} (t) will in general start from an initial value ρ_o which will not be equal to zero. The following observations will help to have an idea of ρ_o and ρ_{lim}.

(i) All crystals even in the annealed state have dislocations in them. The dislocation densities in ordinarily heat treated crystals is $\simeq 10^6 - 10^8$. Therefore the curve 0 - 3 for ρ_{ri}(t) should start from a finite value of $\rho_o \simeq 10^6 - 10^8$ cm^{-2}, at t = 0.

(ii) Even in the heavily deformed materials the dislocation density of only $10^{11} - 10^{12}$ have been reported. Values higher than these do not seem to occur. Therefore, this value may be considered to be the upper

limit for dislocation density in a deforming body. Based on these two observations the curve 0 - 3, for $\rho_{ri}^{o}(t)$ in Figure 4.14a is shown as starting from an initial value of ρ_o and reaching the upper limit ρ_{lim} in a certain period of time which is designated as t_j^o. From the nature of the Equation 3.30 it is clear that if the dislocation velocity is increased somehow, the density of dislocations at the notch will increase at a greater rate than given by curve 0 - 3. In such a case the dislocation accumulation at the notch as a function of time would be shown by the curve 0 - 1 instead of 0 - 3 of Figure 4.14a. It will be seen in the next chapter that the application of an external magnetic field to an asperity junction can cause such an increase in the accumulation of dislocations at the notch. Further, if the dislocation accumulation at the notch becomes preferential, the fracture characteristics at the notch can be different. This would affect the wear characteristics of the sliding pair. These aspects will be further discussed in the following chapter.

CHAPTER IV

EFFECT OF MAGNETIC FIELD ON WEAR

4.1 Ferromagnetism and Magnetic Domains

4.1.1 Origin of Ferromagnetism

Materials which get magnetised when placed in a magnetic field are called ferromagnetic materials and this property ofsuch substances is known as ferromagnetism. The most common ferromagnetic materials are iron, cobalt and nickel. There are two possible atomic origins to ferromagnetism, the orbital motion of electrons and the spin motion of electrons. Atoms which exhibit magnetism are generally called magnetic atoms. Due to the orbital and the spin motion of electrons a magnetic atom has magnetic moment M_e and angular momentum P_e associated with it. The smallest magnetic moment is called the Bohr Magneton. The ratio M_e/P_e is referred to as the gyromagnetic ratio 'g'. On the basis of experiments conducted to measure 'g' it is established now, that the magnetic moment of the important magnetic atoms like Fe, Co and Ni are caused mainly by spin motion of electrons and orbital motion is said to be quenched in these materials (101). In the case of the ferromagnetic state the spins of various atoms are aligned parallel to one another as a result of strong

interaction acting between the spins of the neighbouring atoms.

How the spin magnetic moments are aligned to produce net ferromagnetism is briefly examined in the following paragraphs.

Let a collection of n_1 magnetic atoms each with a magnetic moment M_B be considered. Further, these atoms are assumed to be aligned due to their individual magnetic moments alone, and do not interact. If a magnetic field H_s is applied to such an ensemble, a couple acts on each magnetic moment which is opposed by the thermal agitation of the atom. A simple calculation can give an idea of the order of magnitude of H_s needed to counteract the thermal agitation.

Let $\theta \simeq 300\ ^{o}K$ and $n_1 = 1$.

The value of M_B (Bohr Magneton) $= 1.16 \times 10^{-29}$ Weber - meter.

Maximum value of the couple due to magnetic field is,

$$U_h \simeq M_B H_s \qquad (4.1)$$

$$= 1.17 \times 10^{-29} H_s, \text{ Joules.} \quad (H_s \text{ is in ampere/meter})$$

Energy of the thermal motion of an atom is

$$K\theta \simeq 1.38 \times 10^{-23} \times 300 \simeq 4.1 \times 10^{-21} \text{ Joules.}$$

Thus even with a very strong field $H_s \simeq 10^6$ ampere/meter (the highest available in the laboratories), it is seen

that

$$K\,\theta \gg U_h \qquad (4.2)$$

This shows that even at room temperature thermal agitation is sufficient to make the angular distribution of atomic moments almost random. The magnetic field necessary to counteract the thermal agitation is

$$H_s \simeq \frac{K\,\theta}{M_B} \simeq 10^8 \ \frac{\text{ampere}}{\text{meter}} \ (\simeq 10^6 \text{ Oersteds}) \qquad (4.3)$$

Better calculations show this value to be $\simeq 10^9$ ampere/meter ($\simeq 10^7$ Oe). Figure (4.1) shows for iron, that with no mutual action between atoms how enormous fields, are required to saturate a magnetic material at room temperature. Therefore, it is very hard to magnetise an assembly of free atomic moments to any considerable extent at room temperature. In practice, on the other hand, the external magnetic fields needed to magnetise a ferromagnetic substance are

$H_s \simeq 1 \ \frac{\text{ampere}}{\text{meter}}$ for super alloy, a soft magnetic material,

and, $H_s \simeq 5 \times 10^4 \ \frac{\text{ampere}}{\text{meter}}$ for Alnico, a typical permanent magnetic materials (101).

Most of the ferromagnetic materials can be saturated by magnetic fields whose intensities lie between these two values.

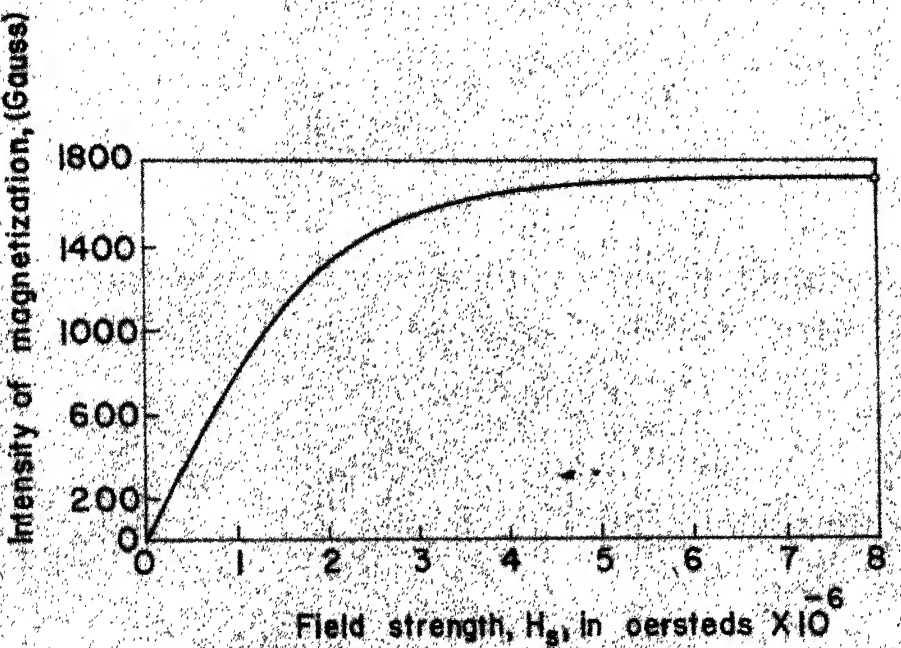

Fig. 4-1 With No Mutual Action Between Atoms, Enormous Fields Are Necessary To Saturate a Magnetic Material; (110)

Weiss (102) was the first to recognize and solve this paradox in the classical manner. He postulated the existence of a strong inherent interaction between the magnetic moments. The interaction is such as to counteract the thermal agitation and resulting in perfect alignment of the atomic spins at room temperature, inspite of the thermal agitation. Thus, a crystal is expected to have this inherent magnetisation called the spontaneous magnetisation. The effect of the external magnetic field is merely to change the direction of this spontaneous field towards the applied field. Weiss called this inherent field as the molecular field acting on each atomic moment and calculated its value for iron to be $\simeq 10^9$ ampere/meter ($\simeq 10^7$ Oersteds).

It was shown by Heisenberg (103) that the molecular field postulated by Weiss can be explained in terms of quantum mechanical forces of exchange acting between electrons in neighbouring atoms. If two magnetic atoms are lying apart, each atom has an associated magnetic moment of one Bohr Magneton. In addition to the usual electrostatic and much weaker magnetic forces between them, a potential energy $\simeq E_{ij}$ between the two spins $\bar{s}_i$ and $\bar{s}_j$ exists which is given by,

$$E_{ij} = - 2 J_{ex} \bar{s}_i \cdot \bar{s}_j \qquad (4.4)$$

where J_{ex} is the exchange integral. If J_{ex} is positive

this energy is minimum when $\bar{s}_i$ is parallel to $\bar{s}_j$. If J_{ex} is negative, the antiparallel state of $\bar{s}_i$ and $\bar{s}_j$ is the stable one. Thus positive value of J_{ex} results in ferromagnetism, whereas negative value of J_{ex} results in anti ferromagnetism. Thus J_{ex} is a measure of the inherent magnetic interaction.

It is not possible to understand the nature of exchange force from classical analysis (101). It is however, recognized now that the 'itinerant' or the 'collective electron model' in which electrons are thought of as wandering through the crystal lattice is the appropriate basis for explaining ferromagnetism in materials like Fe, Co and Ni.

4.1.2 Concept of Magnetic Domains

The internal molecular field of the order of 10^7 Oe postulated by Weiss would lead directly to the prediction that all ferromagnetic crystals below their curie temperatures would exhibit spontaneous magnetisation even in zero fields. But, in actual practice such crystals are observed in a zero state of overall magnetisation. To overcome this difficulty Weiss postulated the existence of 'domains' or 'small regions' which are small volumes of material containing $\simeq 10^{17} - 10^{21}$ atoms. These domains are magnetised spontaneously due to the presence of molecular field,

but their resultant magnetisations are randomly oriented. Due to this, overall magnetisation of the crystal along any direction is zero. The effect of an externally applied field is then, not to induce any magnetisation at atomic level but to align the magnetisation vectors of the domains. This happens either by change of the domain shape or by actual rotation of the magnetisation vector. Experimental works of Barkhausen (104), Sixtus and Tonks (105), Bitter (106) and many others have fully established the physical existence of such domains in all ferromagnetic materials. Landau and Lifshitz (107) showed theoretically that it is necessary for a crystal to break up into domains to reduce its magnetostatic energy. Formation of domains reduces the magnetostatic energy considerably. Thus, a crystal goes on subdividing itself into more and more domains until the energy needed to form an additional boundary separating the domains is greater than the consequent reduction in magnetostatic energy. Bloch (108) showed theoretically that the boundary between neighbouring domains is not sharp on atomic scale but is spread over a finite thickness. Within this boundary the direction of spins changes gradually from one direction to the other. This transition layer is usually referred to as domain wall or Bloch wall. It has also been verified experimentally by several workers (109) that the domain wall has actually a finite width. Figure 4.2 shows the variation of spins

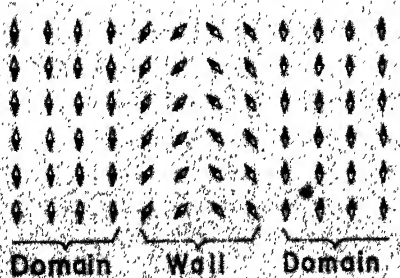

Fig. 4.2

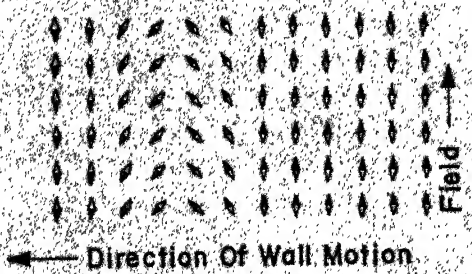

Fig.4.3 Schematic Explanation Of Domain Wall Displacement.

across a domain wall. When a magnetic field is applied to a ferromagnetic material, the domain structure changes in such a way as to increase the resultant magnetisation parallel to the external field. On the application of the field parallel to one of the domains, the spins inside the neighbouring domains experience no torque resulting from the field, because their directions are either parallel or antiparallel to the field. However, since the spins inside the wall make some angle with the field directions, they, under the action of a torque start to rotate towards the direction of the applied field. As a result of this rotation of spins inside the domain wall, the centre of the wall is displaced as shown in Figure 4.3. This results in an increase in the volume of those domains which have their magnetisation parallel to the external field. This process is called domain wall displacement. As the field is increased the domain magnetisations rotate towards the field direction, and ultimately the crystal is saturated. The domain wall shown in Figure 4.2, is referred to as 180° wall as the change in the direction of magnetisation from one domain to the next is through 180°. When the rotation is through 90° the wall is called as 90° wall. Very complex domain patterns are observed in practice depending upon the crystal structure, the impurities of the material and the history of the specimen.

4.2 Interaction of Dislocations and Domain Walls

4.2.1 Magnetostriction

The internal magnetisation in a ferromagnetic crystal causes it to deform along the direction of the magnetisation. This is mainly due to the interaction of the magnetic dipoles (101). The deformation is maximum in the direction of the spontaneous magnetic field and the magnitude of this strain is generally $\simeq 10^{-5} - 10^{-6}$. When a demagnetised crystal is considered the overall change in size due to thespontaneous magnetisation in any direction may be taken to be zero since the spontaneous field is distributed uniformly in all directions in the crystal. But, when an external magnetic field is applied all domain magnetisations tend to lie in one direction and a net change in dimension is observed. This phenomenon is called magnetostriction. When all the domain magnetisations lie in one direction the overall magnetostriction of the crystal has the maximum value. This can be achieved when a saturating magnetic field is applied to the specimen. Figure 4.4 shows the relation between the magnitude of the magnetostriction and the magnetic field intensity.

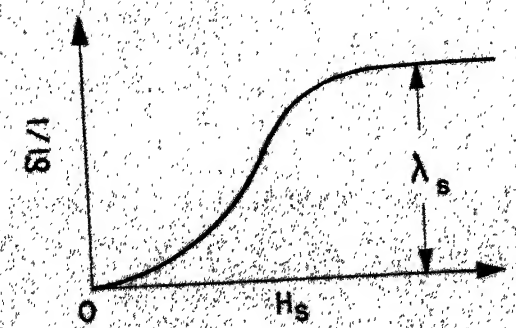

Fig 4.4 Magnetostriction As a Function Of The Field Intensity.

Thus when a saturating magnetic field is applied to a ferromagnetic specimen the change in its dimensions along the direction of the field is $\lambda^* = \delta l/l \simeq 10^{-5} - 10^{-6}$. λ^* is usually called the magnetostriction coefficient. It is also sometimes called the longitudinal magnetostriction coefficient. Experiments have shown that magnetisation also results in magnetostriction at right angles to the field direction. This is called the transverse magnetostriction and is denoted by λ_t. It is negative and its magnitude is half of that of the longitudinal magnetostriction. Thus, $\lambda_t = - \lambda^*/2$; (110). The magnitude of the magnetostriction coefficient also depends upon crystallographic direction considered. This is because of the anisotropic properties of the crystals. Therefore in crystalline materials generally magnetostriction is considered to have an overall average value $\simeq \lambda_s$. In the present work also only such an average value is considered.

4.2.2 Nature of the interaction of dislocations and domain walls.

Many of the properties of ferromagnetic crystals depend upon the structural defects present in the crystals. This is because the lattice defects are associated with stress fields. Dislocation is the most important lattice defect which governs the

behaviour of all materials including ferromagnetic materials. In a ferromagnetic crystal the stress fields of dislocations interact with the magnetostrictive stresses in the crystal. Such an interaction is referred to as the magnetostrictive coupling (111).

It was pointed out in section 3.1 that sources of internal stress exist in materials which hinder the easy movement of dislocations. Dislocations which do not lie on their slip planes also act as source of hinderance to the easy movement of other dislocations (58). In ferromagnetic materials dislocations act as a source of hinderance for the displacement of the domain walls. Dislocations also affect the arrangement of domain walls during and after magnetisation. On the other hand, domain walls also influence the movement of dislocations. The interaction is therefore, mutual in nature. It has been reported (112) that dislocations are pinned by the domain walls. Also, special domain formations around dislocations have been reported (113). On the basis of such experimental observations and also theoretical reasoning (111), the interaction of dislocations and domain walls is considered as a source of internal stress in the body. Such a source of internal stress will not allow free movement of dislocations across a crystal. Consequently, if this

source of internal stress is eliminated, dislocations would travel more freely through a ferromagnetic crystal. Chebotkevich et. al. (114) in their experiments on Fe - 3% Si have observed that the displacement of the domain wall causes a shift in the position of the dislocation. This is considered to be possibly due to the reason that the displacement of the wall relieves some stress on the dislocation causing it to shift its position. Recently, Hayashi (115) has also observed similar movements of dislocations in Ni - Co alloy.

A dislocation is also accompanied by a magnetic moment.. But its interaction with domain walls has been calculated to be too small to affect its motion in a ferromagnetic crystal (114). It is thus recognized that the primary interaction between a dislocation and a domain wall is magnetostrictive in nature. Therefore it is useful to study this in some detail. To start with, the interaction of a screw dislocation with a domain wall is examined, briefly.

Figure 4.5a shows a 180° domain wall in YZ plane with magnetisation H at an angle $\emptyset$ with the Z axis. A screw dislocation lies along the direction OZ subtending an angle $(90^{\circ} - \varphi)$ at a strip $Z_1 Z_2$ of the domain wall.

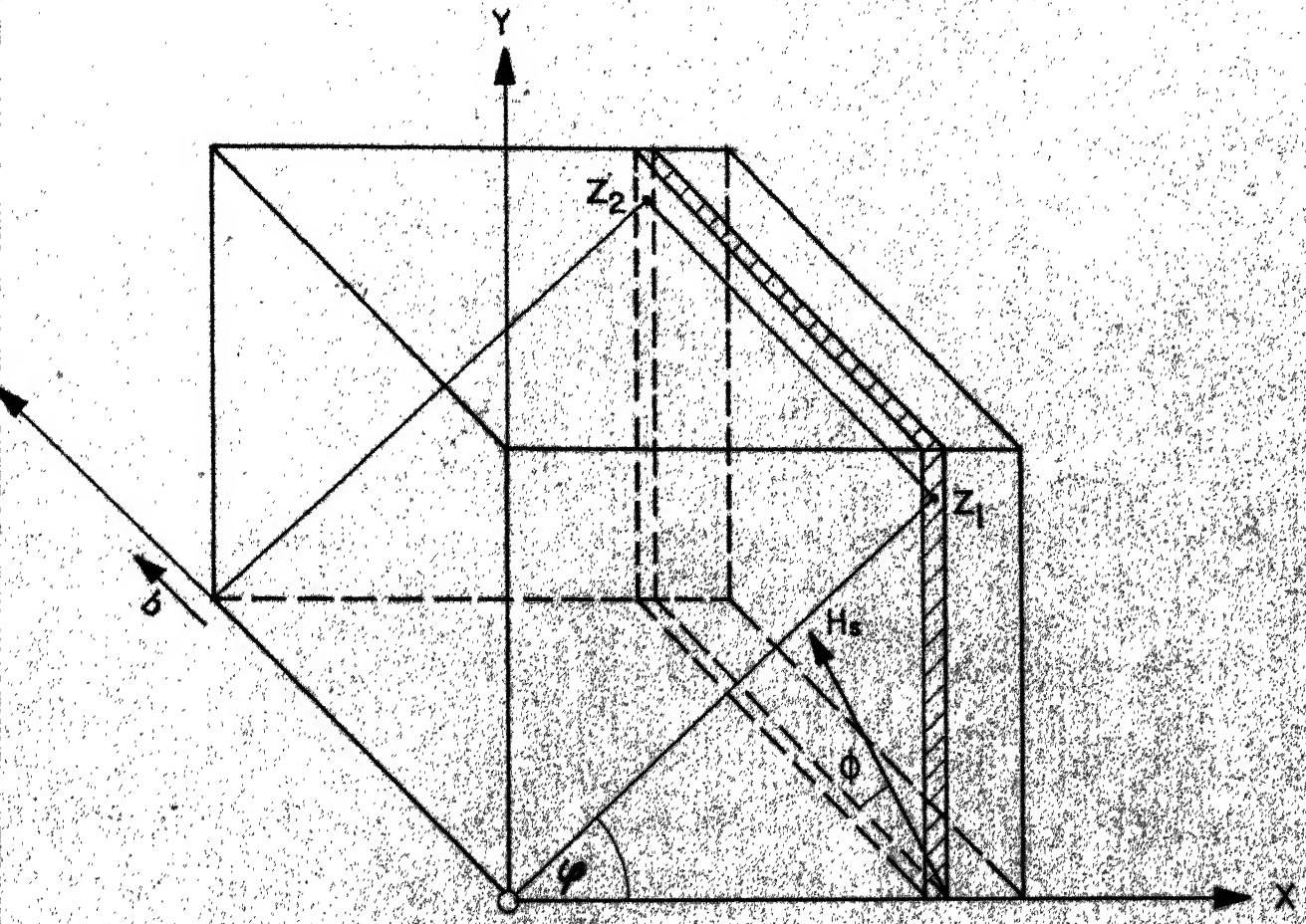

Fig. 4.5 a

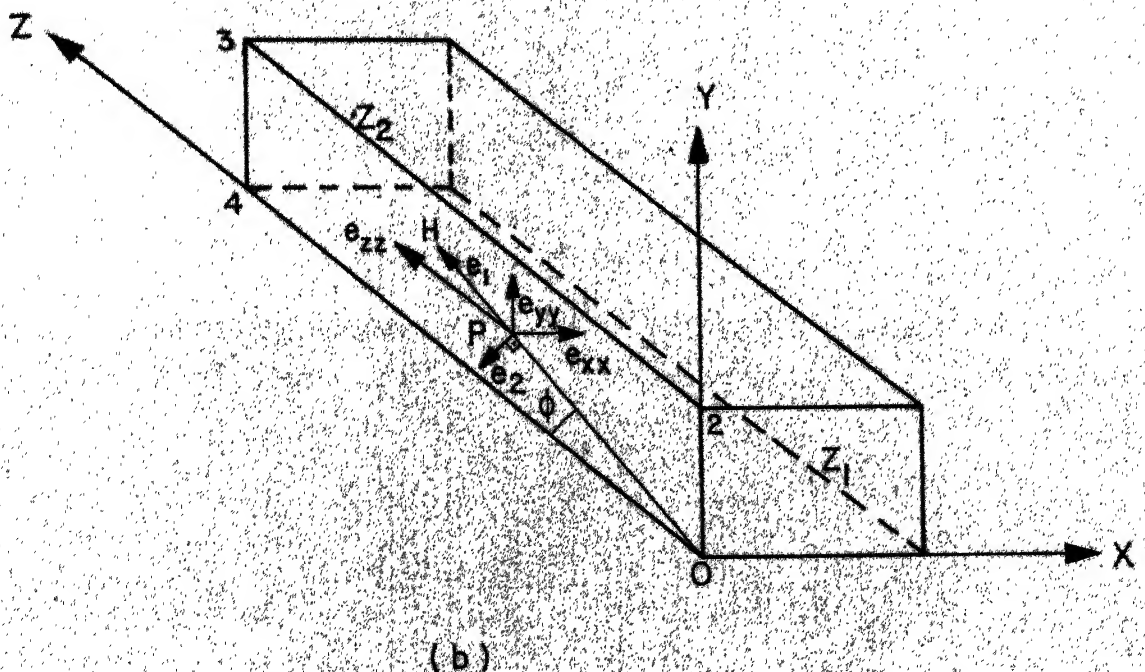

(b)

Fig.4.5 Interaction Of a Screw Dislocation With a 180° Domain Wall.

It was mentioned in section 3.1 that the stress field of screw dislocation is one of pure shear. With reference to Figure 4.5a these stresses in cartesian coordinates are written as

$$\sigma_{xz} = \sigma_{zx} = -\frac{G^* b}{2\pi}\left(\frac{y}{x^2 + y^2}\right) \qquad (4.5a)$$

$$\sigma_{yz} = \sigma_{zy} = \frac{G^* b}{2\pi}\left(\frac{x}{x^2 + y^2}\right) \qquad (4.5b)$$

Substituting $\varphi = \tan^{-1}(y/x)$ these stresses can also be written as,

$$\sigma_{xz} = \sigma_{zx} = -\frac{G^* b}{2\pi}\left(\frac{\sin\varphi \cos\varphi}{x}\right) \qquad (4.5c)$$

and

$$\sigma_{yz} = \sigma_{zy} = \frac{G^* b}{2\pi}\left(\frac{\cos^2\varphi}{x}\right) \qquad (4.5d)$$

The shearing strains caused by these stresses are as follows :

$$e_{xz} = \frac{\sigma_{xz}}{2G^*} = -\frac{b \sin\varphi \cos\varphi}{4\pi x} \qquad (4.6a)$$

and

$$e_{yz} = \frac{\sigma_{yz}}{2G^*} = \left(\frac{2\cos^2\varphi}{4\pi x}\right) \qquad (4.6b)$$

The strip z_1 z_2 of the domain wall may now be examined in isolation. The magnetisation will cause a strain λ_s in the direction of H_s and a contraction of $\frac{\lambda_s}{2}$ in the directions perpendicular to H_s. Thus at a point P on the face 0-2-3-4 of this strip z_1 z_2,

strains $e_1 = \lambda_s$ and $e_2 = -\lambda_s/2$ will be set up along the direction of H and normal to it respectively. Also, strain $e_{xx} = -\frac{\lambda_s}{2}$ will occur normal to yz plane. Transforming the strains e_1, e_2 and e_{xx} into the x, y, z set of coordinates, it is seen that at point P,

$$e_{xx} = -\frac{\lambda_s}{2}, \qquad (4.7a)$$

$$e_{yy} = \lambda_s \sin^2 \phi - \frac{\lambda_s}{2} \cos^2 \phi, \qquad (4.7b)$$

$$e_{zz} = \lambda_s \cos^2 \phi - \frac{\lambda_s}{2} \sin^2 \phi, \qquad (4.7c)$$

and $$e_{yz} = \frac{3}{2} \lambda_s \sin \phi \cos \phi . \qquad (4.7d)$$

Similar strains are also developed at every section of the domain wall which has a finite thickness. Since there are constraints from the surrounding material these strains cannot actually occur. The strains therefore, develop equivalent stresses. Since the direction of magnetisation changes from one section of the domain wall to the other, the magnitude of these magnetostrictive stresses also changes within the wall. The exact calculations of these stresses is quite complicated one and Reider (111) seems to be the only one to have worked out these stresses in detail, for some important types of walls.

Since the objective here is to obtain only order of magnitude of these stresses it is not

considered necessary to pursue the exact analysis.

Therefore, it is adequate for the present work to recognize that due to the magnetostrictive property of the material a state of stress is developed within the domain wall. The stress components at point P will interact with the strain components of the dislocation given by equations 4.7. Thus, a dislocation moving in the neighbourhood of the domain wall would experience a stress field due to the domain wall. This stress field would hinder the free movement of the dislocation across the wall. The component of the magnetostrictive stresses which can exert a force on the screw dislocation shown in Figure 4.5a is σ_{yz}. From Equation 4.7d the magnitude of

$$\sigma_{yz} = \left(\frac{\gamma_{yz}}{2} \right) G^*$$

$$= e_{yz} G^*$$

$$= \frac{3}{2} \lambda_s G^* \sin 2\phi \qquad (4.8)$$

Therefore, the dislocation in the neighbourhood of a domain wall will experience a magnetostrictive shear stress of $\lambda_s G^* \left(\frac{3}{2} \sin 2\phi \right)$. The maximum value of this stress is $\frac{3}{2} \lambda_s G^*$ when $\phi = 45^\circ$. In this situation the dislocation is lying at 45° to the direction of magnetisation H. Reider (111) has made exact estimation of the stresses within a domain wall in important cases of Fe, Co and Ni. In general, all these

stress components have been shown to be of the form

$$\sigma_w \simeq \lambda_s G^* f(\sin \phi) \qquad (4.9)$$

where, ϕ is the angle between the direction of magnetisation and a coordinate axis. The value of $\lambda_s G^*$ for materials like Fe and Ni $\simeq$ 0.5 - 0.6 kg/mm^2 (116). Thus, the maximum contribution of the domain wall to the internal stress may be taken to be $\simeq$ 0.5 - 0.6 kg/mm^2.

A domain wall also exerts a repulsive force on an edge dislocation lying in suitable orientations. Trauble (111) utilized the exact magnetostrictive stress components evaluated by Reider for a 180° wall in iron. He calculated the force on a dislocation lying parallel to a (110) domain wall as shown in Figure 4.6. The magnitude of the stress exerted by such a domain wall on the dislocation is shown in Figure 4.7. It is seen from the figure that the maximum value of the stress acting on a dislocation due to domain wall is $\simeq$ 0.6 kg/mm^2 and it corresponds to the magnitude of product of λ_s and G^*.

On the basis of these investigations a domain wall is generally referred to as an extra source of stress resisting the easy movement of a dislocation across it. Thus, in addition to other sources

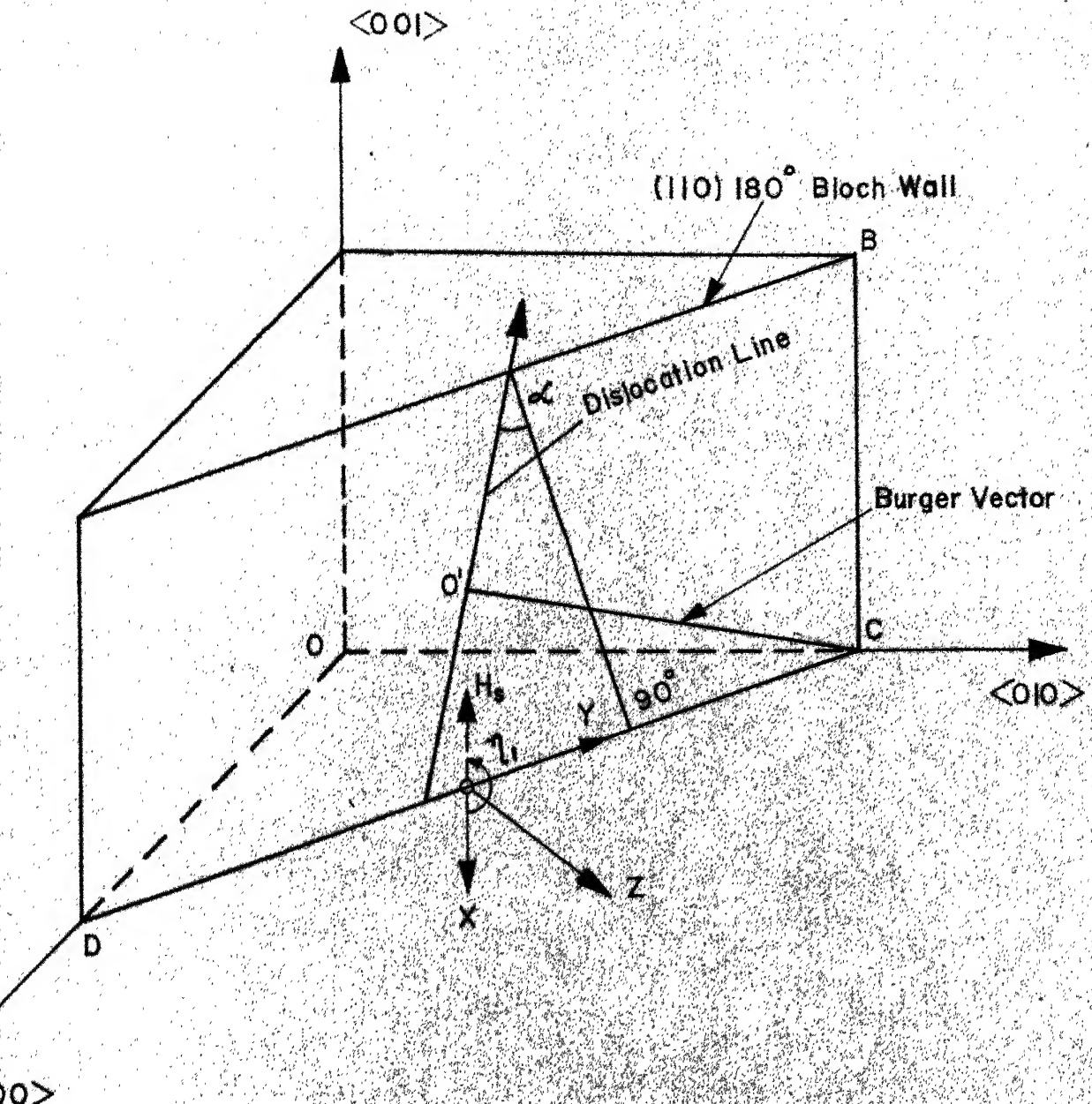

Fig.4.6 Figure Referring To Interaction Between a (110) 180° Bloch Wall And a <111> Dislocation Line. (111)

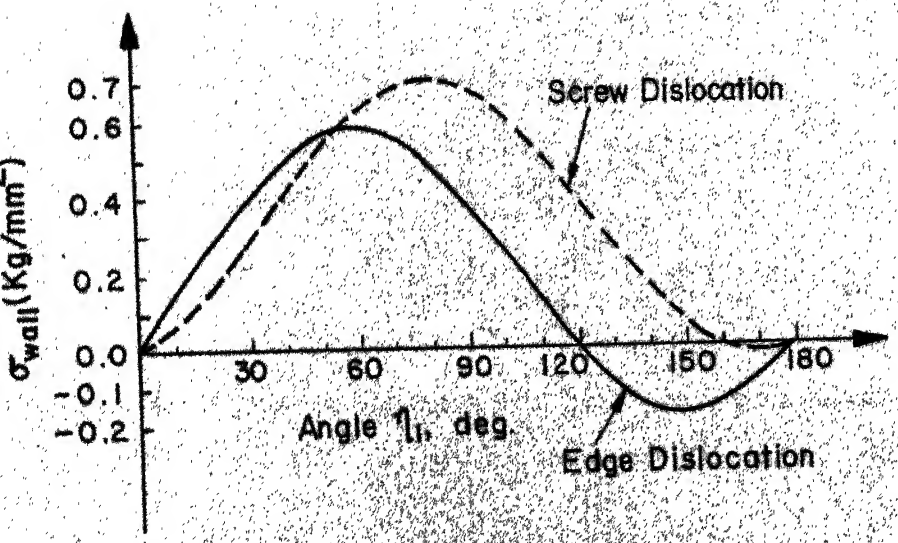

Fig.4.7 Stress At Room Temperature As a Function Of The Displacement Of a (100) 180 Bloch Wall In Iron Going Through Respectively An Edge Or Screw Dislocation, Both Parallel To <110>(111)

of internal stress domain walls are also a source of internal stress in a ferromagnetic body. It seems logical therefore, that if the domain walls of a ferromagnetic body are eliminated this source of the internal stress would be eliminated. Consequently, the dislocation mobility in the ferromagnetic body would increase. It was discussed in section 4.1 that the elimination of domain walls is achieved when a strong constant magnetic field is applied to a ferromagnetic material. In other words, the application of an external magnetic field of sufficient strength to a ferromagnetic body should reduce the internal stress in the body by a magnitude $\simeq G^* \lambda_s$ ($\simeq 0.5$ kg/mm^2).

To verify whether an external magnetic field does in fact reduce the internal stresses in a body, the author proposed to conduct a suitable test for the purpose. Several tests are suggested in the literature (117) which give an idea of the internal stress in a body. The method of stress-relaxation is however, frequently used. In the present work also a stress-relaxation test was conducted. Details of this test will be given in the next chapter.

It was found from these tests that the application of a steady magnetic field ($H_s \simeq 200$ O_e) results

in a decrease in the internal stress as well as in the yield stress. The fall in the yield stress and the internal stress is found to be $\simeq$ 0.9 kg/mm^2 and $\simeq$ 0.6 kg/mm^2, respectively. This reduction in stress confirms that the elimination of domain walls does indeed reduce the internal stress on the average by a magnitude equivalent to the magnetostrictive stress $G^* \lambda_s$. Hayashi (118) has also conducted stress relaxation test on nickel. He has found that the application of an alternating magnetic field to a nickel single crystal also reduces the internal stress in the crystals.

It can be easily seen that a fall in internal stress should also be observed as a decrease in yield stress of a material. The yield stress of a crystalline material is given by equation (119),

$$\sigma_y = \sigma_i + K_y D_g^{-1/2} \qquad (4.10)$$

where

σ_y = yield stress,

σ_i = frictional stress resisting the motion of dislocations,

K_y = measure of extent to which dislocations are piled up at barriers,

D_g = grain diameter.

It is apparent from the Equation 4.10 that any fall in yield stress due to the magnetisation should be primarily a consequence of the fall in the internal stresses in the body which obstruct the free movement of dislocations. This also explains therefore, the fall in the yield stress observed by the author in the present work. Author proposes to substantiate this with the following observation.

When a Frank-Read loop glides through a Frank network, it has to cut across the 'forest' of 'trees' set up by those dislocations which pierce the slip plane of the loop.

The interaction between Frank - Read loop and 'trees' is of short-range order. In B.C.C. and F.C.C. crystals the 'trees' have strong elastic interaction with a moving loop. Just as two dislocations can attract or repel each other, a 'tree' can attract or repel a moving loop depending upon their mutual orientations. If the two attract it results in an 'attractive junction' and if they repel it results in a 'repulsive junction'. Carrington et al (84) have shown how in B.C.C. iron two $\frac{a}{2} \langle 111 \rangle$ dislocations join to make one $\frac{a}{2} \langle 100 \rangle$ type of dislocation, resulting in an attractive junction as shown in Figure 4.8. In this figure the lines x - x' and y - y' designate two

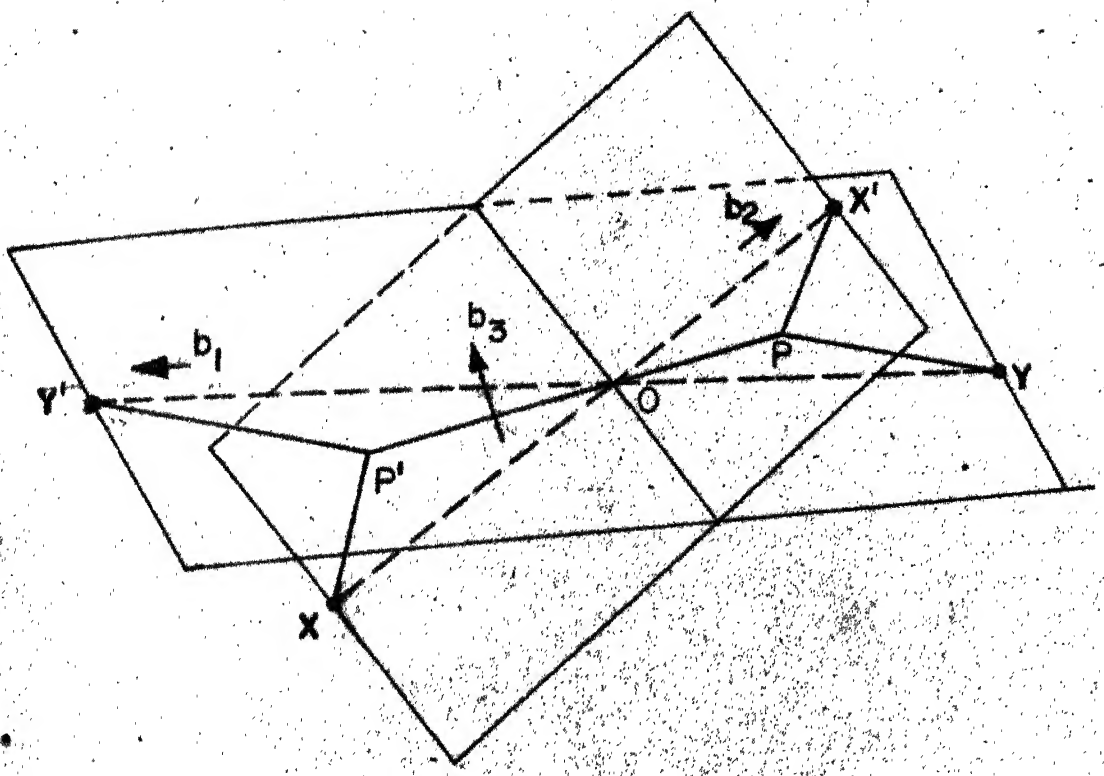

Fig. 4.8 Formation Of An Attractive Junction. XX', YY' Denote The Dislocations Before Intersections XP'Y' – P'P – X'P'Y' Shows The Configuration After Attractive Interaction.

$\frac{a}{2} \langle 111 \rangle$ dislocations before interaction, separated by a certain distance. When they approach each other under attractive force they react to form a third $\frac{a}{2} \langle 100 \rangle$ dislocation P P'. These intersections act as sources of resistance for a dislocation loop because a net force is needed to break up such an intersection. Saada (120), Carrington et. al. (84) have shown that the stress σ_j needed to break such a junction is,

$$\sigma_j \simeq \frac{0.3\, G^* b}{l} \qquad (4.11)$$

where, G is the shear modulus,

b is the Burgers vector,

and l is the network size.

This expression gives large enough stresses to make it probable that attractive junctions contribute substantially to flow stress. Also Carrington et. al. have studied the arrangement of dislocations experimentally, in iron in various conditions like annealed, cold worked, recovered and after creep. In all these cases they have confirmed the existence of attractive junctions formed by inter section of two $\frac{a}{2} \langle 111 \rangle$ dislocations to make one $\frac{a}{2} \langle 100 \rangle$ dislocation. In this manner it is possible that a definite contribution to the flow stress in ferromagnetic materials

can come from the interaction between attractive junction and the domain wall. Consequently, when the domain wall is eliminated the extra stress of interaction is eliminated and the 'attractive junctions' would be overcome at a relatively smaller stress. This should be seen in the lowering of yield stress as observed by the author.

The following calculations will show that the internal stress due to domain wall,

$$\sigma_w = G^* \lambda_s \qquad (4.12)$$

is a significant fraction of σ_j, the stress needed to break an attractive junction. The values, for b, l, and λ_s are assumed as follows :

$$b \simeq 2.8 \times 10^{-8} \text{ cm},$$

$$l \simeq 0.2 \times 10^{-3} - 2.0 \times 10^{-3} \text{ cm}$$

$$\lambda_s \simeq 0.1 \times 10^{-5} - 1.0 \times 10^{-5}.$$

Substitution of these values in Equations 4.11 and 4.12 yields the values for σ_w and σ_j as

$$\sigma_j \simeq 0.04 \times 10^{-4} G^* - 0.4 \times 10^{-4} G^* \qquad (4.13)$$

and $$\sigma_w \simeq 0.01 \times 10^{-4} G^* - 0.1 \times 10^{-4} G^* \qquad (4.14)$$

respectively.

Thus, it is seen that the resistance to dislocation motion due to the presence of domain walls is

expected to be upto about 25% of the resistance due to the presence of attractive junctions. Thus if the domain walls are absent this source of internal stress may be eliminated and the yield stress should show a decrease.

On the basis of these evidences it is concluded that the major effect of the application of an external magnetic field to a deforming body is to reduce the internal stress in the body by an amount of $\simeq$ 0.5 kg/mm^2. This is indeed a very small quantity compared to the yield strength of materials. Nevertheless, it plays a significant role in phenomenae which are sensitively dependent upon the changes in the internal stress. Several workers (91, 121 - 123) have emphasized the significance of internal stress in plastic deformation particularly creep. It will be shown in the following sections how this small reduction in the internal stress caused by the application of an external magnetic field plays a significant role in changing the wear characteristics of sliding bodies.

4.3 Enhancement of Dislocation Mobility by an External Magnetic Field

4.3.1 Effect of magnetic field on Static Diffusion

Literature survey has revealed that the effect of an external magnetic field on diffusion coefficient D has not been investigated so far. The author therefore, investigated this aspect in the following manner.

Figure 4.9a shows the nature of the constriction which restricts the motion of an adjacent atom into a vacancy in a f.c.c. lattice. The atom movements required for an atom 1 to jump are shown in Figures a-c. Figure 4.9a and Figure 4.9c show the initial and final states while Figure 4.9b shows the intermediate configuration referred to as the activated state. If crystals were free from defects other than vacancies the activation barrier as shown in Figure 4.9d would be the sole controlling factor for diffusion-by-vacancy mechanism. However, in the case of a demagnetised ferromagnetic crystal which is always divided into domains the contribution of exchange energy to the activation energy has also to be considered. This is examined with the aid of Figure 4.10. Figure 4.10a shows that an atom in order to go from position 1 in domain 1 to position 1' in domain 2

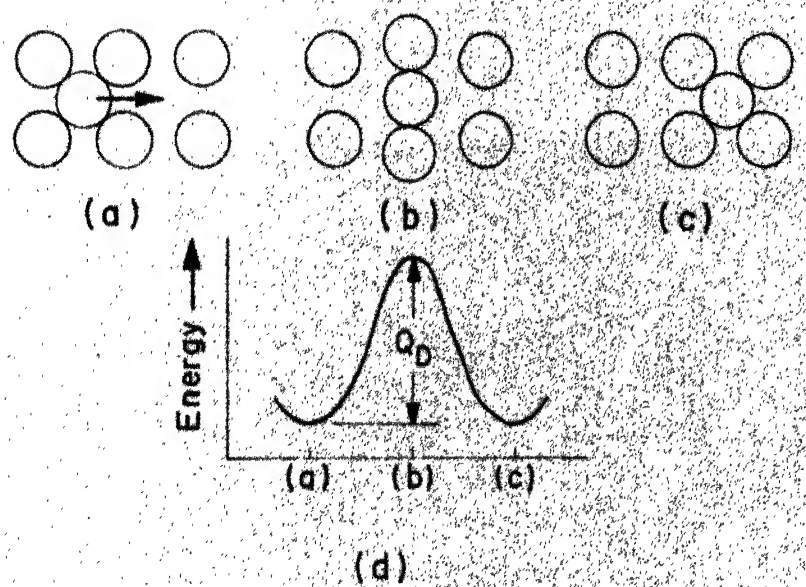

Fig.4.9 Schematic Diagram Showing The Sequence Of Configuration Involved When An Atom Jumps From One Normal Site To a Neighbouring One.

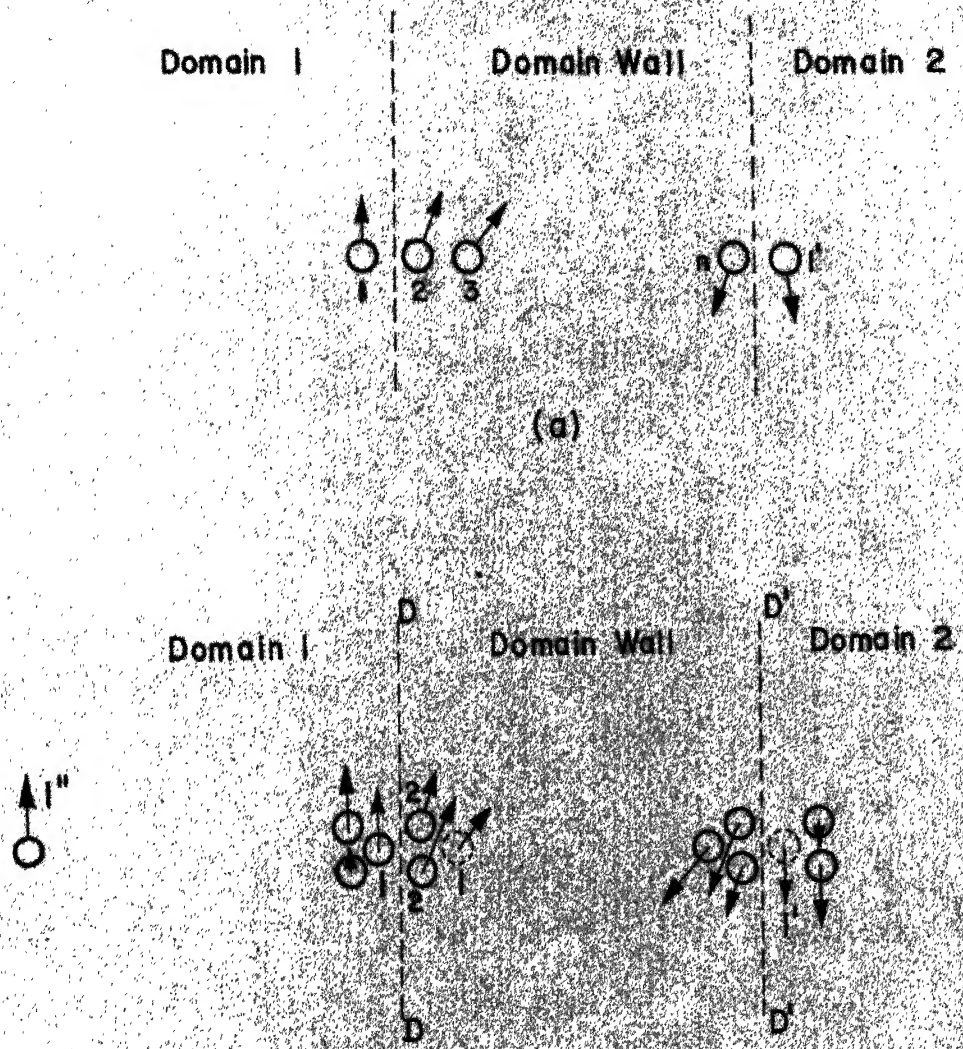

Fig. 4.10 Movement Of An Afom In a Ferromagnetic Material

has to go through the intermediate configurations 2, 3 ... n, 1'. Figure 4.10b shows that atom 1 in domain 1 is just in a position to go through the constriction between atoms 2 - 2 in order to diffuse into vacancy 1 in the wall. Atom 1 has to undergo a variation in the direction of the magnetic moment while diffusing from position 1 in domain 1 to position 1' in domain 2. This is shown in the figure. At each stage of its diffusion atom 1 has to break the magnetic bond of one nature and get into a different magnetic configuration due to the change in the spin direction. To do so an atom must possess enough energy to overcome the activation energy barrier as shown in Figure 4.9d, as well as to overcome the exchange energy effect. Thus, if in a ferromagnetic crystal atom 1 (in domain 1) were imagined to diffuse to 1" in its own domain the controlling barrier would be Q_D as shown in Figure 4.9d and Figure 4.10b would indicate that the direction of magnetic moment essentially remains constant during this diffusion process. In such a case the energy barrier, encountered by atom 1 to go to 1', would be as shown in Figure 4.11a. However, when the atom 1 has to traverse across a domain wall to position 1', the variation in the potential energy of the atom is as shown in Figure 4.11b. It is obvious that the atom 1

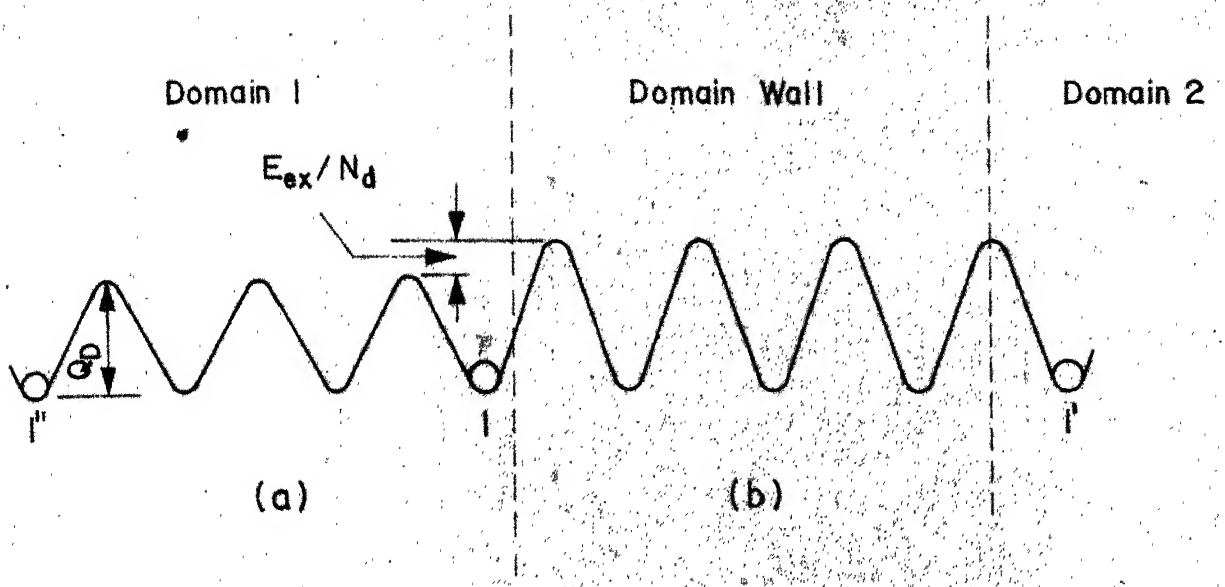

Fig.4.11 Energy Of Activation, Within a Domain And Across a Domain Wall.

in order to reach position 1' has to overcome at every stage an energy barrier,

$$Q \simeq Q_D + E_{ex} / N_d \qquad (4.15)$$

where E_{ex} is the exchange energy.

It is to be observed that the crossing of an atom from position 1 to position 1' occurs over large number of steps, given by the thickness of the domain wall. Therefore, the actual contribution of E_{ex} to the activation energy of diffusion is only E_{ex} / N_d, where N_d are the number of steps involved in crossing the domain wall. Usually N_d is of the order of several hundred. The contribution of the domain wall to the activation energy of diffusion may therefore, be taken to be $\simeq E_{ex}/100$. Thus, the activation energy for self diffusion in presence of magnetic field, Q_H, is given by

$$Q_H = Q - \frac{E_{ex}}{N_d} \qquad (4.16)$$

Now, it may be considered that an external constant magnetic field of sufficient strength has been applied so as to reduce the multidomain configuration of a crystal to a single domain configuration. Thus, the magnetic moments of all atoms point in one direction i.e. in the direction of the field. In view of the discussion related to Figure 4.10 the activation energy

for diffusion in the magnetised state should be obviously less by the order of magnitude of exchange energy per step of domain wall. This reduction may be considered to be equal to $\simeq \frac{K\ \theta_c}{100}$ per atom (110).

Therefor, $E_{ex} / N_d \simeq \frac{K\ \theta_c}{100}$ (4.17)

where, K = Boltzman constant

θ_c = curie temperature.

For an iron atom the value of E_{ex} / N_d, is equal to, 7×10^{-16} ergs/atom ($\simeq 10^{-2}$ kcal/gm - mole).

Thus, $Q_H = Q - 0.01$ (Cal/mole) (4.18)

If the activation energy of self-diffusion of iron is taken to be $\simeq$ 50 kcal/mole the application of an external magnetic field should result in a reduction of the activation energy of diffusion by $\simeq 0.02\%$. This is an extremely small quantity and would not influence the self diffusion of a ferromagnetic body to any observable degree. This can be easily seen as follows.

The ratio of diffusivities in unstrained state with and without an external magnetic field, is given by

$$\frac{D_u^H}{D_u^o} = \frac{\exp\ (-Q_H)}{\exp\ (-Q)} = e^{0.01} \simeq 1 \qquad (4.19)$$

where,

D_u^o = Diffusivity in unstrained state, and in the absence of an external magnetic field.

D_u^H = Diffusivity in unstrained state, but in the presence of an external magnetic field.

Therefore, the application of an external magnetic field to a ferromagnetic body cannot affect the self-diffusion in the body to any measurable degree.

To test this hypothesis the author conducted a static diffusion test. The details of this test will be discussed in the next Chapter.

These experiments did not yield any change in the diffusivity due to the application of the magnetic field. Therefore, on the basis of these experiments and the theoretical reasoning it is concluded that an external magnetic field has no influence on the diffusivity of a ferromagnetic body.

4.3.2 Enhancement of Dislocation Velocity by an External Magnetic Field.

In section 3.1 it was shown that at sufficiently high stresses the velocity of dislocations is given by

$$V(\sigma, \theta) = D \exp\left(\frac{v^* \sigma^*}{K \theta}\right) \qquad (4.20)$$

where, σ^*, the effective stress is the difference between the applied stress σ_a and the internal stress σ_i as already defined.

Since the application of an external magnetic field reduces the internal stress in the body by a magnitude of $G\lambda_s^*$, obviously the effective stress σ^* is increased by the same magnitude. Also, there is no evidence that the application of a steady magnetic field influences the activation volume for a particular process. Accordingly, for the present analysis v^* has been considered to remain unaffected by the application of a magnetic field. In light of the analysis given in the preceeding section diffusion coefficient D will also be treated as constant in the following analysis. Therefore, if the velocity of dislocations in presence of magnetic field is denoted by V_H it can be written as

$$V_H = D \exp\left(\frac{v^* \sigma_H^*}{\theta K}\right) \qquad (4.21)$$

where, σ_H^* represents the effective stress in presence of the magnetic field.

Also, the dislocation velocity without magnetic field may now be rewritten as

$$V_o = D \exp\left(\frac{v^* \sigma_o^*}{\theta K}\right) \qquad (4.22)$$

where, σ_o^* is the effective stress when magnetic

field is absent. The ratio of these velocities at a particular temperature θ is therefore given by,

$$\frac{V_H}{V_o} = \frac{\exp\left(v^* \overset{*}{\sigma_H} / \theta K \right)}{\exp\left(v^* \overset{*}{\sigma_o} / \theta K \right)} \qquad (4.23)$$

Now since

$$\overset{*}{\sigma_o} = \sigma_a - \sigma_i \qquad (4.24)$$

$$\overset{*}{\sigma_H} = \sigma_a - (\sigma_i - G^* \lambda_s)$$

or $$\overset{*}{\sigma_H} = \overset{*}{\sigma_o} + G^* \lambda_s \qquad (4.25)$$

Substituting this value of $\overset{*}{\sigma_H}$ in the Equation 4.23 and treating all other quantities unaffected, the ratio of the two velocities is obtained to be,

$$\frac{V_H}{V_o} = \exp\left(\frac{v^* G^* \lambda_s}{\theta K} \right) \qquad (4.26)$$

The following sample calculation will show the order of magnitude of this ratio. For this purpose the following values have been assumed

$$v^* \simeq 1.5 \times 10^{-21} \text{ cm}^3$$

This value of the activation volume at room temperature has been obtained by extrapolating the values provided by Watanabe and Karashima (89) for high temperature creep. This is shown in Figure 4.12. Also from earlier discussion it is clear that

$$G^* \lambda_s \simeq 50 \text{ kg/cm}^2.$$

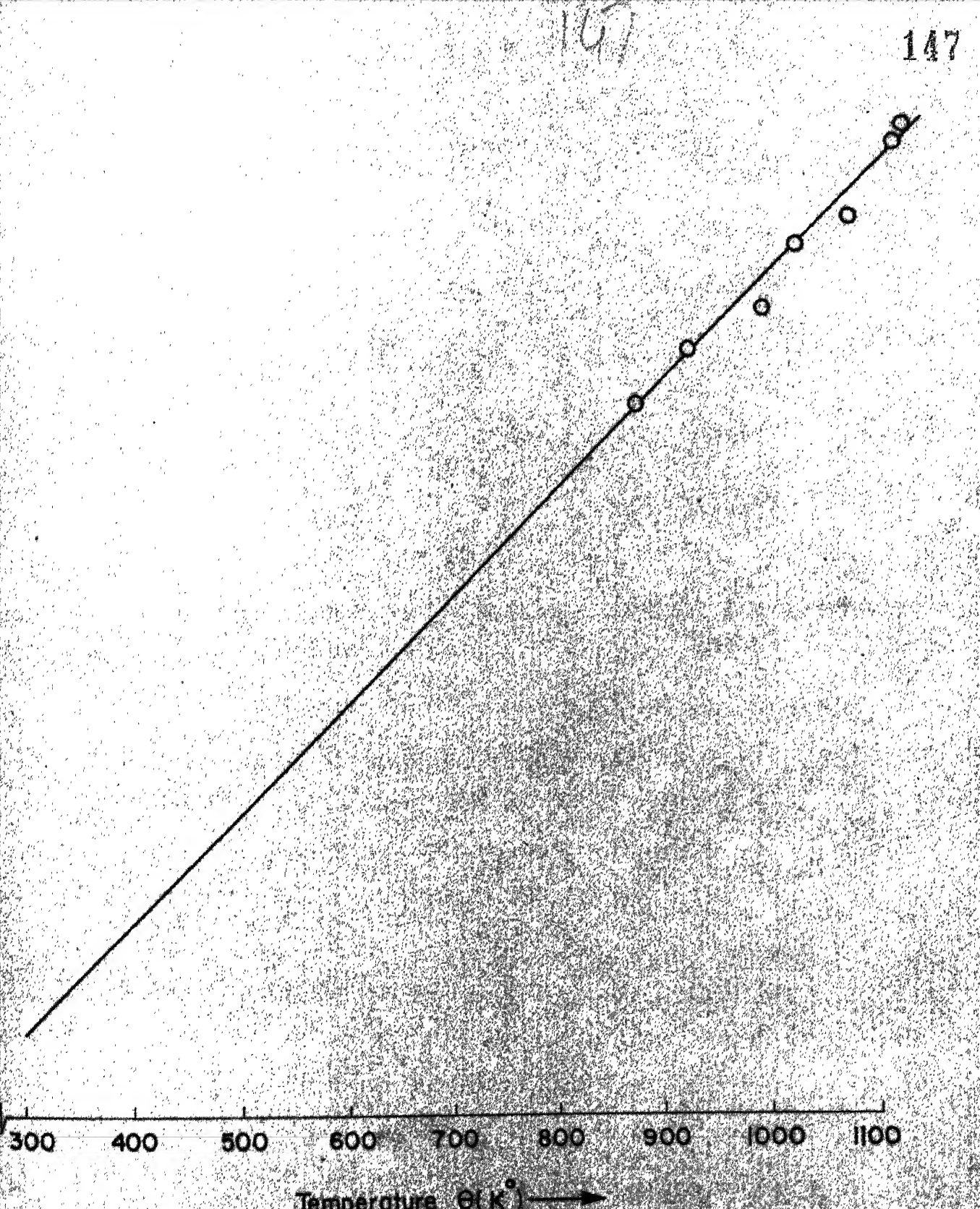

Fig. 4.12 Activation Volume For ∝ - Iron, (89).

Therefore, using $K \simeq 1.4 \times 10^{-23}$ Joules/deg. K

and $\theta \simeq 300\ ^{o}K$ (room temperature)

magnitude of $v^* G^* \lambda_s \simeq 75 \times 10^{-21}$ kg cm

$= 735 \times 10^{-23}$ Joules,

and, $K\theta = 420 \times 10^{-23}$ Joules.

So, $$\frac{v^* G^* \lambda_s}{K\theta} \simeq \frac{735}{420} = 1.75 \qquad (4.27)$$

and, $$\exp\left(\frac{v^* G^* \lambda_s}{K\theta}\right) \simeq \exp(1.75) = 5.75 \qquad (4.28)$$

Thus, at room temperature,

$$\frac{V_H}{V_o} \simeq 5.75 \qquad (4.29)$$

The dislocation velocity at room temperature is therefore found to increase by a factor of about 6 by the application of magnetic field. In other words, a decrease in the internal stress in a ferromagnetic material by a small amount $\simeq 0.5$ kg/mm^2 is likely to enhance the dislocation velocity by nearly 500%. This is a significant enhancement. Accordingly, physical phenomenae which depend upon the dislocation velocity should be influenced to a considerable extent by a magnetic field. Author establishes this by examining the creep strain rate of a ferromagnetic material like iron. The creep strain rate $\dot{\epsilon}_o$ in absence of a magnetic field is given by,

$$\dot{\epsilon}_o = V_o\, b \rho_m \qquad (4.30)$$

Again, in presence of the magnetic field strain rate $\dot{\epsilon}_H$ may be written as,

$$\dot{\epsilon}_H = V_H \, b \, \rho_m \qquad (4.31)$$

If it is assumed that the effect of an external magnetic field is only to increase the dislocation velocity without affecting b and ρ_m, the ratio of the creep strain rates $\dot{\epsilon}_H$ and $\dot{\epsilon}_o$ is given by,

$$\frac{\dot{\epsilon}_H}{\dot{\epsilon}_o} = \frac{V_H}{V_o} \qquad (4.32a)$$

From equation 4.29 this ratio is seen to be $\simeq$ 6, for iron.

$$\therefore \dot{\epsilon}_H \simeq 6 \dot{\epsilon}_o \qquad (4.32b)$$

Thus, if an external magnetic field is applied to a ferromagnetic material, the enhancement of dislocation velocity should manifest itself in enhancement of the creep strain rate to a considerable extent. This has indeed been confirmed by experiments of Kamnetskaya et. al. (124). These workers performed creep tests on iron samples at room temperature and found that the influence of magnetic field is to increase the creep strain rate considerably. Their results are shown in Figure 4.13. It can be seen from this figure that the application of magnetic field has increased the steady state creep strain rate

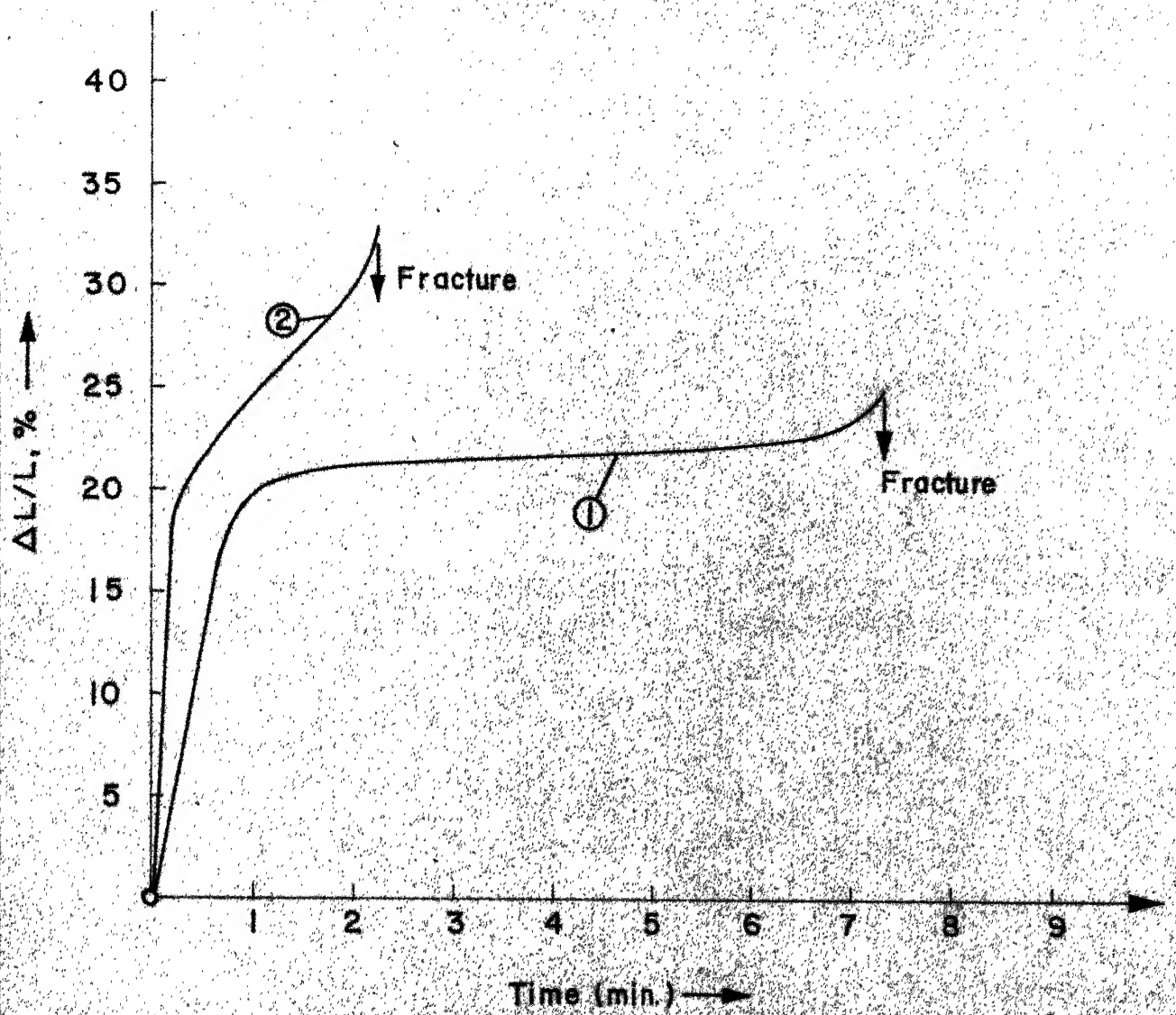

Fig.4.13 Creep Curves Of Fe_{cg} At Room Temp. And 29.6 kg/mm^2 ① Without Field, ② In Steady Magnetic Field Of 860 Oe, (54)

from $\simeq$ 1%/min in absence of the field to $\simeq$ 5%/min in presence of field. Thus, these experimental results yield,

$$\dot{\epsilon}_H \simeq 5\ \dot{\epsilon}_o \qquad (4.33)$$

This result is in very good agreement with that provided by Equation 4.32b and confirms that the major effect of an external magnetic field to a deforming body is to enhance the mobility of dislocations in the body.

It can now be examined how the enhancement of the dislocation velocity can significantly affect the wear behaviour of a sliding pair.

4.4 Effect of Magnetic Field on Adhesion Wear

It was pointed out in section 3.2 that a dislocation barrier can act as a potential nucleus for the initiation of a crack. The barriers could be the grain boundaries, second phase particles or 'dislocation forests'. Therefore, both in polycrystalline as well as in single crystal materials dislocation accumulation can affect a crack.

It was also discussed how dislocations get accumulated at the junction between the two grain size asperities of a sliding pair. The rate of accumulation of dislocations at the notch was shown to be approximately obtainable in the form,

$$\overset{o}{\rho}_{ri}(t) = \rho_o \left\{ 1 + \frac{V_o\, t}{ri^2} \left(2\, ri + V_o\, t + \frac{1}{\sqrt{F_o}} \right) \right\} \qquad (3.30)$$

where, V_o is the uniform dislocation velocity, when no magnetic field is applied to the asperity junction. Also, thesuperscript 'o' on $\overset{o}{\rho}_{ri}(t)$ denotes that the magnetic field is absent. Asperity junction of Figure 2.4 may now be considered with asperity I representing a ferromagnetic material and asperity II a non-magnetic material. Further, as shown in the figure a magnetic field H_s is applied across the asperity junction.

The condition for crack initiation at a point derived in section 2 was obtained to be

$$n \sigma_a \geq 0.7 G^* \qquad (3.17)$$

Thus for a given dislocation density at a point the stress has to reach a certain value to initiate the crack. Conversely, if the dislocation density at a particular point increases the crack initiation can occur at a lower stress.

In a bimetallic junction crack does not initiate on both sides of the junction, simultaneously. In view of the preceeding discussion, for a given junction, the probability of failure on a particular side of the junction should depend upon the dislocation density on that side of the junction. Now, when the asperity junction of Figure 2.4 starts deforming, the agglomeration of dislocations on the side of asperity I will be much faster than on the side of the asperity II. This is because the magnetic field enhances the velocity of dislocations only on the side of the asperity I and has no such effect on the asperity II. When both the asperities are ferromagnetic in nature, the one with a higher permeability would represent asperity I, of Figure 2.4. The discussion on the crack initiation at the asperity junction could still proceed in the same manner as for the junction formed by a ferromagnetic and a non-magnetic body. In both the cases,

application of an external magnetic field leads to an increased dislocation density on the side of the asperity I compared to that on the side of asperity II. Therefore, taking recourse to the earlier discussion, in section 3.3, the application of the magnetic field can lead to increased probability of failure of the junction on the side I and correspondingly to a decreased probability of failure on the side of II provided the duration of the time considered is less than t_j^o . Thus, during a given period of time, junctions should fail more often on the side of asperity I than on the side of asperity II. This leads to an important conclusion that the application of an external magnetic field should increase the wear rate of body I and consequently reduce the wear rate of body II. To analyse it further, the gain factor G may be redefined as

$$G = \frac{W^o - W^H}{W^o} \qquad (4.34)$$

where,

W^o = volume of wear in time T, when no magnetic field is applied,

and W^H = volume of wear in time T in presence of magnetic field.

On the basis of the preceeding observations the gain factor G should turn out to be a negative quantity for

the ferromagnetic body, I. On the same reasoning G should turn out to be a positive quantity for the non-magnetic body, II. In brief, body I should show a negative gain, while body II a positive gain when they are sliding in presence of the magnetic field. The magnitude of this positive or negative gain should obviously depend upon the relative enhancement of the dislocation density caused by the application of the magnetic field. An expression for such enhancement may now be obtained.

The density of dislocations on the side of body I (ferromagnetic body) with and without magnetic field is expressed as,

$$\rho_{ri}^{H}(t) = \rho_o \left\{ 1 + \frac{V_H\, t}{ri^2} \left(2\, ri + V_H\, t + \frac{1}{\sqrt{\rho_o}} \right) \right\} \tag{4.35}$$

and,

$$\rho_{ri}^{o}(t) = \rho_o \left\{ 1 + \frac{V_o\, t}{ri^2} \left(2\, ri + V_o t + \frac{1}{\sqrt{\rho_o}} \right) \right\} \tag{4.36}$$

In these equations, $\rho_{ri}^{H}(t)$ and $\rho_{ri}^{o}(t)$ denote the dislocation densities on the side of I in presence and absence of an external magnetic field, respectively. Both these equations are, however, valid only for their respective time limits t_j^H and t_j^o, respectively. The graphical representation of equations 4.35 and 4.36 is

shown in Figure 4.14a. In this figure curves 0 - 1 and 0 - 3 represent equations 4.35 and 4.36 respectively. The enhancement of dislocation density during any time $t < t_j^o$ is given by,

$$\delta \rho_{ri}(t) = {}^{H}\rho_{ri}(t) - {}^{o}\rho_{ri}(t) \qquad (4.37)$$

where, both ${}^{H}\rho_{ri}(t)$ and ${}^{o}\rho_{ri}(t)$ attain the same, limiting value of ρ_{lim} but at different times t_j^H and t_j^o respectively. Figure 4.14b shows how this enhancement in dislocation density $\delta \rho_{ri}(t)$ varies as a function of time. This enhancement of dislocation agglomeration at the notch, on the side of the ferromagnetic body I increases upto time t_j^H. Thereafter, it decreases continuously reaching a value of zero at t_j^o. Therefore, if the sliding velocity of a pair is such that the junction life falls in the range of 0 - t_j^o, then the enhancement of the dislocation density will be given by a corresponding point on the profile 0 - 1' - 3'. For instance, if the junction time is t_j^{x1}, the corresponding enhancement in dislocation density is $\delta \rho^{x1}$ as shown by point 1" on the line 0 - 1' in Figure 4.14b. For a given asperity size the junction life t_j is inversely proportional to the sliding velocity V_s. Consequently, the nature of variation of the enhancement of dislocation density $\delta \rho_{ri}(t)$ as a function of sliding velocity, can, be easily obtained using the Figure 4.14b and

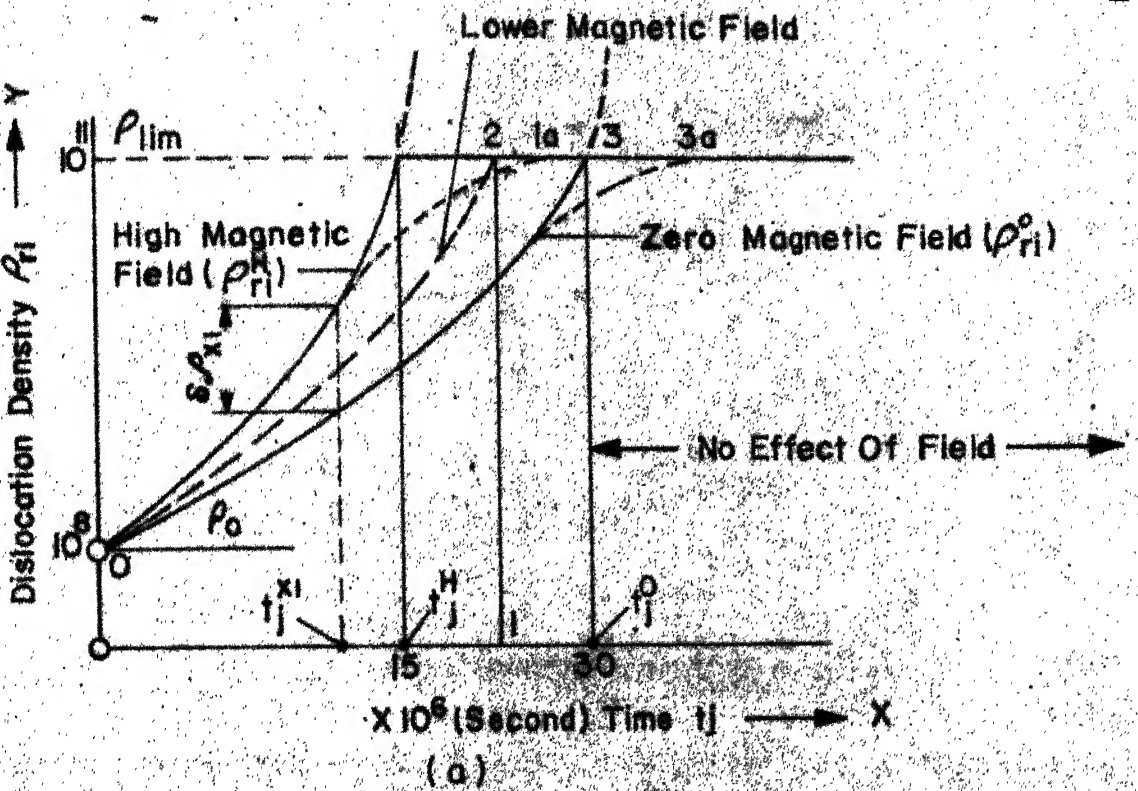
Lower Magnetic Field
Y
Dislocation Density ρ_{ri}
10^{11}
ρ_{lim}
1
2
1a
3
3a
High Magnetic Field (ρ_{ri}^{H})
Zero Magnetic Field (ρ_{ri}^{o})
$\delta\rho_{xi}$
No Effect Of Field
10^{8}
ρ_o
0
t_j^{xi}
t_j^{H}
t_j^{o}
15
30
X 10^6 (Second) Time t_j
X

(a)

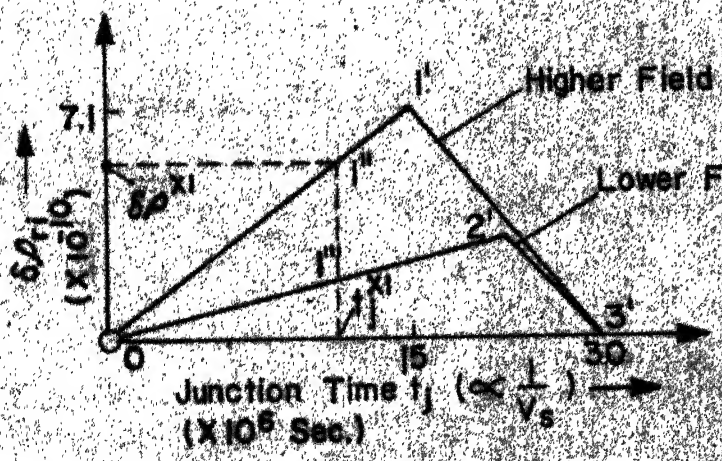
7.1
$\delta\rho_{ri}$ (X 10^{-10})
1'
Higher Field
1''
$\delta\rho^{xi}$
Lower Field
2'
1'''
t_j^{xi}
3'
0
15
30
Junction Time t_j ($\propto \frac{1}{V_s}$)
(X 10^6 Sec.)

(b)

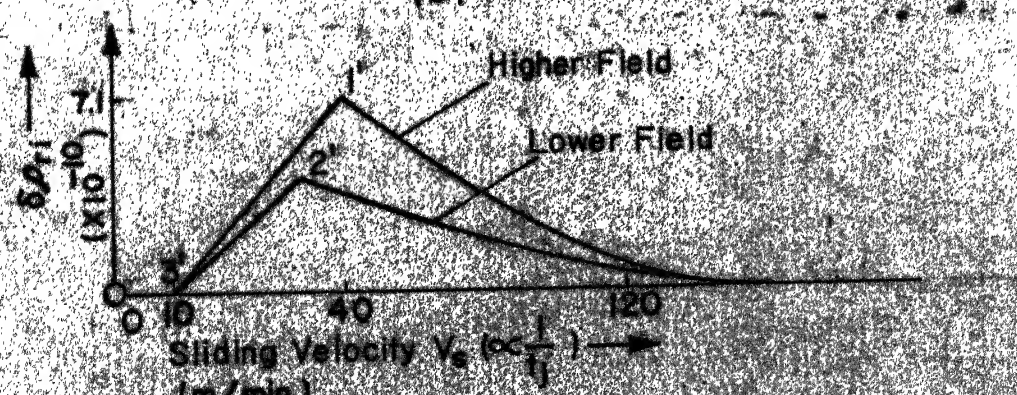
7.1
$\delta\rho_{ri}$ (X 10^{-10})
1'
Higher Field
Lower Field
2'
3'
0
10
40
120
Sliding Velocity V_s ($\propto \frac{1}{t_j}$)
(m/min.)

(c)

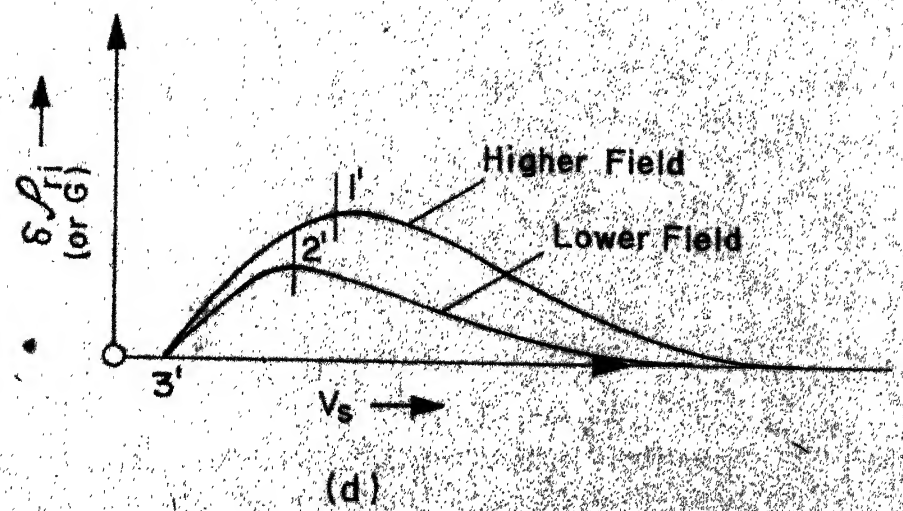

(d)

Fig.4.14 Diagram Showing Trend In The Densities Of Dislocations At The Notch Under Magnetic And Non - Magnetic Conditions.

is shown in Figure 4.14c. The consequences of the enhancement of dislocation density may now be further analyzed.

If ρ^{H}_{ri} curve is shifted towards ρ^{o}_{ri} curve, the point of maxima 1' in Figure b gets shifted towards the higher junction life. Also, the magnitude of the enhancement $\delta \rho_{ri}$ is also reduced. This is shown in Figure b, where the point of maxima 1' is now shown as point 2'. Shifting of thecurve ρ^{H}_{ri} to a position closer to ρ^{o}_{ri} implies that a magnetic field of lower strength be employed. This is because a lower magnetic field would enhance the dislocation velocity to smaller extent. This would result in shifting the curve 0 - 1' in Figure 4.14a, to a position like 0 - 2' in the same figure. Also, for the same junction time t^{x1}_{j}, $\delta \rho^{x1}$ will be given by point 1''' on the line 0 - 2'. The value of the enhancement of dislocation density at 1''' is obviously lower than $\delta \rho^{x1}$. Consequently, the enhancement of dislocation accumulation at the notch due to the application of the magnetic field is related to both the sliding velocity and the field strength. This, can be seen in Figure 4.14c. It was explained in section 3.3 how a notch acts as a focal point for the agglomeration of dislocations. And, the intense agglomeration of dislocations at the notch increases the probability of crack initiation at

the notch. Therefore, with reference to the discussions in the preceeding paragraphs it is realised that the enhancement in the dislocation density, $\delta \rho_{ri}$ in the ferromagnetic body I is also a measure of the enhancement of wear δW $(= W^{O} - W^{II})$ of the same body. Consequently, the variation of gain factor G $(= \frac{\delta W}{W^{O}})$ with the sliding speed V_s is of the same form as the variation of $\delta \rho_{ri}$ with V_s. It is difficult to bring out a numerical equivalence between $\delta \rho_{ri}$ and G. In this work therefore only qualitative relationship between $\delta \rho_{ri}$ and G is attempted. On the basis of the discussions in the preceeding paragraphs, it is therefore adequate to consider that the nature of variation of G with V_s is similar to that of $\delta \rho_{ri}$ with V_s. This is shown in Figure 4.14b and 4.14c.

To have an idea about the enhancement of dislocation density, $\delta \rho_{ri}$, Equations 4.35, 4.36 and 4.37 have been evaluated. A sample set of calculations is shown in Table 4.1. In evaluating these equations the following values for the various parameters have been assumed.

$V_o = 10^3$ Cm/sec

$V_H = 2 \cdot V_o$

$a = 10^{-3}$ Cm.

$\rho_o = 10^8$ Cm^{-2}

$\rho_{lim} = 10^{11}$ Cm^{-2}

TABLE 4.1

Dislocation accumulation at the asperity notch.

$t_j \times 10^6$ (sec.)	V_s m/min	${}^{o}\rho_{ri} \times 10^{-8}$ Eqn. 4.35 (Cm^{-2})	${}^{H}\rho_{ri} \times 10^{-8}$ (Cm^{-2}) ; Eqn 4.36		$\delta\rho_{ri} = ({}^{H}\rho_{ri} - {}^{o}\rho_{ri}) \times 10^{-8}$ (Cm^{-2})		$\rho_{ri} / {}^{o}\rho_{ri}$	
			$V_H = 2\ V_o$	$V_H = 1.28 V_o$	$V_H = 2\ V_o$	$V_H = 1.28 V_o$	$V_H = 2\ V_o$	$V_H = 1.28\ V_o$
1	2	3	(4a)	(4b)	(5a)	(5b)	(6a)	(6b)
60	10	964	964	-	negligible	-	negligible	-
30	20	964	964	-	negligible	-	negligible	-
25	24	678.5	964	-	285.5	-	0.42	-
20	30	443	964	-	521	-	1.17	-
15	40	257.5	964	-	706.5	-	2.74	-
10	60	122	443	-	321	-	2.63	-
8	75	81.8	290.6	-	208.8	-	2.55	-
7	86	64.7	226.4	-	161.7	-	2.49	-
5	120	36.5	121	-	84.5	-	2.31	-
4	150	25.4	81.8	38.1	56.4	12.7	2.24	0.5
2	300	9.2	25.4	12.9	16.2	3.0	1.76	0.4
1	600	4.1	9.2	5.33	5.1	1.2	1.24	0.3

The numerical values given in Table 4.1 have also been indicated in Figure 4.14. It can be observed that the calculations have been done over a speed range of 10 - 600 m/min. The range of speeds employed in actual wear experiments was $\simeq$ 10 - 150m/min.

From the calculated values of $\delta \rho_{ri}$, it can be seen that for speeds $<$ 10 m/min and $>$ 600 m/min, $\delta \rho_{ri}$ is negligible. Actually $\delta \rho_{ri}$ should start falling to zero much earlier because of the rise in temperature as the speed increases. This can be examined as follows.

As temperature increases the magnetostriction coefficient λ_s decreases, reaching a value of zero at thecurie temperature, θ_c. Consequently, the magnitude of the magnetostrictive stress is also considerably reduced at these high temperatures. The variation of magnetostrictive stress with temperature may be taken to be, in general, of the same form as the variation of magnetisation with temperature. This is shown in Figure 4.15. From the figure it is seen that at a temperature of 0.9 θ_c, the magnetisation has half the value of its value at room temperature. If as a first approximation the magnetostrictive stress is also considered to be reduced to nearly half of its value at room temperature, the velocity ration $\frac{V_H}{V_o}$ (calculated in Equation 4.27)

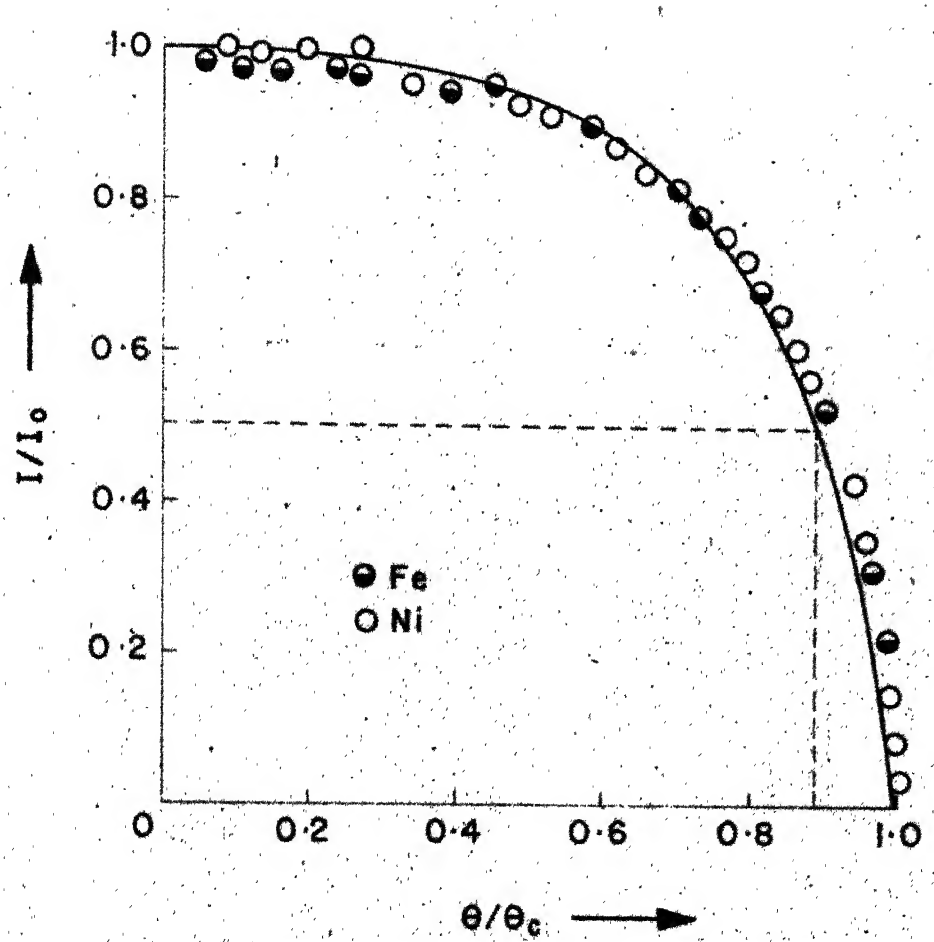

Fig. 4·15 Temperature Dependence Of Spontaneous Magnetisation (101).

can be re-calculated as

$$\frac{V_H}{V_o} = \exp\left(\frac{G^* \lambda_s/2}{K\ 0.9\ \theta_c}\right)$$

For iron the room temperature value of $\lambda_s\ G^*$ is $\simeq 0.5$ kg/mm^2 and $\theta_c = 1043\ ^oK$. With these values introduced in the above equation, the ratio $\frac{V_H}{V_o}$ is calculated to be

$$\frac{V_H}{V_o} = \exp(0.25)$$
$$= 1.28$$

Therefore, at temperature $\theta = 0.9\ \theta_c$ ($\simeq 693\ ^oC$) which is nearly the recrystallization temperature of iron, the dislocation velocity is enhanced by only about 28%. This is considerably smaller as compared to the enhancement in velocity at room temperature.

If at higher speeds, therefore, the velocity of dislocations is considered to be enhanced by only such a smaller amounts, the enhancement in dislocation density at the asperity junction would be reduced considerably. If, for instance, at speeds $\gg$ 150 m/min V_H is considered to be equal to 1.28 V_o, the factor $\delta\rho_{ri} / \overset{o}{\rho}_{ri}$ is considerably reduced as can be seen from the last column of Table 4.1. It was already discussed that $\delta\rho_{ri} / \overset{o}{\rho}_{ri}$

is a measure of the gain factor G. Thus, the gain factor G should also show a considerably faster reduction at high speeds, than that indicated by values given in column 6a of Table 4.1. While it would be helpful to have exact calculations for $\delta \rho_{ri}$ at high temperature, such calculations cannot serve any purpose, without the exact knowledge of dislocation velocities.

It is concluded therefore that the enhancement in dislocation density, $\delta \rho_{ri}$, is realisable only when the times considered are in the range of 10^{-6} - 10^{-5} sec. Out side this range of times, $\delta \rho_{ri}$ is negligible and so the magnetic field will not be seen to have any effect on the fracture and wear characteristics. This point will be further brought to focus in Chapter 5 when the experimental observations on the fracture of large samples will be discussed. For the present it is adequate to postulate that, in general, the influence of magnetic field is to enhance the wear rate of the ferromagnetic body I, and decrease that of the non magnetic body, II.

It is to be observed that as the dislocation density at the notch increases the velocity of dislocations coming towards the notch would get reduced more and more. This is due to the increasing repulsive force exerted on the incoming dislocation by the

dislocations agglomerated on the notch. Due to this the rate of build up of dislocations at the notch would get reduced as can be easily seen from Equations 4.35 and 4.36. Consequently, the build up is no longer given by such sharply rising curves as 0 - 1 or 0 - 3 of Figure 4.14a. Rather, the dislocation density would attain the value ρ_{lim} in an asymptotic manner. For instance, the curve 0 - 3 would be then obtained as 0 - 3a and the curve 0 - 1 as 0 - 1a. As a result the $\delta\rho_{ri}$ versus V_s curve will not exhibit a sharp maxima. On the other hand, it will show a smooth changeover from an increasing trend to a decreasing trend. The relation between the gain factor G and the sliding velocity V_s also would be then more appropriately given by Figure 4.14d. It will be seen in Chapter 5 that the experimental results are also exhibiting the trend indicated by Figure 4.14d.

4.5 Effect of Magnetic Field on Diffusion Wear

It was pointed out in section 2.4 that several workers have established that considerable diffusion occurs, during plastic deformation. It has also been shown by Hirano et.al.(61) that the diffusivity in the strained condition D_s is related to that in the unstrained condition D_u, in the following manner :

$$\left(\frac{D_s}{D_u} - 1 \right) = \frac{n_x}{n_v} = B\dot{\epsilon} \qquad (4.38a)$$

where,

n_x = steady-state atomic fraction of excess vacancies introduced by the deformation process,

n_v = atomic fraction of vacancies at thermal equilibrium.

$\dot{\epsilon}$ = strain rate

and B = constant, which depends only on temperature.

In the case of α - iron Hirano et. al. have also found that over a wide range of temperatures and strain rates, the value of $\left(\frac{D_s}{D_u} - 1 \right)$ varies from above 100 to 2500. Above equation may therefore be written in simpler form as follows :

$$\frac{D_s}{D_u} = \frac{n_x}{n_v} \qquad (4.38b)$$

It is therefore, well established that plastic deformation enhances the diffusivity of the material. The author proposes that the application of an external magnetic field to sliding asperity junction should further enhance the diffusivity at the junction. This is substantiated in the following manner.

As the dislocations intersect one another a jog is produced on them. If the jog is dragged along with the dislocation it can produce a vacancy in each successive step. The number of such defects produced during a given period of time will depend upon the number of dislocations involved in the intersection process. In other words, the number of excess vacancies n_x, introduced by the deformation process can be related to the density of dislocations at a particular point in the deforming body. Turkovich and Calvo (125) have shown mathematically that in the metal cutting process, the number of excess point defects produced in the shear zone is proportional to the number of dislocations being produced in the process. This argument can now be extended to an asperity junction. At the asperity junction the dislocations are continuously being attracted towards the notch. This should lead to increased dislocation intersections near the notch. As a result, the number of excess vacancies generated would be larger compared to the case when there would be no such preferential agglomeration.

It has already been shown that the application of an external magnetic field enhances the dislocation mobility near the asperity junction. This leads to the enhanced agglomeration of dislocations at the notch formed at the junction of two asperities. Obviously therefore, the application of magnetic field will enhance the generation of point defects at the notch.

If as a first approximation the number of excess vacancies produce, n_x, is considered to be linearly dependent on the dislocation density, the following equations

$$n_x^o = k_1 \overset{o}{\rho}_{ri} \qquad (4.39a)$$

and

$$n_x^H = k_1 \overset{H}{\rho}_{ri} \qquad (4.39b)$$

can be immediately written.

In these equations, the superscript H denotes that magnetic field has been applied, while the superscript 'o' denotes that no such field has been applied. Substitution of 4.39a and 4.39b in the Equation 4.38 yields,

$$\frac{D_s^H}{D_u^H} = \frac{n_x^H}{n_v} = \frac{k_1 \overset{H}{\rho}_{ri}}{n_v} \qquad (4.40a)$$

and

$$\frac{D_s^o}{D_u^o} = \frac{n_x^o}{n_v} = \frac{k_1 \overset{o}{\rho}_{ri}}{n_v} \qquad (4.40b)$$

where,

D_s^H , D_s^o denote the diffusivity in the strained condition in the presence and absence of magnetic field, respectively,

and D_u^H , D_u^o denote the diffusivity in the unstrained condition in the presence and absence of magnetic field, respectively.

As already mentioned experiments conducted by the author have conclusively shown that

$$D_u^H = D_u^o \qquad (4.41)$$

Therefore, combining Equations 4.40 and 4.41,

$$\frac{D_s^H}{D_s^o} = \frac{n_x^H}{n_x^o} = \frac{{}^H\rho_{ri}}{{}^o\rho_{ri}} \qquad (4.42)$$

Equation 4.42 is an important relation as it shows that thediffusivity in the vicinity of the asperity junctions would always increase in proportion to the increase in the dislocation density. Thus, the application of magnetic field to a sliding asperity junction of Figure 2.4 would increase the self diffusivity on the side of the ferromagnetic body, I. Consequently, the diffusivity of the ferromagnetic element of body I into body II would also get enhanced.

With reference to Figure 2.10, the author has already shown in section 2.4.2 how in a sliding

It is to be mentioned that in the present discussion, body I is considered to be ferromagnetic and of greater hardness than body II. In such a case the hardness gradient in body II would be negative. This would lead to larger and larger material removed from body II as diffusion process would be enhanced. This is shown as follows.

After introducing Equation 4.42 into Equation 4.45, it can readily be seen that

$$\frac{m_{II}^{H}}{m_{II}^{o}} = \left(\frac{{}^{H}\rho_{ri}}{{}^{o}\rho_{ri}} \right)^{1/6} = \bar{\beta} \quad (> 1) \qquad (4.46)$$

Equation 4.46 shows that the diffusion wear of body II is also related to the dislocation density and thus the fracture probability on the side of body I.

Now, from Equations 4.35 and 4.36 and the Figure 4.14a, it is clear that the ratio ${}^{H}\rho_{ri} / {}^{o}\rho_{ri}$ is nearly unity for very low and also very high values of the time t_j. For intermediate values of t_j this ratio changes in the manner already shown in the Figure 4.14b and is always greater than 1. Thus, the ratio of diffusivities D_s^H / D_s^o will also follow a similar profile. The following example shows what contribution the enhancement of D_s^o to D_s^H, will make in the net wear of body II and to the gain factor G_{II}, of body II. (In the present analysis the gain factor of body I will be denoted by G_I, and that of body II by G_{II}).

For a typical asperity junction width 'a' $\simeq 15 \times 10^{-4}$ cm and sliding speed of 100 m/min, the junction life is $\simeq 10^{-5}$ sec. If the dislocation velocity in presence of magnetic field is assumed to be $\simeq \frac{10^5}{2}$ (m/sec) then during the junction life $t_j \simeq 10^{-5}$ sec, the dislocation density at the notch would get enhanced from its initial value of $\simeq 10^6$ cm^{-2} to the limiting value of $\simeq 10^{12}$ cm^{-2}. This can be calculated from Equation 4.35. If the value of the dislocation velocity in the absence of magnetic field is assumed to be $\simeq \frac{V_H}{4}$, then during the same time $t_j \simeq 10^{-5}$ secs, the dislocation density at the notch, ${}^{H}\rho_{ri}$, would reach a value of only $\simeq 0.7 \times 10^{11}$ cm^2. This value is calculated from Equation 4.36. Therefore, for this example the maximum value of the ratio $\frac{{}^{H}\rho_{ri}}{{}^{o}\rho_{ri}}$ which occurs at $t_j \simeq 10^{-5}$ sec is given by

$$\frac{{}^{H}\rho_{ri}}{{}^{o}\rho_{ri}} = \frac{10^{12}}{.7 \times 10^{11}} \simeq 15$$

From Equation 4.42 it is clear that the ratio

$$\frac{D_s^H}{D_s^o} \text{ is also } \simeq 15$$

Thus, the diffusivity in the magnetised case is about 15 times that in the unmagnetised case. Referring back to Equation 4.45 and Figure 2.10 the wear of body II

should increase in the ratio,

$$\frac{m_{II}^{H}}{m_{H}^{o}} = (15)^{1/6} \simeq 1.57 = \bar{\beta} \quad (>1)$$

Thus, at the sliding speed considered the wear rate of body II would be increased by $\simeq$ 57% due to the application of the magnetic field. It can now be shown that the gain factor on the side of body II, G_{II}, is related to the gain factor G_{I}, on the side of body I. For this purpose the following quantities are defined.

m_{I}^{o}, m_{II}^{o} = mass removed in one asperity interaction from body I, and II, respectively, when no magnetic field is applied.

m_{I}^{H} , m_{II}^{H} = mass removed in one asperity interaction from body I and II, respectively, when magnetic field is applied.

and n_{I}^{o}, n_{I}^{H} = number of fractures during a given time occuring on the side of body I, when no magnetic field is applied and when magnetic field is applied, respectively.

From the definition of gain factor it follows immediately, that

$$G_{II} = \frac{m_{II}^{o}\, n_{II}^{o} - m_{II}^{H}\, n_{II}^{H}}{m_{II}^{o}\, n_{II}^{o}} = 1 - \frac{m_{II}^{H}}{m_{II}^{o}} \times \frac{n_{II}^{H}}{n_{II}^{o}}$$

using the value, for $\frac{m_{II}^{H}}{m_{II}^{o}}$, from Equation 4.46,

$$G_{II} = 1 - \bar{\beta} \times \frac{n_{II}^{H}}{n_{II}^{o}} \qquad (4.47)$$

Also, since magnetic field has no effect on the size of the wear particle removed from body I,

$$m_{I}^{o} = m_{I}^{H} \qquad (4.48)$$

Consequently, the gain factor for body I can be written as

$$G_{I} = \frac{n_{I}^{o} - n_{I}^{H}}{n_{I}^{o}}$$

$$= \frac{(1 - n_{II}^{o}) - (1 - n_{II}^{H})}{n_{I}^{o}}$$

$$= \frac{(n_{II}^{H} - n_{II}^{o})}{n_{I}^{o}}$$

or $$G_{I} = \left(\frac{n_{II}^{H}}{n_{II}^{o}} - 1 \right) \frac{n_{II}^{o}}{n_{I}^{o}} \qquad (4.49)$$

Combining Equations 4.47 and 4.49 it is easily seen that

$$G_{II} = 1 - \bar{\beta} \left(\frac{G_{I}\, n_{I}^{o}}{n_{II}^{o}} + 1 \right)$$

$$= 1 - \bar{\beta} \left(1 + \frac{G_{I}\, n_{I}^{o}}{1 - n_{I}^{o}} \right) \qquad (4.50)$$

Since G_I is actually a negative quantity

$$G_{II} = G_I \left(\frac{\bar{\beta}\, n_I^o}{1 - n_I^o} \right) - (\bar{\beta} - 1)$$

where, G_I now represents only modulus of G_I. Since, body I is considered to be harder than body II, the factor $n_I^o / (1 - n_I^o) (= \lambda)$ is most often likely to be less than unity. The above equation may therefore be written as

$$G_{II} = 1 - \bar{\beta} (1 - G_I \lambda) \qquad (4.51)$$

Equation 4.51 shows that the gain of non-magnetic body, II is a function of

i) the gain of ferromagnetic body, I.

ii) the enhancement in the diffusivity of body I,

and iii) $\lambda = \frac{n_I^o}{(1 - n_I^o)}$, which may be defined as the 'mechanical interaction factor' of the sliding pair. This factor will always be less than one, when body I is harder than body II.

It is clear therefore, that the sign as well as the magnitude of G_{II} depends upon the magnitude of the quantity $\bar{\beta} (1 - G_I \lambda)$. Since, both G_I and λ are less than unity and $\bar{\beta} > 0$, the quantity $\bar{\beta} (1 - G_I \lambda)$ is always positive. Therefore, G_{II} will be positive, zero or negative depending upon whether

$$\bar{\beta}(1 - G_I\lambda) \begin{cases} < 1 \\ = 1 \\ \text{or} > 1 \end{cases}$$

Therefore, the nature of variation of G_{II} will be controlled by the nature of variation of G_I. This aspect can be further discussed in Chapter 5, when the experimental results are presented. For the present, it is therefore adequate to observe that the enhanced diffusivity of body I would cause a characteristic change in the wear behaviour of the sliding pair and can cause the gain of body II, G_{II}, to attain negative values also.

CHAPTER V

EXPERIMENTAL RESULTS AND DISCUSSIONS

5.1 Introduction

In order to establish the most prominent mechanism through which magnetic field affects the wear of sliding surfaces, it was found necessary to conduct appropriate tests. These tests can be grouped in five broad categories as follows :

Category A : Material Property Tests

Under this category the following two experiments were performed :

(i) Tensile strength test.

(ii) Impact strength test.

Category B : Cutting force test.

Category C : Static diffusion test.

Category D : Stress-relaxation test.

Category E : Wear tests.

Under this category four kinds of experiments were performed. These are, as follows :

(i) Machining of non-magnetic job by ferromagnetic cutting tools.

(ii) Rubbing of non-magnetic job by ferromagnetic tools.

(iii) Rubbing of ferro-magnetic specimens against non-magnetic body.

(iv) Rubbing of non-magnetic specimens agsint ferro-magnetic body.

(v) Rubbing tests with different magnetic field strengths.

Details of these tests conducted are given below.

5.2 Details of Experiments

5.2.1 Effect of Magnetic Field on Tensile Strength

Test specimens of mild steel of standard dimensions were prepared according to ISI specifications. These samples were tested on Instron Testing Machine (Model TCTML). Following are the conditions under which this test was conducted.

(i)	Diameter of the specimen at the test section	= 6.0 $\pm$ .01 mm
(ii)	Temperature	= room temp.
(iii)	Cross head speed of the Instron Machine	= 0.5 cm/min.
(iv)	Chart speed used	= 1.0 cm/min.
(v)	Magnetic field strength	= 125 Oe.

The magnetic field was applied to the test specimen by means of a solenoid surrounding the specimen. The magnetic field was thereby acting along the

axis of the specimen. A schematic diagram of the set up is shown in Figure 5.1. A typical load elongation curve with and without the presence of magnetic field is shown in Figure 5.2. From this figure it is to be observed that the curve for the magnetised case is lower than that for the unmagnetised case. The yield strength and the ultimate strength both have reduced. This reduction is about 0.8 kg/mm^2, and only about 2.7% of the yield strength of the material. Obviously this change is too small to be considered as a significant change in the bulk property of the material.

From these observations it was inferred that the magnetic field is probably influencing only the microscopic properties rather than the macroscopic ones, of materials.

5.2.2 Effect of Magnetic Field On The Impact Strength of Materials

To investigate whether the energy required to cause a body to fracture would be affected in presence of an external magnetic field an impact strength test was conducted. It was found convenient to carry out the Izod impact test, for, in this case the solenoid which was used to magnetise the specimen could be placed in a manner that the striking hammer would not damage it. A schematic diagram for the set up is shown in Figure 5.3. The test was conducted on

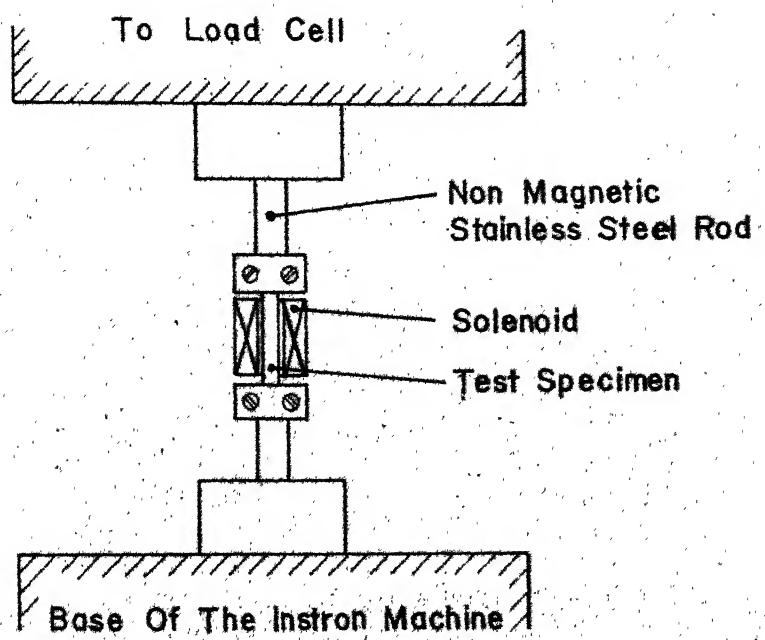

Fig. 5.1 A Schematic Diagram Of a Tensile Test Set-Up.

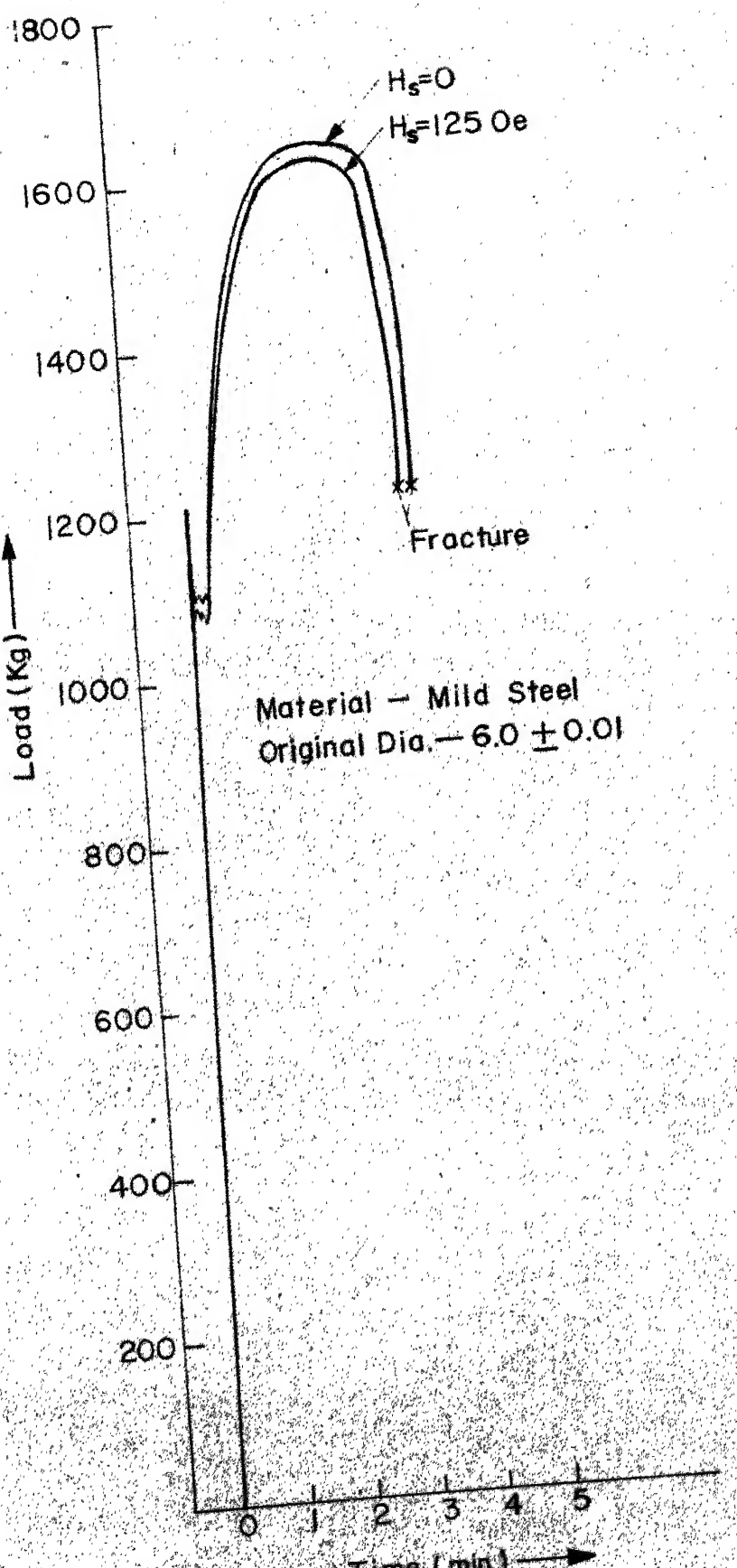

Fig 5.2 Tensile Test Of a Mild Steel Specimen

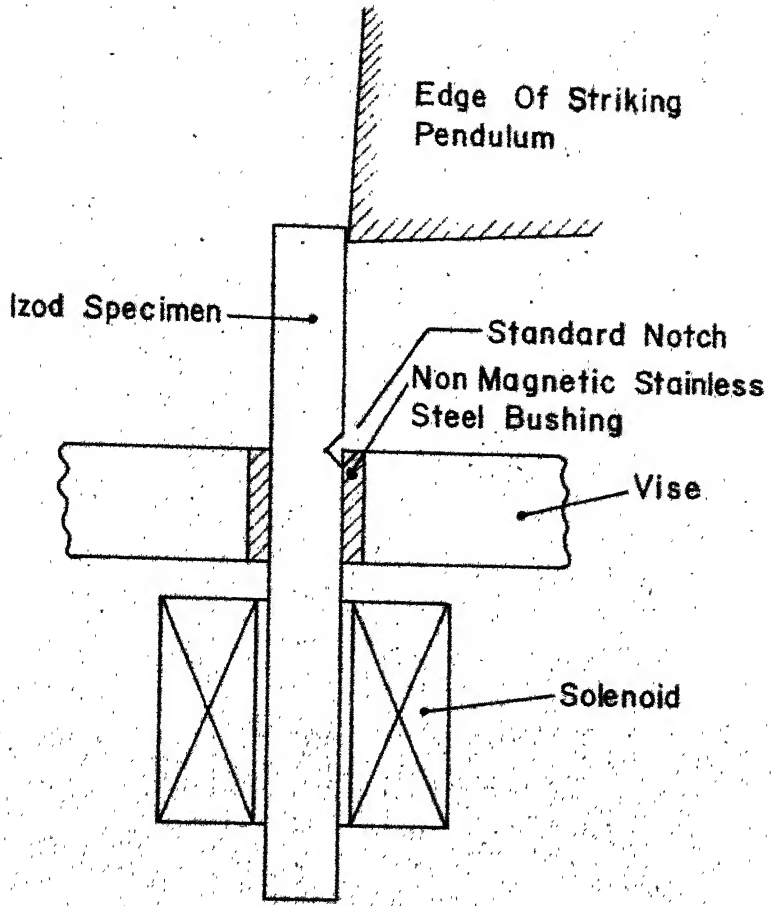

Fig. 5.3 Schematic Diagram Of The Izod Impact Test

Tinus - Olsen Impact Testing Machine. The test conditions were as follows :

(i)	Material tested	= Mild Steel
(ii)	Diameter of the specimen	= 10 ± 0.01 mm
(iii)	Depth of the notch	= 2 mm
(iv)	Angle of the notch	= 45°
(v)	Magnetic field strength	= 125 Oe
(vi)	Temperature	= Room Temp.

Twenty identical specimens were tested for impact strength. Ten specimens were tested in the magnetised state and other ten specimens in the unmagnetised state. The magnitudes of the energy absorbed in fracturing the specimens in the two cases are given in Table 5.1

It can be seen from the tabulated readings that the difference in the energy absorbed in the two cases is within errors of observation, both in regard to the individual readings as well as in their average values.

The fractured surfaces were also examined under microscope (x 200) for any characteristic effect on the type of fracture by the magnetic field. No obvious difference was discovered between the two cases. The macroscopic behaviour of materials therefore seemed to remain unaffected by an external magnetic field.

TABLE 5.1

IMPACT STRENGTH OF MILD STEEL SPECIMEN

Test : Izod Test Magnetic Field Strength = 125 Oe

Material Tested : Mild Steel

Specimen Number	Energy Absorbed	
	Without field (cm kg) x 1/13.6	With field (cm kg) x 1/13.6
1	74	-
2	-	73
3	71	-
4	-	69
5	69	-
6	-	73
7	70	-
8	-	74
9	73	-
10	-	69
11	74	-
12	-	73
13	72	-
14	-	73
15	70	-
16	-	72
17	68	-
18	-	70
19	70	-
20	-	71
Average	71.1	71.9

This result signifies that the bulk fracture strength of ferromagnetic materials is not observed to be affected by the application of an external magnetic field. This is, however, so because the observation itself is made over a considerable period of time. The time required for the fracture of an impact test specimen is substantial compared to that involved in the fracture of an asperity junction. For, if the velocity at which the impact test specimen is sheared is overestimated to be $\simeq 10^5$ cm/sec (shear wave velocity) it takes $\simeq 10^{-4}$ sec to shear a 10 mm x 10 mm test specimen. Even this gross underestimate of the time is considerably larger than the usual asperity junction life, during which the effect of magnetic field on wear is observable. During such large times the dislocation density near the notch of an impact test specimen will always reach ρ_{lim}, during the testing time, both in the magnetised case as well as in the unmagnetised case.

It is therefore, worth pointing out that if specimens of the order of asperity size could be tested for impact strength the effect of magnetic field could be observable. Perhaps, the fracture strength would be observed to be reduced. For the present, however, it is concluded that the application of an external magnetic field has no effect on the fracture strength of materials.

5.2.3 Effect of Magnetic Field On the Machining Force

To investigate whether magnetic field affects the gross plastic deformation at high strain rates it was considered to perform some appropriate tests. Accordingly, metal cutting tests were performed in which the components of the cutting force were recorded on a recorder. The general arrangement of the set up is shown in Figure 5.4. The test conditions are indicated below.

(i)	Job material	Mild Steel
(ii)	Tool material	H.S.S.
(iii)	Magnetic field strength (applied to tool only)	125 Oe (d.c.)
(iv)	Cutting speeds used	40 m/min, 100 m/min.
(v)	Feed rate	.05 mm/rev.
(vi)	Cutting conditions	dry
(vii)	Tool geometry	(12-8-10-10-15-10-1.5)

A three component Lebow Dynamometer was used for sensing the components of the cutting force. The signal from the dynamometer was recorded on a Sanborn Recorder. A typical trace obtained in such a test is shown in Figure 5.5. It is seen from the trace that the application of the magnetic field does not have any effect on the force components.

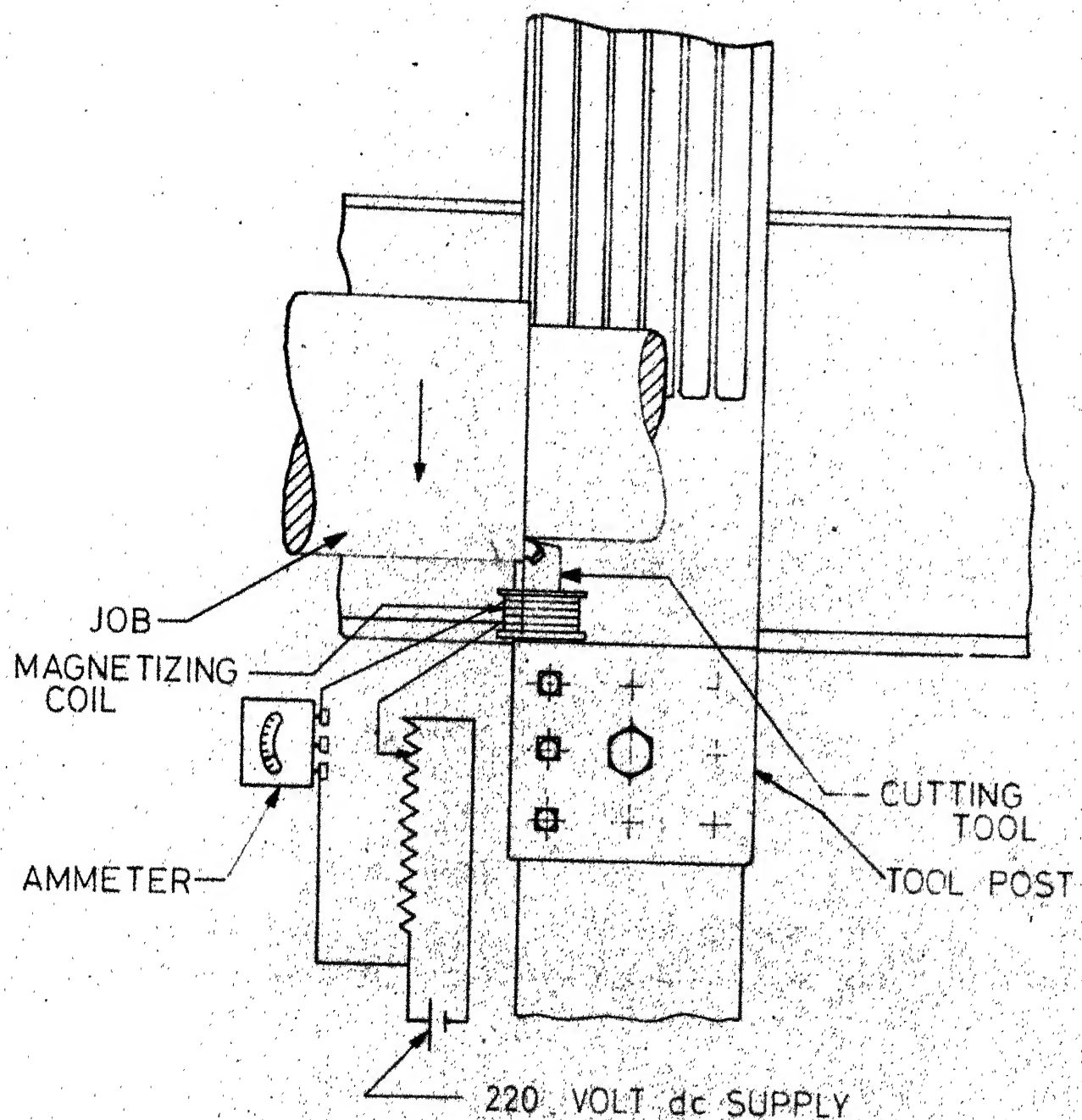

Schematic view of the experimental set-up for cutting tests.

Fig. 5.5 Recorder Trace Of Cutting Force

It is to be observed that the components of the cutting force, are dependent on, η_o, φ_s and α_o where,

η_o = Angle of friction

φ_s = Shear plane angle

α_o = Rake angle.

Since none of the components of the forces showed any change on the application of the field it is concluded that η_o and φ_s are not influenced to any observable extent.

Since changes in cutting forces occur as a result of change in the strength of the job or changes in η_o, φ_s and α_o, it is concluded from this test that neither the strength nor the mechanism of cutting has been influenced by the magnetic field. The change in η_o and φ_s would also be affected as a result of change in material property only. Therefore, this series of tests confirmed that the magnetic field has no influence on the macroscopic properties of the materials, during plastic deformation at high strain rates.

5.2.4 Effect of Magnetic Field on Static Diffusion

In order to investigate whether the application of a steady magnetic field has any influence on the diffusivity of a ferromagnetic material a static

diffusion test was conducted. The details of the test conducted are as follows :

(i)	Materials of the diffusion couple	Commercial Copper and mild steel.
(ii)	Temperature	650 ^{o}C ± 5 ^{o}C
(iii)	Duration of Diffusion	48 hrs and 72 hrs.
(iv)	Strength of the magnetic field used.	200 Oe.

Figure 5.6a shows the experimental set up used for the purpose. The vertical sliding furnace of the Riehle Creep machine was found to be the most convenient for the purpose. Two identical diffusion couples were placed side by side in the furnace which could be opened on both the sides. One of the diffusion couples formed a link in the magnetic circuit while the other one was kept beside it within the furnace. This ensured that both the diffusion couples were maintained at exactly same temperature, while only one of them was subjected to the influence of the magnetic field. The diffusion couples consisted of a tapered copper pin press fitted into an identical tapered hole in a short steel cylinder. Press fitting was done between two flats of a compression testing machine. A typical specimen under preparation is shown in Figure 5.6b.

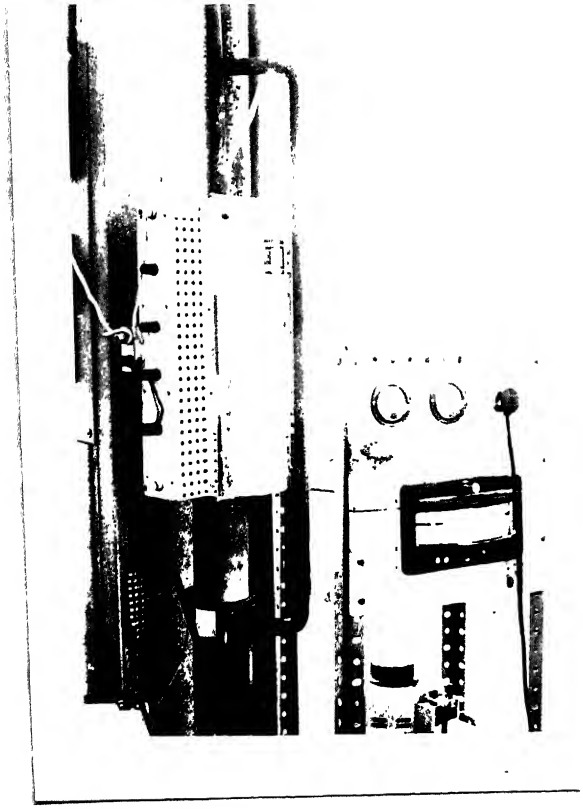

(a)

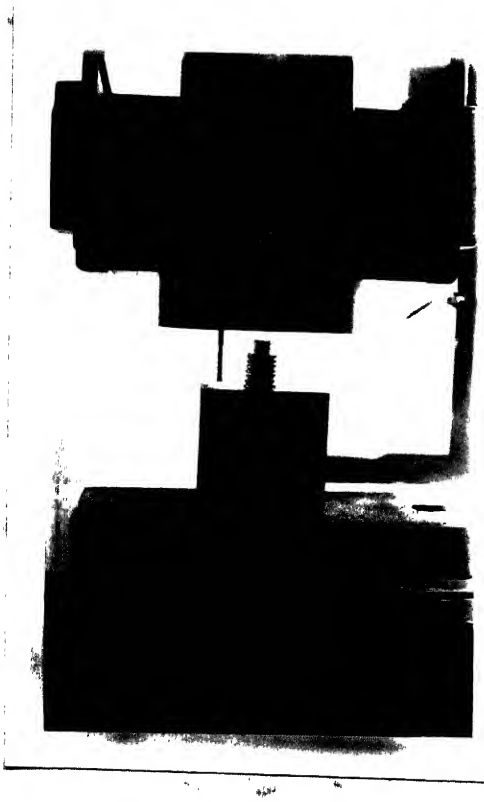

(b)

Fig.5·6 (a) Experimental Set-up For Static Diffusion Test.
(b) A Test Specimen Under Preparation.

After diffusion anneal for specified time (48 hrs. in one test and 72 hrs. in another), the faces of the samples were ground on a surface grinder and polished on a vibrator, to yield mirror finish. Micro-indentations were made at several locations on both sides of the copper-steel interface. These indentations were made under specified conditions on a PMT-3 (USSR) Microhardness tester fitted with a diamond pyramid 60° - indentor. The typical variation of the size of these indentations across the interface is shown in Figure 5.7. The size of these indentation markings is a measure of the hardness variation across the interface and also that of the transfer of material across the interface. Transfer of iron from the steel side into the copper side would increase the hardness on the copper side of the interface. The size of the indentations on the copper side would correspondingly be smaller. As seen from Figures 5.7a and 5.7b, the size variation of indentations is almost identical in both the magnetised and the nonmagnetised samples. Tests at various temperatures and for different timings showed repeatedly that there was no measurable difference in size variation of indentations in the two cases. The actual hardness values are directly related to the length of the diagonal of the indentations. Values of the diagonals of these indentations in a typical test are given in Table 5.2. It can be seen

(a)

(b)

Fig. 5·7. Indentation Across Copper–steel Interface, In The
(a) Absence Of Magnetic Field.
(b) Presence Of Magnetic Field.

Table 5.2

Dimensions of the indentations across the interface of a Copper-Steel Diffusion-Couple

Operating Temperature = 650 °C ± 5 °C

Indentation Load = 100 grams

Duration of diffusion = 72 hours

Duration of the load = 15 sec.

Strength of the magnetic field = 200 Oe

Serial number of the indentations measured from the interface into the bulk of the Copper	Lengths of the diagonals of the indentations (mm). (x 200)					
	Without field			With field		
	a′	b′	Average	a′	b′	Average
1	13.22	13.13	13.175	13.21	13.22	13.215
2	13.05	13.02	13.035	12.03	12.01	12.02
3	13.51	13.21	13.36	12.20	12.05	12.125
4	-	-	-	12.51	12.11	12.31

from these values, that there is no perceptible difference in hardness of copper in the two cases.

Chemical analysis of a thin surface layer of the copper pin was done in order to test whether iron has at all diffused from steel side into copper. The iron estimation in copper was done according to IS : 440 - 1964. In both the magnetised and the unmagnetised cases, the percentage of iron in copper was found to be about 2%. This estimation cannot be considered to be absolutely reliable, since only 0.2 grams of the sample were available for chemical analysis. According to IS : 440 : 1964 a minimum of 2 grams of the sample have to be used for this test. In any case, the test clearly showed that there was no perceptible difference in the percentage of iron in the two cases, even though there was perceptible quantity of iron in copper in both the cases.

These static diffusion tests and the iron analysis, led the author to draw the conclusion that magnetic field has no significant effect on static diffusion. Since, at a particular temperature, diffusion rate is strongly dependent upon the activation energy for diffusion, magnetic field has obviously no observableinfluence on the activation energy for diffusion. This is an important result as it suggests that there is no fundamental change in the energy of

formation or movement of a vacancy. It was shown in section 4.3 that the application of an external magnetic field cannot affect the activation energy for diffusion to any measurable extent. Correspondingly the results of the static diffusion test presented here are in conformity with the theoretical postulate test of that section. Thus it is confirmed that in unstrained conditions an external magnetic field has no influence on the diffusivity of a ferromagnetic material. But,as discussed in section 4.5, in a deforming ferromagnetic body the magnetic field can enhance the diffusivity under some conditions.

5.2.5 Effects of Magnetic Field on Internal Stress

This test was conducted to find out to what extent an external magnetic field reduces the internal stress of a ferromagnetic material. For this purpose several identical test specimens of mild steel were prepared according to IS : 1608 - 1972. Few of them were tested for stress relaxation under magnetic field and few without any magnetic field.

The stress relaxation tests were conducted on an Instron testing machine (Model No. TCTML). The test samples were mounted between the grips of the machine and were subjected to the usual tensile test. When the load reached a value close to the ultimate

level, the cross head motion was stopped and specimen was allowed to relax. After a sufficiently long time the stress is expected to reach the value of the internal stress. However, since in the present test the objective was only to find out the change caused by the influence of the magnetic field it was considered unnecessary to carry on the test for a long period. Accordingly, this test was terminated after about twenty minutes.

The results of this test are shown in Figure 5.8. As can be seen from these test results, there is a reduction in the internal stress of the mild steel specimen when tested in presence of magnetic field. The magnitude of this reduction is approximately 0.6 kg/mm^2. This value agrees quite well with the theoretical value of $\lambda_s G$,* the magnetostrictive stress opposing the motion of dislocations through the domain wall. This test clearly demonstrated that the prominent effect of an external magnetic field to deforming body is to reduce the internal stress by a small amount of $\simeq$ 0.5 kg/mm^2. Correspondingly, the bulk strength of the material also decreases roughly by the same magnitude as discussed in section 4.2.

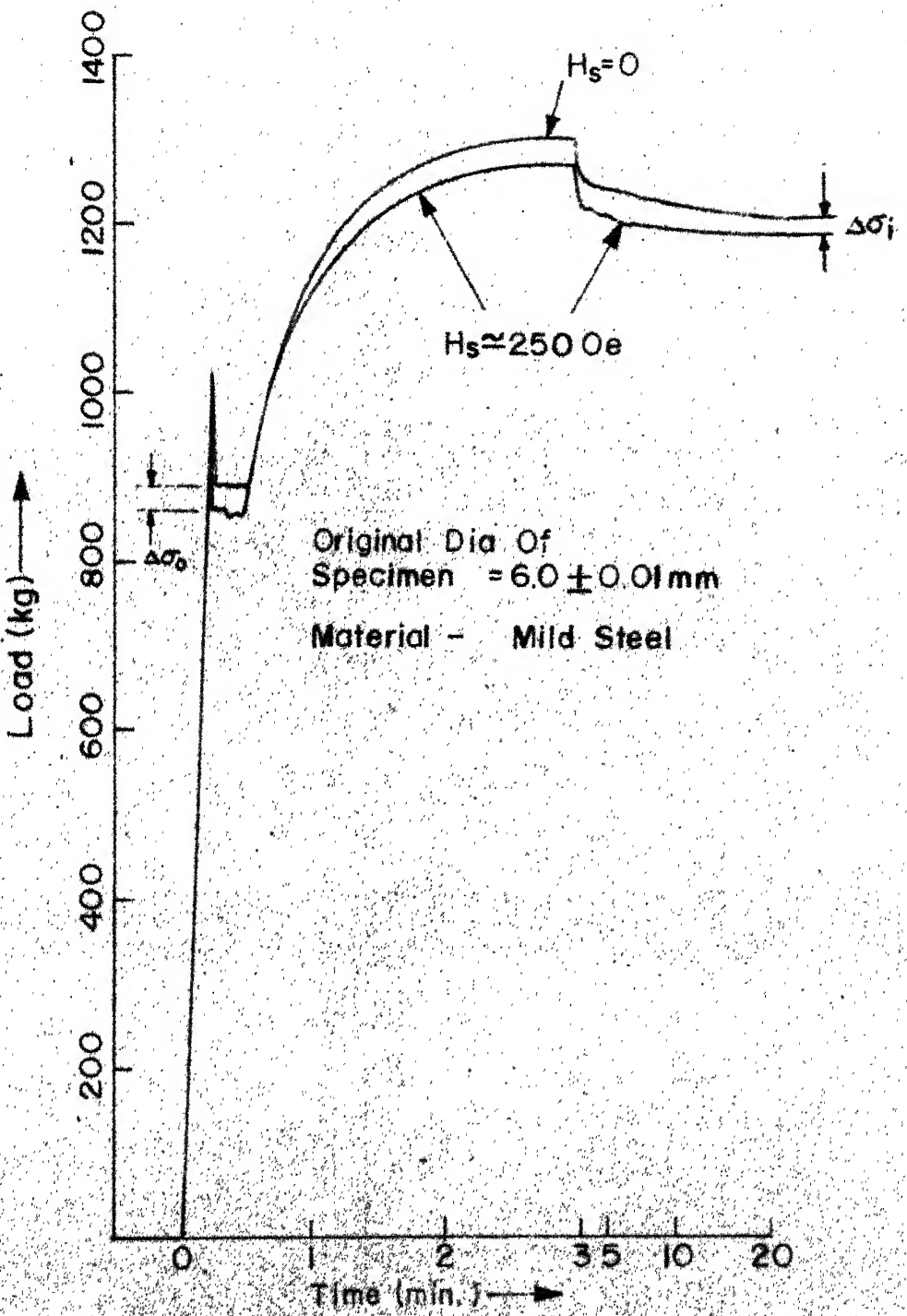

Fig.5.8 Stress Relaxation Test

5.2.6 Wear Experiments

General features common to all the wear tests presented in this work, are indicated below :

All the wear tests were performend on a HMT Lathe (Model - LB 25). machine.

All rubbing tests were performed in dry condition and against a fresh surface of a cylinder mounted on the lathe. Figures 5.4 and 5.9 show the general experimental set up used in the rubbing tests. Whenever, the job or the tool was to be magnetised a suitable solenoid designed for the purpose was energized. The solenoid was put in series with a d-c power supply which was adjusted so that a specified current passed through the solenoid coil. All the wear tests were conducted within the speed limits of about 10 m/min to 200 m/min. Also, for all the tests only one feed rate of 0.05 mm/rev., was employed. Care was taken that roughly same magnitude of wear occurred at various speeds. This is important for keeping the results within same order of errors at various speeds. If rubbing time is keptsame at different speeds it results in different volumes of metal removal. This would naturally introduce different percentage errors at different speeds. To ensure uniform order of errors, the rubbing times were so adjusted that the linear dimensions of the worn regions were of nearly same magnitude.

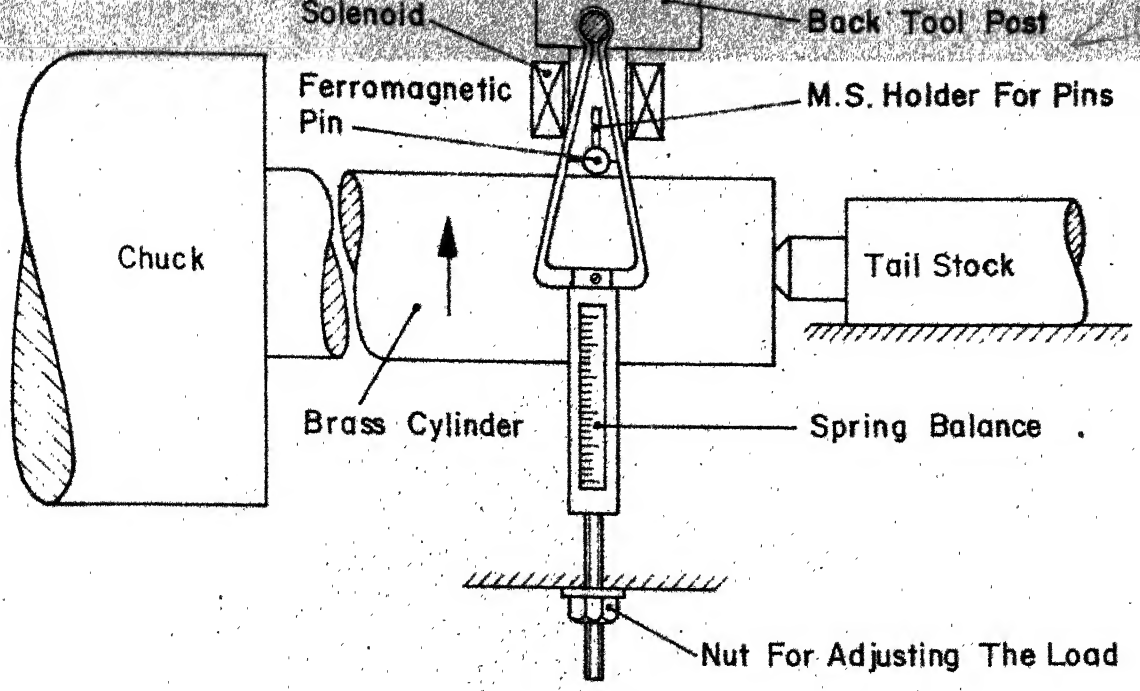

(b) Rubbing Of Ferromagnetic Pins Against a Non-Magnetic Body.

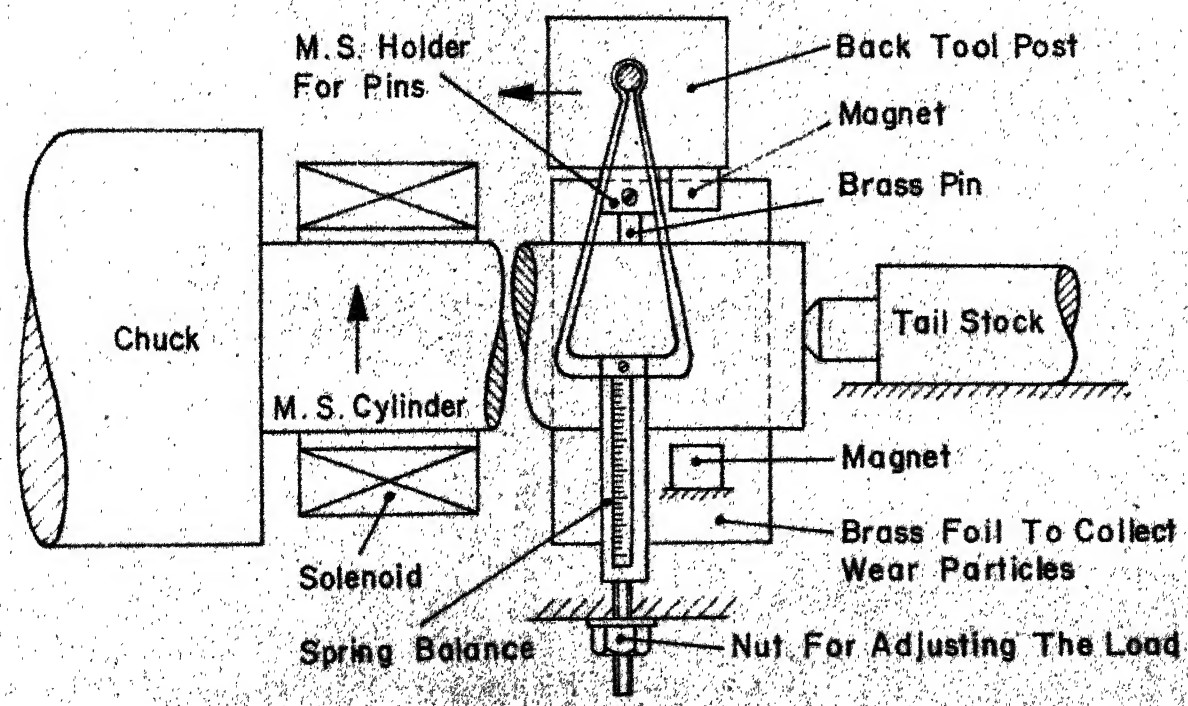

(c) Rubbing Of Non-Magnetic Pins Against a Ferromagnetic Body.

Fig. 5.9 Schematic View Of The Experimental Set Ups For Rubbing Experiments On Pins.

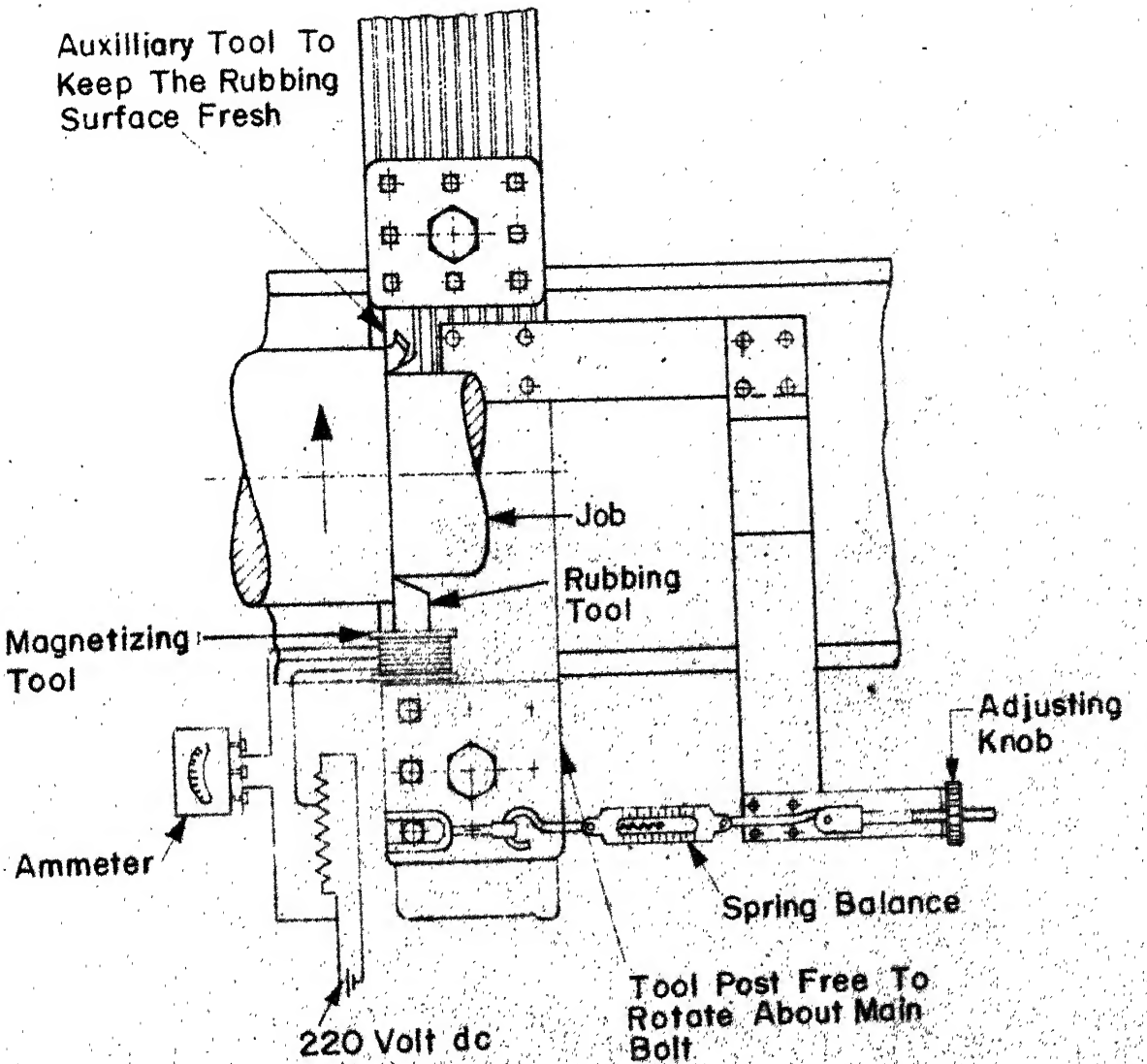

Fig.5.9a Schematic View Of The Experimental Set-Up For Rubbing Experiments On Tools.

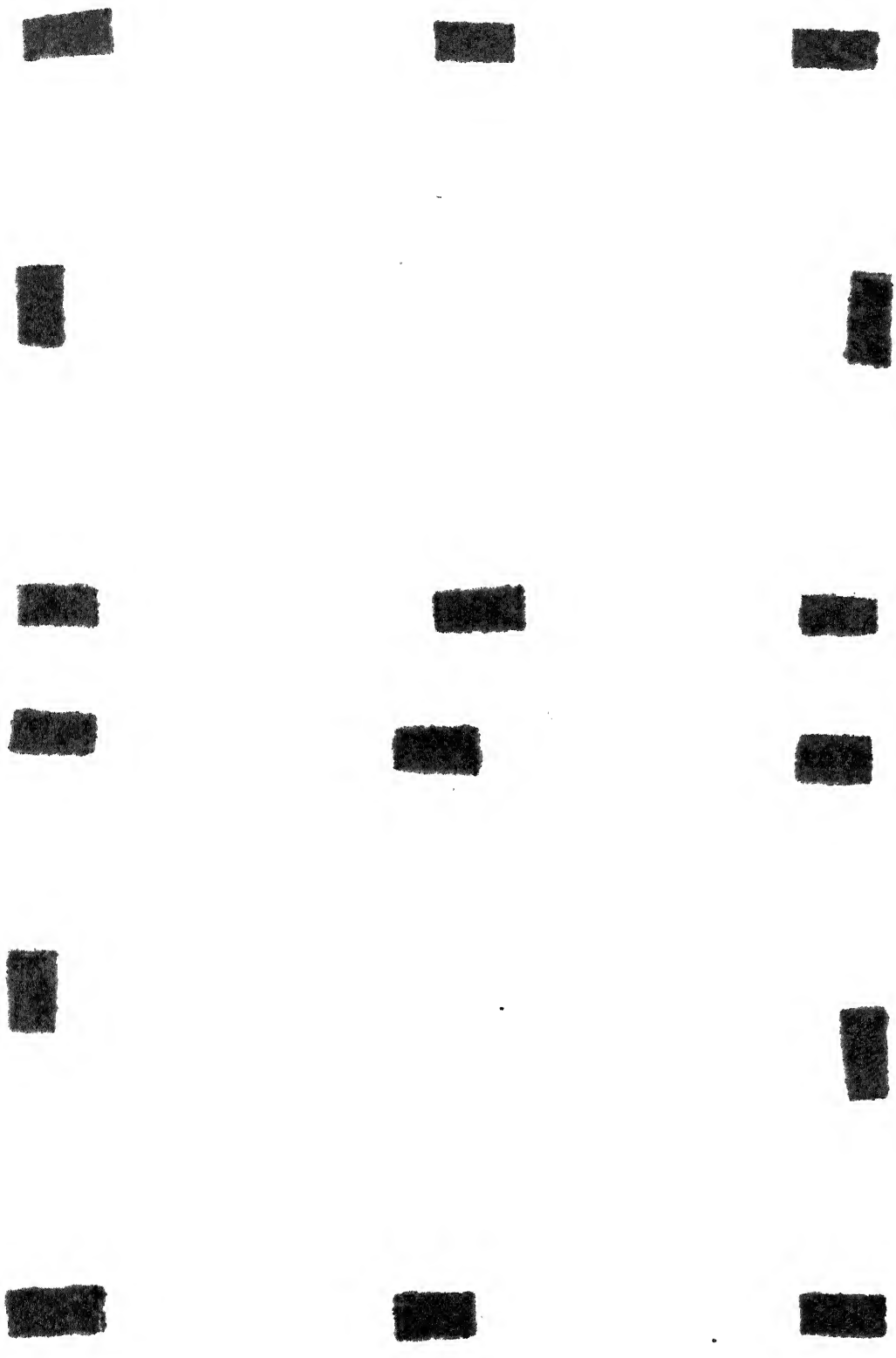

Fig.5·9d. An Actual Experimental Set-up For Wear Experiments.

Measurements of wear was done with the help of a travelling microscope, optical projector and microbalance depending upon the particular case.

When rubbing experiments were performed the load was applied by means of a spring balance as shown in Figure 5.9. The insertion and the removal of the tool or pin was done in a manner so that the spring balanced was not disturbed. This ensured that for a particular set of experiments the load once adjusted was maintained unchanged. Also the overhang of the tool or the holder for pins was always kept the same.

All the readings were repeated five times and the average value of wear was derived from these readings. This was done both for the magnetised as well as for the unmagnetised cases.

The details about the individual tests are presented in the following sections.

5.2.7 Machining of Non-Magnetic Job By Ferromagnetic Tools

In this series of tests an aluminium bar was machined at various speeds with the help of mild steel (0.25%C) tools. A large number of identical tools of mild steel (0.25%C) were prepared. Blanks for these tools were cut from the same plate taking care that all the tools had their longitudinal axes in

the direction of the grain of the plate. This was done to ensure that all the tools had fairly identical distribution of crystallographic directions. Since the magnetostriction coefficient is different in different directions, an identical distribution of grain directions would possibly ensure identical magnetisation effects in all the tests. All these tools were ground to the geometry 0 - 10 - 15 - 10 - 15 - 0 - 1 (mm) (ASA lathe tool designation). Grinding of the tools was done on Tool and Cutter Grinder. Whenever required a steady current was passed through the solenoid to magnetise the tool. Flank wear was measured with and without magnetic field and gain factor $G \left(= \frac{h_o - h_m}{h_o}\right)$ calculated. Measurements of the flank wear were done using a travelling microscope with a least count of 0.02 mm.

It was found that the wear of the mild steel tools was always increased when cutting was done in presence of magnetic field. Every reading was repeated five times to put this observation on a firm footing. The net wear was calculated as the average of the five readings. Gain factor G was calculated from these average values. These observations of flank wear are shown in Table 5.3.

It was observed that as the cutting velocity was changed the gain factor G varied in the manner

TABLE 5.3

MACHINING OF ALUMINIUM CYLINDER BY MILD STEEL TOOLS

Feed = .05 mm/rev. Magnetic Field Strength = 125 Oe

Width of cut (t) = 1.5 mm.

Cutting speed (m/min)	Time of machining (min.)	Flank Weak, h_o, without Field (mm) 1	2	3	4	5	Average wear, h	Flank wear (mm) with Field (h_m) 1	2	3	4	5	Average wear h_m	Gain Factor
10	5	.84	.84	.90	.93	.89	.88	.97	.95	.96	.98	.97	.968	-0.1
15	5	.94	.85	.93	.92	.89	.92	1.01	1.20	1.18	1.15	1.02	1.15	- .25
50	2	.46	.49	.48	.48	.50	.482	.68	.66	.66	.72	.69	.682	- .42
65	2	.48	.48	.52	.54	.46	.496	.74	.71	.70	.72	.71	.720	- .51
90	1.5	.50	.51	.50	.52	.51	.508	.75	.75	.74	.73	.75	.74	- .45
100	1.5	.51	.52	.50	.51	.51	.508	.76	.75	.74	.75	.76	.75	- .50
105	1.5	.51	.49	.49	.56	.55	.519	.63	.66	.64	.63	.64	.64	- .2
130	1	.66	.66	.65	.62	.65	.65	.90	1.10	.92	.91	1.09	1.95	- .4
145	1	.77	.76	.79	.83	.83	.790	1.03	1.01	1.05	1.04	1.04	1.03	- .3
170	1	1.00	1.02	1.10	1.00	.90	1.004	1.05	1.10	1.00	1.04	1.06	1.05	- .07

CC-0. Mumukshu Bhawan Varanasi Collection.

shown in Figure 5.10. It can be observed that G is throughout a negative quantity. Also, as speed increases, the magnitude of G also increases. But, after reaching a maximum value of $\simeq$.47 at a speed of $\simeq$100 m/min., the gain factor G decreases in magnitude as speed is further increased.

The general features of the curve are therefore tallying with the theoretical predictions presented in section 4.4.

5.2.8 Rubbing of Ferromagnetic Tools Against a Non-magnetic Job.

This test was conducted essentially to confirm whether the kind of results obtained in the previous test are restricted to cutting operation only. It was also necessary to check whether the effect was due to the particular combination of materials or not. In this test therefore, identical mild steel tools were rubbed against a brass cylinder. Similar, but different tools than those used in the cutting test were used in this test. Rubbing was always done against a fresh surface as shown in the general experimental set up shown in Figure 5.9a. A constant load of 12.0 kg was applied to the tool by means of a spring balance. Table 5.4 gives the magnitude of the flank wear of the rubbing tools obtained in this test. The gain factor G was calculated

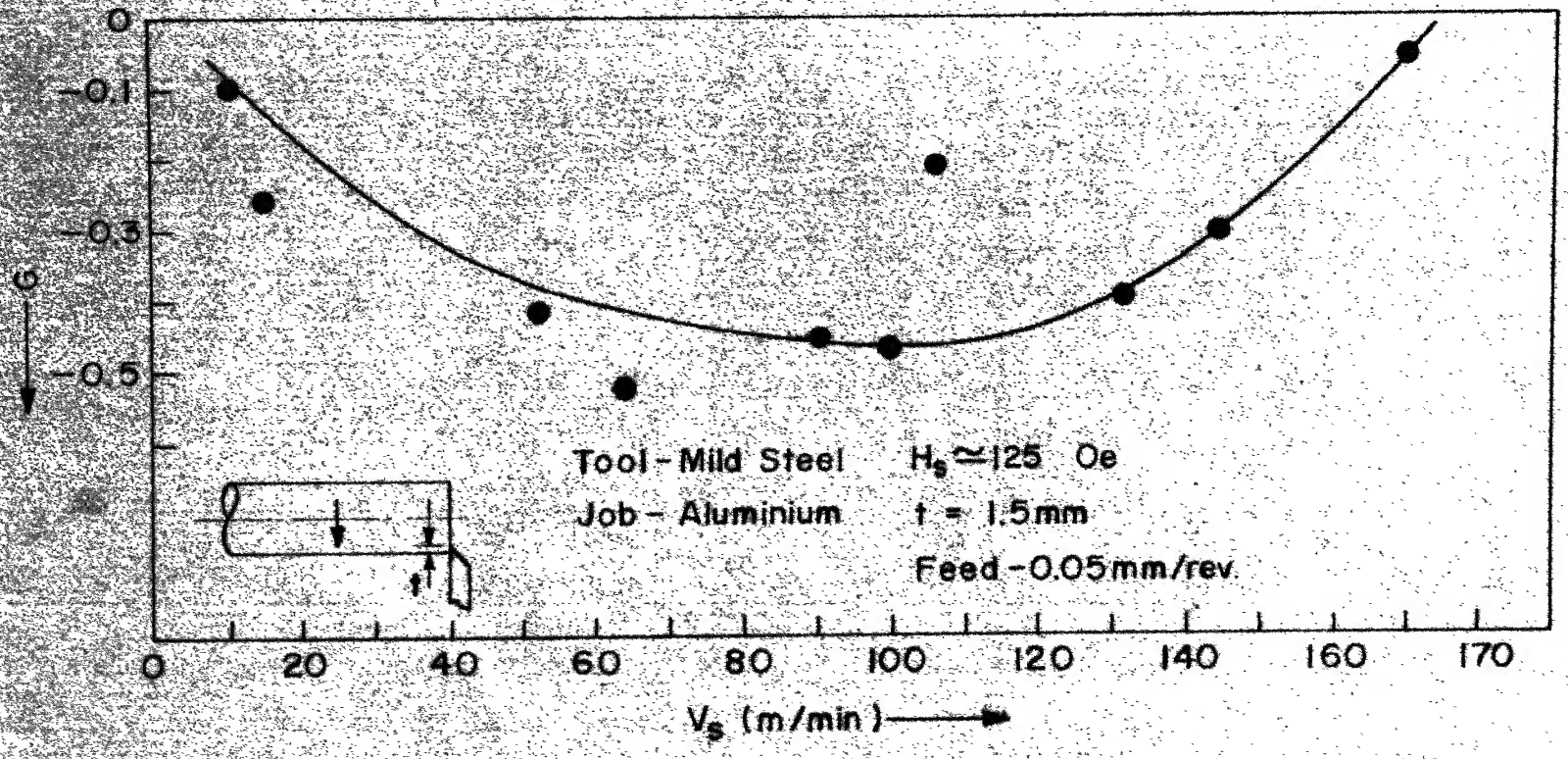

Fig5.10 Variation Of Gain Factor With Cutting Velocity

TABLE 5.4

RUBBING OF MILD STEEL TOOLS AGAINST BRASS JOB

Feed = .05 mm/rev. Magnetic Field Strength 125 Oe

Width =1.5 mm Load (N) = 12 kg
cut 't)

Rubbing speed (m/min.)	Rubbing time (min.)	Flank wear (mm) without field (h_o)					Average (h_o)	Flank wear (mm) with field h_m)					Average (h_m)	Gain factor
		1	2	3	4	5		1	2	3	4	5		
10	3	.47	.48	.49	.49	.47	0.481	.53	.54	.52	.53	.53	.530	- .1
40	3	.81	.82	.82	.81	.81	.814	1.20	1.21	1.20	1.22	1.21	.977	- .2
80	3	1.02	1.04	1.01	1.00	1.01	1.016	1.37	1.38	1.36	1.35	1.35	1.37	- .35
130	2	.86	.85	.84	.83	.85	.848	1.14	1.14	1.16	1.16	1.5	1.1	- .35
155	1.5	.78	.80	.80	.81	.77	.792	1.08	1.09	1.09	1.07	1.08	1.0	- .37
180	1	1.01	1.00	.99	.98	.97	.990	1.14	1.14	1.14	1.17	1.12	1.1	- .15

again in the same manner as discussed in the preceeding section. The results of this test are shown in Figure 5.11. These results are in good agreement with those obtained in the earlier test as well as the theoretical predictions of section 4.4.

This test therefore, clearly demonstrated that application of magnetic field to a sliding pair results in greater wear of the ferromagnetic body.

5.2.9 Rubbing of Ferromagnetic Pins Against Non-magnetic Surface

In this kind of test three separate series of experiments, mentioned below were conducted.

5.2.9.1 Rubbing of mild steel pins against a brass cylinder

5.2.9.2 Rubbing of pure iron pins against a brass cylinder

5.2.9.3 Rubbing of pure nickel pins against a brass cylinder.

These above mentioned tests were performed in an identical manner. The pins were mounted firmly in a holder designed for the purpose. The general experimental set up, common to all these tests is shown in Figure 5.9b. It can be seen from this figure that the manner of the contact between the pin and the cylinder was such that their axes were normal to one another.

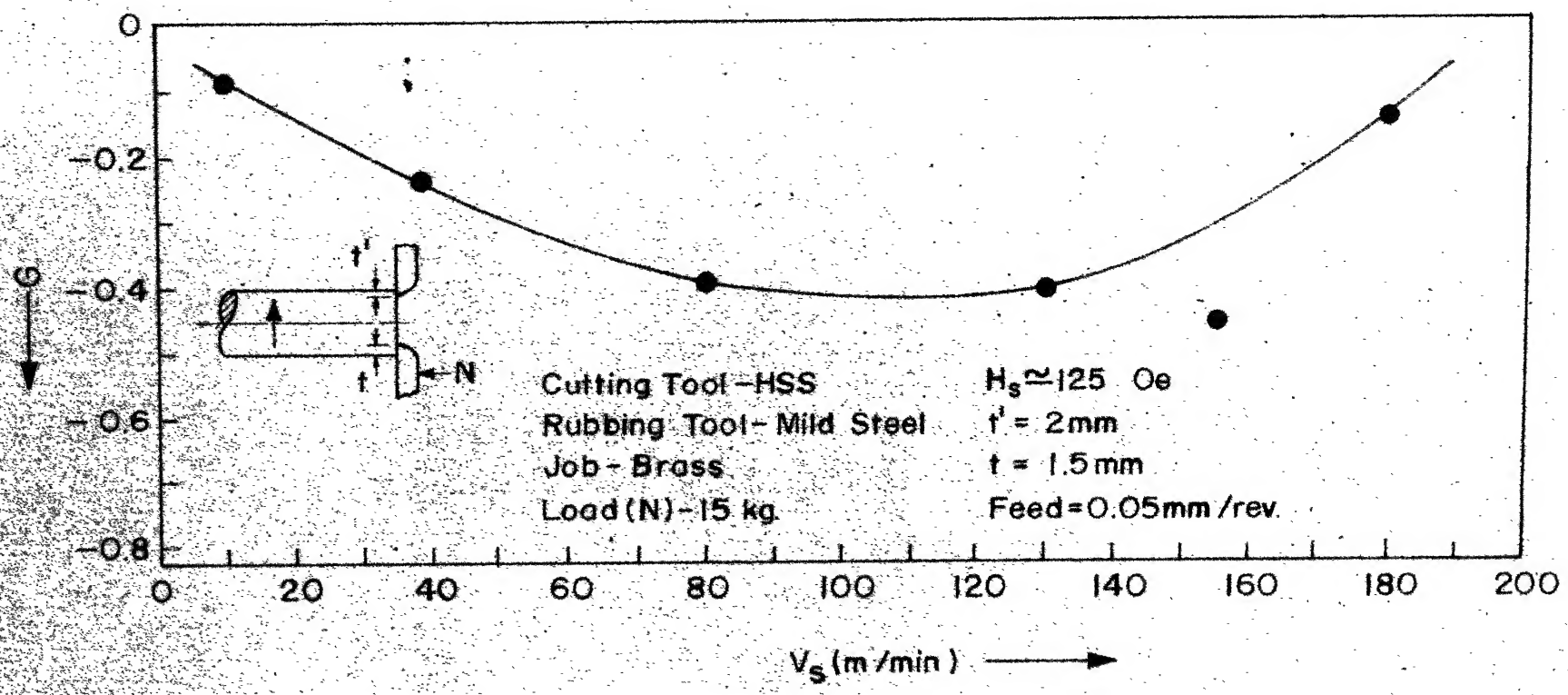

Fig.5.11 Variation Of Gain Factor With Rubbing Velocity

As in the previous tests in these tests also rubbing was performed at various speeds and at a feed rate of .05 mm/rev. The shape of the wear scar produced on these pins was elliptical as can be easily visualised from the geometrical configuration of the contact. Photograph of such a typical wear scar is shown in Figure 5.12. The volume of wear removed from the pin in such a contact is proportional to the fourth power of the major axis of the elliptical scar on the pin (Appendix). The values of the major axis of the wear scar obtained in these rubbing experiments are shown in Tables 5.5 - 5.7.

Thus in these experiments the gain factor G was calculated as :

$$G = \frac{K_1 d_{o,o}^4 - K_1 d_{o,H}^4}{K_1 d_{o,o}^4}$$

$$= \frac{d_{o,o}^4 - d_{o,H}^4}{d_{o,o}^4} \qquad (5.1)$$

In all these experiments, the gain factor G turned out to be a negative quantity. Also, the variation of G with the rubbing speed has the same trend as seen in the case of mild steel tools rubbing or cutting a brass cylinder or an aluminium job, respectively. This can be seen from Figures 5.13 - 5.15. Other features relevant to the particular experiment considered are also shown in these figures. The measurements of these wear scars was done on an Optical Projector.

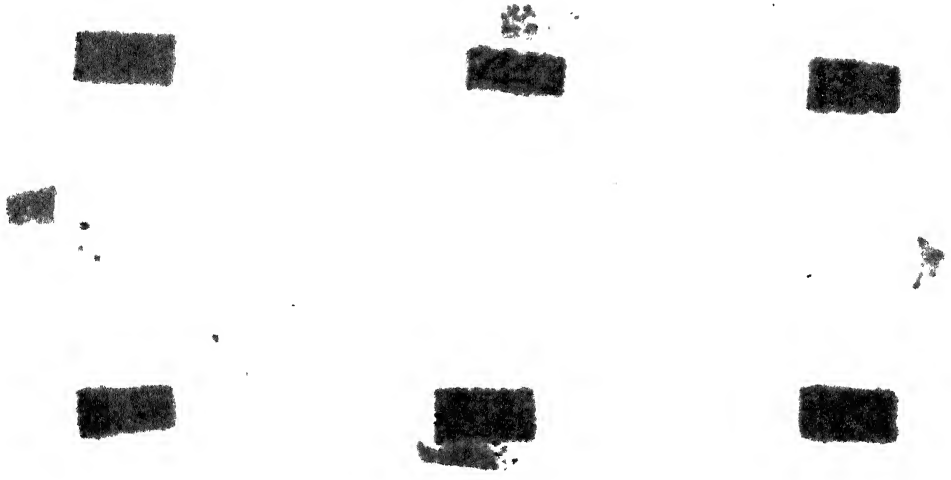

Fig. 5·12 Photograph Of Typical Wear Scars.

TABLE 5.5a

RUBBING OF MILD STEEL PINS AGAINST BRASS CYLINDER

Feed = 0.05 mm/rev.
Dia of m.s. pins = 6.0 mm
Dia of brass cylinders = 55 mm

Magnetic Field Strength = 250 Oe
Load = 16 kg

Rubbing speed (m/min)	Rubbing Time (mtn)	Wear of pin, $d_{o,o}$ without field (mm)	Average $d_{o,o}$ (mm)	Wear of pin, $d_{o,H}$, with field (mm)	Average $d_{o,H}$ (mm)	Gain factor
8	5	1.805, 1.951, 1.985 2.105, 2.210	2.012	2.161, 2.110, 2.090 2.160, 2.210	2.152	- .33
15	5	4.673, 4.752, 4.735 4.712, 4.692	4.712	5.14, 5.10, 5.11, 5.09, 5.08	5.109	- .375
35	5	6.330, 6.271, 6.320 6.341, 6.286	6.311	7.121, 7.145, 7.109 7.125, 7.090	7.122	- .61
55	4	5.940, 5.940, 5.930 5.921, 5.920	5.930	5.981, 6.250, 6.301 6.352, 6.333	6.240	- .61
70	2	4.322, 4.310, 4.315 4.326, 4.327	4.322	4.861, 4.864, 4.860 4.855, 4.866	4.861	- .57
95	2	5.521, 5.540, 5.501 5.485, 5.500	5.510	6.352, 6.409, 6.381 6.380, 6.390	6.382	- .825
120	1	4.07, 4.031, 4.009 3.981, 4.010	4.020	4.331, 4.381, 4.362 4.352, 4.381	4.361	- .375
150	1	7.730, 7.720, 7.701 7.709, 7.711	7.714	7.920, 7.940, 7.910 7.952, 7.951	7.940	- .15

TABLE 5.5b

RUBBING OF MILD STEEL PINS AGAINST BRASS CYLINDER

Feed = .05 mm/rev.

Dia of m.s. pins = 6 mm

Dia of brass cylinder = 55 mm

Magnetic Field Strength = 125 Oe

Load = 16 kg

Rubbing speed (m/min)	Rubbing Time (min)	Wear of pin, $d_{o,o}$, without field (mm)	Average $d_{o,o}$ (mm)	Wear of pin, $d_{o,H}$ with field (mm)	Average $d_{o,H}$ (mm)	Gain factor
8	5	4.510, 4.531, 4.511, 4.509, 4.489	4.510	4.694, 4.749, 4.770 4.760, 4.759	4.750	- 0.225
35	5	6.410, 6.403, 6.415, 6.412, 6.399	6.409	6.190, 6.160, 6.120 6.152, 6.141	6.151	0.30
55	4	5.930, 5.921, 5.909, 5.932, 5.911	5.921	6.330, 6.292, 6.116 6.431, 6.273	6.280	0.255
70	2	4.729, 4.710, 4.730, 4.724, 4.720	4.721	4.908, 4.921, 4.899 4.903, 4.915	4.909	- 0.165
95	2	4.509, 4.524, 4.530, 4.523, 4.520	5.521	5.549, 5.602, 5.522 5.538, 5.592	5.541	- 0.15

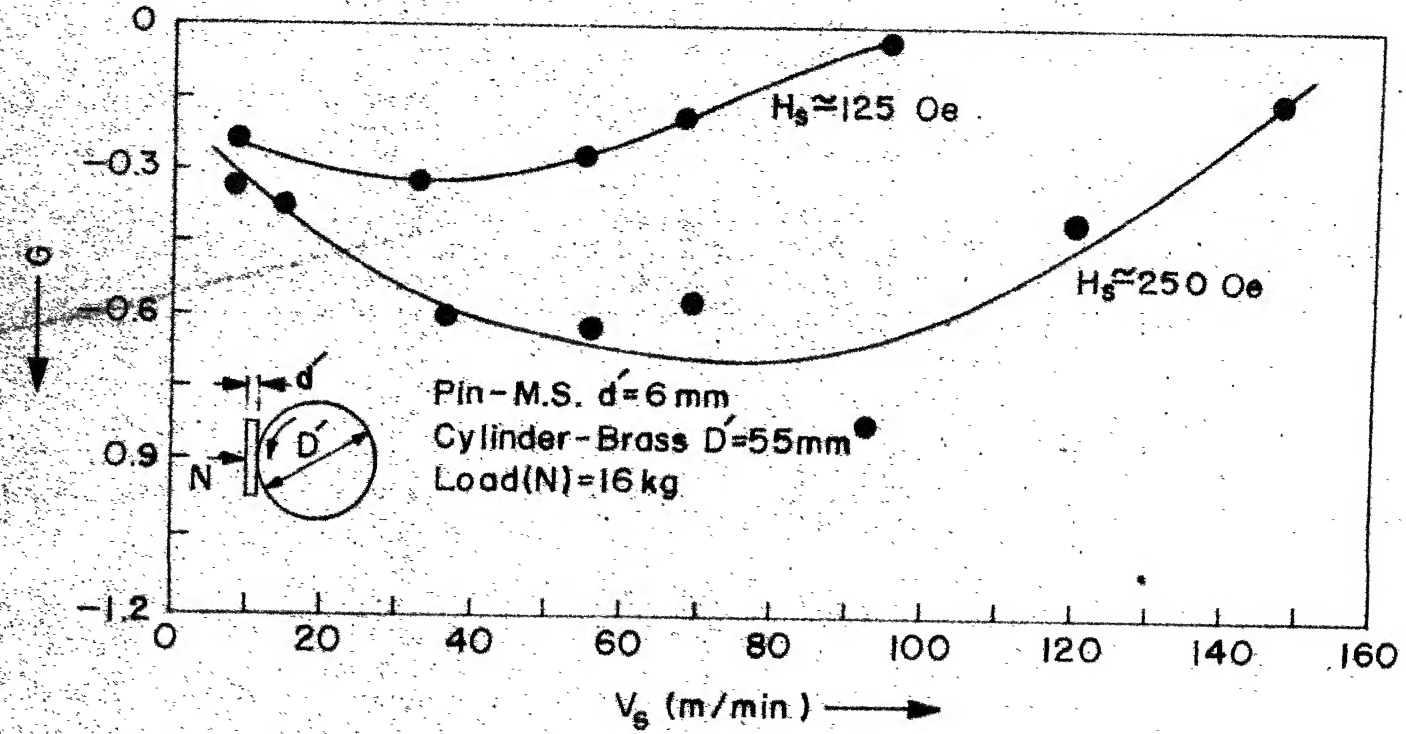

Fig.5.13 Variation Of Gain Factor With Rubbing Velocity

TABLE 5.6

RUBBING OF PURE IRON PINS AGAINST BRASS CYLINDERS

Feed = 0.05 mm/rev.

Dia of iron pin = 4.0 mm

Dia of brass cylinder = 53 mm

Magnetic Field Strength = 250 Oe

Load = 16 kg

Rubbing speed (m/min)	Rubbing time (min)	Wear of pin, $d_{o,o}$, without field (mm)	Average $d_{o,o}$	Wear of pin, $d_{o,H}$ with field (mm)	Average $d_{o,H}$	Gain factor
10	4	2.941, 2.933, 2.934, 2.915, 2.940	2.932	3.050, 3.090, 3.070 3.080, 3.078	3.076	- 0.2
18	4	3.051, 3.101, 3.009, 3.019, 3.021	3.052	3.201, 3.222, 3.212 3.192, 3.178	3.205	- 0.2
35	4	3.112, 3.151, 3.142, 3.109, 3.125	3.129	3.331, 3.380, 3.319 3.325, 3.320	3.335	- 0.3
55	4	3.251, 3.257, 3.270, 3.261, 3.250	3.257	3.471, 3.482, 3.472 2.468, 3.469	3.472	- 0.3
80	4	3.535, 3.512, 3.490, 3.501, 3.531	3.535	3.761, 3.780, 3.778 3.767, 3.765	3.770	- 0.3
120	2	2.660, 2.651, 2.648, 2.623, 2.641	2.651	2.710, 2.732, 2.751 2.743, 2.735	2.733	- 1.0
145	2	2.880, 2.871, 2.865, 2.857, 2.860	2.862	2.021, 3.015, 3.009 2.998, 3.004	3.005	+ 0.20

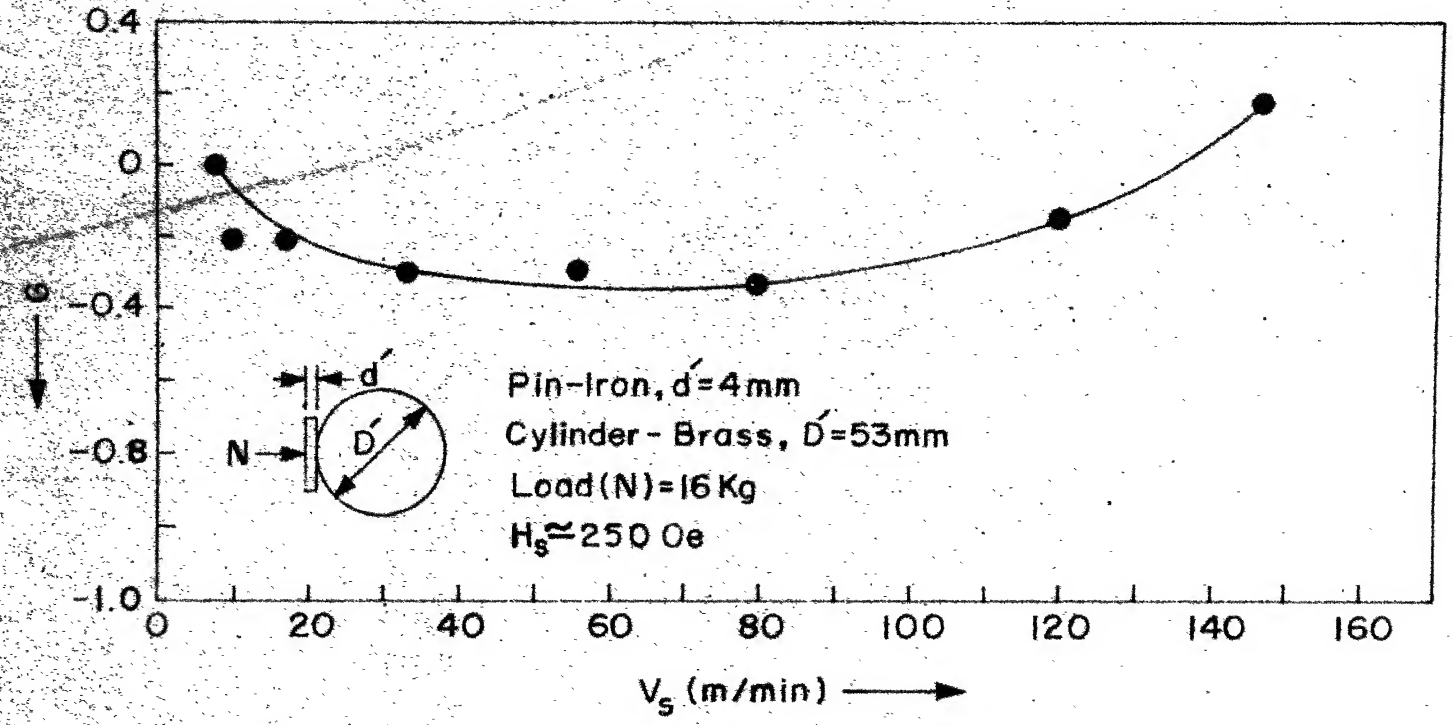

Fig.5.14 Variation Of Gain Factor With Rubbing Velocity

TABLE 5.7a

RUBBING OF NICKEL PINS AGAINST BRASS CYLINDER

Feed = 0.05 mm/rev.

Dia of Nickel Pins = 5 mm

Dia of Brass Cylinder = 50 mm

Magnetic field strength = 250 Oe

Load = 16 kg

Rubbing speed (m/min)	Rubbing time (min)	Wear of pin, $d_{o,o}$ without field (mm)	Average $d_{o,o}$	Wear of pin, $d_{o,H}$ with field (mm)	Average $d_{o,H}$	Gain factor
8	6	2.105, 2.182, 2.190 2.101, 2.019	2.119	2.241, 2.307, 2.302 2.300, 2.240	2.263	- 0.30
13	5	2.005, 2.001, 1.988 1.979, 1.990	1.993	2.205, 2.090, 2.199 2.209, 2.187	2.180	- 0.44
30	4	2.152, 2.200, 2.184 2.134, 2.160	2.169	2.651, 2.850, 2.712 2.652, 2.661	2.702	- 0.55
54	2	1.451, 1.402, 1.432 1.417, 1.410	1.422	1.511, 1.540, 1.509 1.482, 1.498	1.508	- 0.23
68	2	2.192, 2.183, 2.179 2.165, 2.178	2.179	2.221, 2.191, 2.192 2.192, 2.202	2.199	- 0.04

TABLE 5.7b

RUBBING OF NICKEL PINS AGAINST BRASS CYLINDER

Feed = .05 mm/rev

Dia of pin = 5 mm

Dia of Brass cylinder = 45.8 mm

Magnetic Field Strength = 125 Oe

Load = 16 kg

Speed (m/min)	Rubbing time (min)	Wear of pin, $d_{o,o}$ without field (mm)	Average $d_{o,o}$	Wear of pin, $d_{o,H}$ with field (mm)	Average $d_{o,H}$	Gain factor
8	6	2.151, 2.131, 2.136 2.141, 2.109	2.133	2.202, 2.211, 2.213 2.000, 2.178	2.202	0.15
13	5	2.001, 2.054, 1.981 2.024, 2.018	2.015	2.115, 2.149, 2.163 2.095, 2.143	2.135	0.23
20	5	2.100, 2.090, 2.110 2.110, 2.122	2.105	2.221, 2.224, 2.257 2.237, 2.254	2.240	0.29
30	4	2.752, 2.732, 2.741 2.756, 2.759	2.752	2.861, 2.843, 2.840 2.856, 2.843	2.848	0.15
54	2	1.527, 1.520, 1.502 1.512, 1.493	1.511	1.519, 1.511, 1.529 1.510, 1.528	1.514	0.01

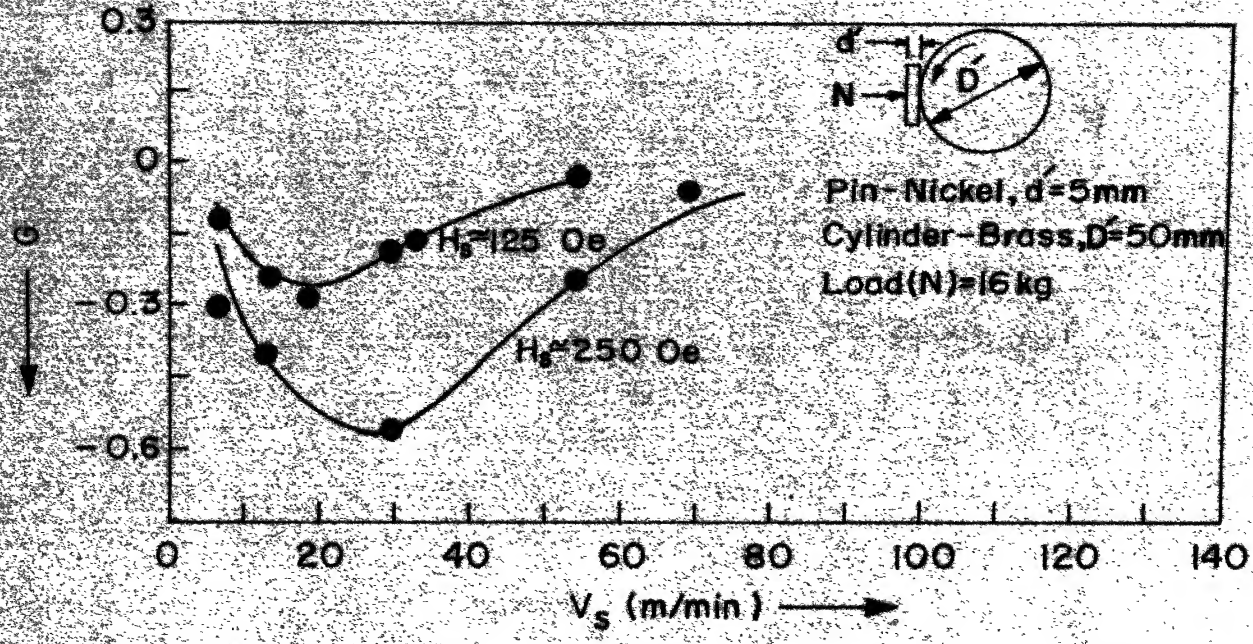

Fig.5.15 Variation Of Gain Factor With Rubbing Velocity

5.2.10 Rubbing of Non-magnetic Specimens Against a Ferro-magnetic Body

This test was conducted essentially to verify the hypothesis put forth by the author in section 4.3. In this section it was postulated that the increased probability of failure on one side of the asperity junction should lead to decreased probability of failure on the other side. Correspondingly, the application of an external magnetic field should reduce the wear rate of the non-magnetic body. To test this postulate large number of brass pins were rubbed against a mild steel cylinder at various speeds. The pins were rubbed with their ends pressed against the mild steel cylinder. The mild steel cylinder was magnetised by means of the solenoid mounted on it. These details of the experimental set up can be studied in Figure 5.9c.

The wear of the pins was calculated as the difference in weight of the pins before and after rubbing. The weight was found by means of a micro balance which had a least count of $\pm$ .00005 gms. The loss in weight of these pins at various speeds is given in Table 5.8 and plotted in Figure 5.16.

In this experiment an interesting trend of the gain factor G was observed. Upto a certain rubbing velocity the gain factor was positive. But,

TABLE 5.8

RUBBING OF BRASS PINS AGAINST MILD STEEL CYLINDER

Feed = 0.05 mm/rev.

Dia of brass pin = 6 mm

Dia of steel cylinder = 56 mm

Magnetic field strength = 125 Oe

Load = 8 kg

Rubbing speed (m/min)	Rubbing time (min)	Wear of pin, W^o without field (grams) x 10^3	Average W^o x 10^3	Wear of pin, W^H with field (grams) x 10^3	Average W^H x 10^3	Gain factor
10	2.5	13.21,13.21,13.60, 13.90,14.0	13.58	12.01,11.80,11.71, 12.10,11.91	11.9	+ 0.15
20	2.0	37.51,37.70,37.61, 37.70	37.62	28.62, 28.64,28.84, 28.64,28.80	28.7	+ 0.23
35	1.5	38.08,38.05,37.95, 38.02,38.06	37.82	30.25,30,62,30.01, 30.15,30.20	30.25	+ 0.25
40	1.5	45.10,45.07,44.95, 44.90,45.03	45.01	37.58,37.95,37.45, 38.01,37.05	37.51	+ 0.20
60	1.5	59.95,60.05,60.00, 59.90,59.97	59.98	55.95,55.76,55.80, 55.73,55.91	55.81	+ 0.075
70	1.5	75.57,75.28,75.40 75.38,75.45	75.42	79.01,79,15,79.11, 79.23,79.50	79.19	- 0.05
90	1.0	80.45,80.51,80.30 80.24,80.01	80.38	92.62,92.40,92.51, 92.38,92.30	92.44	- 0.15
104	1.0	100.16,100.25,99.982 100 .092,100.22	100.13	118.27,118.17,118.09 118.10,118.15	118.15	- 0.18

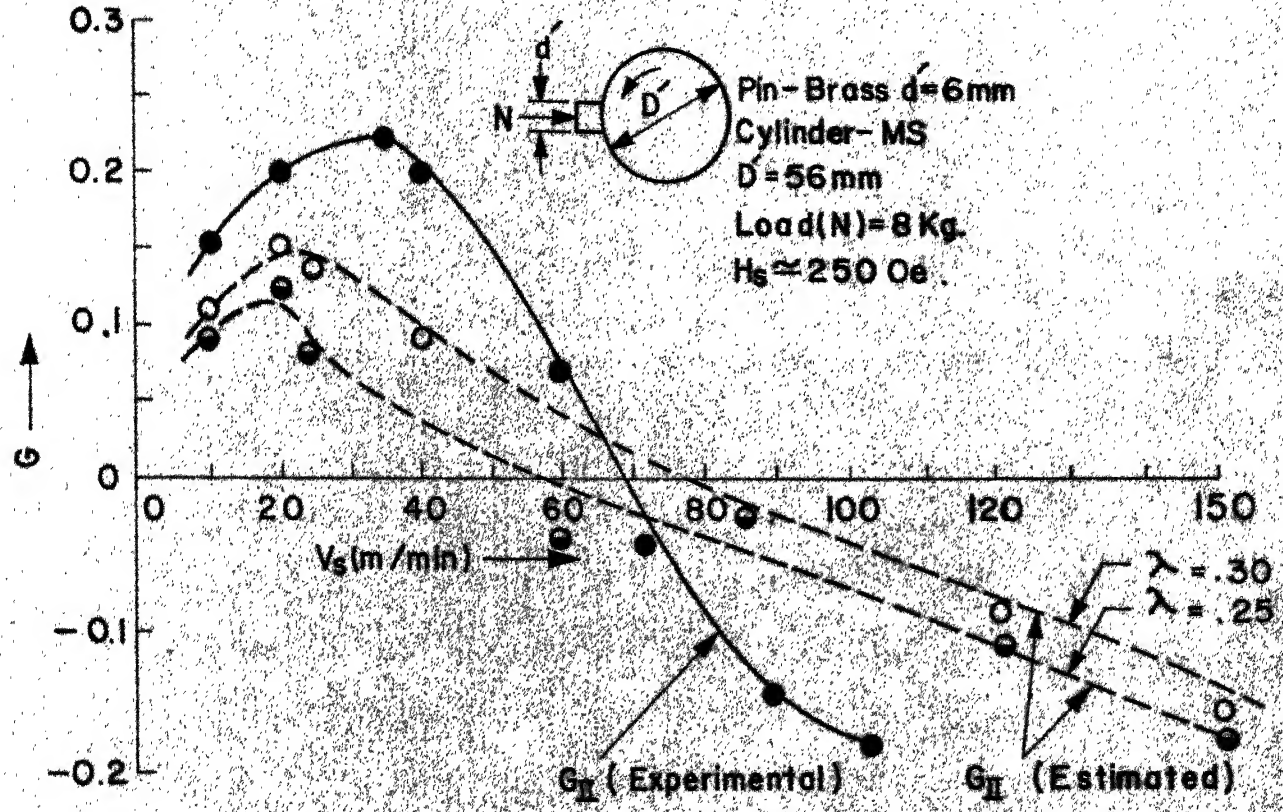

Fig. 5.16 Variation Of Gain Factor With Rubbing Velocity (Experimental And Estimated)

beyond this velocity the gain factor had a negative value. It is interesting to observe that the negative value of gain factor G is achieved only at higher speeds while at lower speeds it is positive as postulated by the model in section 4.5.

The negative values of gain factor G can be explained as follows :

As the speed increases the diffusion of iron into the brass pins increases. Therefore larger and larger chunks of brass can be removed as postulated in section 4.5. When a magnetic field is applied to the asperity junction at these high speeds, the diffusivity of iron is further enhanced. This leads to further increase in the depth 'd' of the fracture zone $C_1 X_1 C_2$ shown in Figure 2.10. Consequently, even though the probability of fracture initiation has increased only on the side of the ferromagnetic body, the net weight lost by the non-magnetic body has increased considerably. This leads to the negative gain factor for the non-magnetic body, II at these high speeds. This crossing over of gain curve from positive side to the negative side was explained in section 4.5. The results of this experiment therefore, agree well with the argument presented in that section.

The preceeding discussion relating to the possibility of negative gain of non-magnetic body, II, is further illustrated through the following calculations.

Equation 4.50 may be re-written as,

$$G_{II} = 1 - \bar{\beta}(1 + \lambda G_I) \qquad (5.2)$$

where, λ represents the factor n_I^o / n_{II}^o.

The values of G_{II} at various speeds can thus be evaluated for known values of λ, $\bar{\beta}$ and G_I. The estimation of the 'mechanical interaction factor', λ, is apparently not so straight forward. It should, in general, depend upon the hardness ratio of the two bodies, their diffusion characteristics, bonding affinity as well as their fatigue strength. Therefore, it varies with temperature. Also, its magnitude should be always less than unity. And it should increase as the sliding velocity (and so the temperature) increases. In the absence of exact calculations, λ, can be taken to be constant.

Sample calculations of G_{II} for two different values of λ have been made. These calculations are presented in Tables 5.9a and 5.9b. The values of G_I; shown in this table, have been taken to be those found for the mild steel pins rubbing against brass

TABLE 5.9a

Calculation of gain factor for body II, G_{II}, using Equation 5.2

$\lambda = 0.3$; $\quad G_{II} = 1 - \bar{\beta}(1 + G_I\lambda)$; $\quad \lambda = n_I^o / n_{II}^o$

$a = 10^{-3}$ cm

$t_j \times 10^6$ (sec.)	V_s (m/min)	G_I (Fig.5.13	$H_{\rho ri} / \rho_{ri}^o$ (Table 4.1)	$\bar{\beta}$ (Eqn. 4.46	$G_I\lambda$	$(1 + G_I\lambda)$	$\bar{\beta}(1+G_I\lambda)$	G_{II} (estimated)
60	10	- .37	1.00	1.00	- .111	.889	0.889	+ .111
30	20	- .50	1.00	1.00	- .150	.850	0.850	+ .150
25	24	- .53	1.12	1.06	- .180	.820	0.869	+ .131
15	40	- .63	3.74	1.246	- .195	.805	0.905	+ .095
10	60	- .65	3.63	1.239	- .204	.796	0.986	+ .014
7	86	- .68	3.49	1.232	- .204	.796	0.981	+ .009
5	120	- .375	3.31	1.221	- .113	.888	1.084	- .084
4	150	- .150	3.24	1.215	- .045	.955	1.160	.160
2	300	0	2.76	1.152	0	1	1.152	- .152

Table 5.9b

Calculation of gain factor of body II, G_{II}, using Equation 5.2

$\lambda = 0.25$

$a = 10^{-3}$ cm.

$$G_{II} = 1 - \bar{\beta}(1 + G_I\lambda); \quad \lambda = n_I^o / n_{II}^o$$

$t_j \times 10^6$ (sec.)	V_s (m/min.)	G_I (Fig.5.13)	$\rho_{ri}^H / \rho_{ri}^o$ (Table4.1)	$\bar{\beta}$ (Eqn.4.46	$G_I\lambda$	$1 + G_I\lambda$	$(1+G_I\lambda\bar{\beta}$	G_{II} (estimated)
60	10	- .37	1.0	1.0	-.0925	.9075	.9075	+ .093
30	20	- .50	1.0	1.0	-.125	.875	.875	+ .125
25	24	- .53	1.12	1.060	-.1325	.8675	.919	+ .081
15	40	- .63	3.74	1.246	-.1573	.8408	1.037	- .037
10	60	- .65	3.63	1.239	-.1625	.8375	1.039	- .039
7	86	- .68	3.49	1.2317	-.1700	.8300	1.023	- .023
5	120	- .375	3.31	1.221	-.0898	.9100	1.11	- .11
4	150	-.150	3.32	1.215	-.0375	.9625	1.169	- .169
2	300	0	2.76	1.152	0	1	-1.152	- .152

cylinder (Figure 5.13). Values for $\bar{\beta}$ are calculated using Equation 4.46 and the values for dislocation densities given in Table 4.1. The calculated values of G_{II} for the two known values of λ are plotted in Figure 5.16 along with the experimentally observed values.

It is interesting to observe that the estimated curves for G_{II} have the same nature of variation as the experimental curves have. This is inspite of the fact that the experimental values of G_I used in the estimation of G_{II} are obtained from independent experiments. Also, the experiments for G_I (Table 5.5a - Figure 5.13) and G_{II} (Table 5.8 - Figure 5.16) have not been conducted under exactly identical conditions. It therefore, appears that if experiments were conducted under controlled conditions and the wear of both the bodies measured simultaneously, a very close agreement between G_{II} (experimental) and G_{II} (estimated) would be expected. This could also lead to an estimation of the 'mechanical interaction factor', λ, if $\bar{\beta}$ is known.

It is obvious from Equation 5.2 that a decrease in λ would influence G_{II} in a manner similar to that of an increase in $\bar{\beta}$. Both these effects produce the effect of reducing the gain of body II (which is normally positive). At higher

speeds, however, the increase in β results in negative gain of body, II. Decrease in λ is seen to be having an identical effect. The effect of λ on gain of body II, G_{II}, is also postulated by Equation 2.37 which relates the depth of fracture zone 'd', in body II, to β_1 which is a measure of hardness of body I. If λ is also considered to be primarily related to hardness only, then the effect of ' $1/\lambda$ ' on 'd' is same as that of β. As seen from Equation 2.37, an increase in β_1 increases 'd'. So, a decrease in λ also should increase 'd', the depth of fracture zone in body II. Consequently, for the same effect of magnetic field a decrease in λ would further increase the negative gain of body I at higher speeds. This is seen in Figure 5.16, wherein the G_{II} (estimated) curve for $\lambda = 0.25$ is lower than G_{II} (estimated) curve for $\lambda = 0.30$.

While it may not be justified to extend these conclusions too far, nevertheless, the results of this section confirm that the 'complimentary' nature of adhesion wear postulated in section 4.4 is realised in actual rubbing of bodies.

5.2.11 Rubbing Under Reduced Magnetic Field Strengths

According to the theoretical model presented in section 4.4, if a magnetic field of lower strength is applied to the sliding pair, the magnitude of the gain factor is reduced. Also, at reduced magnetic field strengths there is a shift in the location of the maxima of gain factor G. The point of maxima is shifted towards lower velocity side. This was shown in Figure 4.14d.

To test these two hypothesis author repeated some tests described in section 5.2.9, under reduced magnetic field strength. A field strength $\simeq$125 Oe was employed in these tests. All other features of the tests remained essentially unchanged. The results of these experiments are given in Tables 5.5b and 5.7b and shown in Figures 5.13 and 5.15. It can be observed that both of the theoretical postulates mentioned earlier stand confirmed by these experiments. The magnitude of the gain factor G has reduced. Also, the optimum point on the gain curve has shifted to the lower velocity side.

CHAPTER VI

CONCLUSIONS

Based on the results and discussions in the preceeding chapters the following conclusions can be drawn.

(i) A steady magnetic field of the order of few hundred Oersteds has no significant effect on the bulk properties of the ferromagnetic materials.

(ii) Application of external magnetic field reduces the internal stress and the yield stress. For saturation level, reduction in internal stress is of the order of 0.5 kg/mm^2.

(iii) The reduction in internal stress causes considerable enhancement in dislocation velocity. This enhancement causes a difference in the dislocation density at the notches of a deforming asperity junction during a small interval of time (10^{-5} - 10^{-6} secs.) after the application of the magnetic field.

(iv) The enhancement of dislocation density can increase the probability of crack initiation

in a body. Since the life of asperity junctions is usually $\simeq 10^{-5} - 10^{-6}$ secs., such an influence becomes effective and observable.

(v) In the 'adhesion wear' of a sliding pair the magnetic field enhances the probability of crack initiation on the side of the body which has a higher permeability. This leads to the increased rate of wear of that body. This, consequently, leads to the decreased rate of wear of the other body.

(vi) An external steady magnetic field of few hundred Oersteds does not seem to have any influence on the diffusivity of a ferromagnetic body when the body is not under dynamic strain. But, in a deforming asperity junction the diffusivity is enhanced during a small time interval of $10^{-5} - 10^{-6}$ secs. after the magnetic field is applied. This also influences the wear characteristics of a sliding pair quite significantly.

(vii) In a bimetallic junction the magnetic field enhances the wear rate of both the bodies. At high speeds, where the effect of diffusion is prominent a negative hardness

gradient of considerable magnitude may be created in the softer body. This results in significant changes in the 'adhesion wear' characteristics of the sliding pair.

BIBLIOGRAPHY

1. Taylor, F.W. — " On the art of metal cutting" Trans. A.S.M.E., 28 (1907) 31.

2. Nakajima, K. and Isogai, A. — "Electron microprobe study of the effect of abrasion of the surface of alloy crystals" Wear, 10 (1967) 151.

3. Rabinowitz, E. — "Friction and Wear of self lubricating metallic materials" J. of Lubr. Tech., 97 (1974) 217.

4. Naik, S.K. and Suh, N.P. — "The investigation of enhancement mechanisms of oxide treatment on cemented carbide tools" Trans. A.S.M.E., Series B, 97 (1975) 112.

5. Krauss, H. — "Tribochemical reactions in the friction and wearing process of iron". Wear, 18 (1971) 403.

6. Hurricks, P.L. — "The fretting wear of mild steel from room temperature to 200 °C. Wear, 19 (1972) 207.

7. Suh, N.P. — "The delamination theory of wear". Wear, 35 (1973) 111.

8. Suh, N.P. — "The delamination theory of wear and the wear of a composite surface". Wear, 32 (1975) 33.

9. Doyle, E.D. — "A mechanism of spherical particle formation in wear debris". J. Aust. Inst. Metals, 19 (1974) 276.

10. Simpson, F.F. and Russell, R.W. — "Influence of magnetic field and the passage of electrical currents on the deterioration of ball-bearings". Proc. Conf. Lub. and Wear, London, Oct. (1957) 477.

11. Ghosh, A. — "Mechanism of cutting tool wear". Ph.D. Thesis - Calcutta University, (1968) 123.

12. Bagchi, P.K. and Ghosh, A. — "Effect of magnetisation on the wear characteristics of cutting tools". J. Instn. Engrs. (INDIA), 50 (1970) 264.

13. Bagchi, P.K. and Ghosh, A. — "Mechanism of cutting tool wear in the presence of magnetic field". Indian J. Tech., 9 (1971) 165.

14. Chakravarty, S. — "Why magnetised cutting tools has a greater life - probable causes." Presented at the semi-annual convention of the Instn. of Engrs. (INDIA), (1971).

15. Pal, D.K. and Gupta, N.C. — "Some experimental studies on drill wear in presence of alternating magnetic field". J. Instn. Engrs. (India), 53, ME 4, March (1973) 195.

16. Kragelskii, I.V. — "Friction and Wear" Butterworths, Washington, (1965)1.

17. Holm, R. — "Electrical Contacts" Almquist and Wiksells, Stockholm, (1948).

18. Bowden, F.P. and Tabor, D. — "The Friction and Lubrication of Solids" Oxford University Press, N.Y. (1950).

19. Dyson, J. and Hirst, W. — "The true contact area between solids". Proc. Phy. Soc. (London), B 67 (1954) 309.

20. Ming Feng, I. — "Metal Transfer and Wear" J. Appl. Plys., 23 (1952) 1011.

21. Rabinowitz, E. — "Investigation of size effects in sliding by means of statistical techniques". Inst. Mech. Engrs; Conference on Lubrication and Wear (1957). 1.

22. Rabinowitz, E. "Auto correlation analysis of the sliding process". J. Appl. Phys., 27 (1956) 131.

23. Ling, F.F. "On asperity distribution of metal surface". J. Appl. Phys., 29 (1958) 1168.

24. Greenwood, J.A. and Williamson J.B.P. "Contact of Nominally Flat surfaces". Proc. Roy. Soc. (London), A 295 (1966) 300.

25. Whitehouse, D.J. and Archard, J.F. "The properties of random surfaces of significance in their contact". Proc. Roy. Soc. (London), A316 (1970) 97.

26. Tskada, T. and Anno, Y. "An evaluation of machined surface topography". Bull. Japan. Soc. Prec. Engg., 9 - 1 (1975) 1.

27. Gupta, P.K. and Cork, N.H. "Statistical analysis of mechanical interaction of rough surfaces". J. Lubr. Tech., Jan (1972) 19.

28. Barwell, J.T. and Strang, C.D. "Metallic Wear", Proc. Roy. Soc. (London), A212 (1952) 470.

29. Archard, J.F. and Hirst, W. "An examination of a mild wear process". Proc. Roy. Soc. (London), A238 (1957) 515.

30. Radchik, A.S. and Radchik, V.S. "Deformation of surface layers during sliding". Dokl. Akad. Nauk SSR, 119 (1958) 933.

31. Archard, J.F. "Elastic deformation and the laws of friction". Proc. Roy. Soc. (London), A243 (1957) 190.

32. Archard, J.F. "Contact and rubbing of flat surfaces". J. Appl. Phys., 24 (1953) 981.

33. Barwell J.T. and Strang, C.D. "On the empirical laws of adhesive wear". J. Appl. Phys., 23 (1952) 18.

34. Trigger, K.J. and Chao, B.T. "Mechanism of crater wear, of cemented carbide tools". Trans. A.S.M.E., 79 (1956) 1119.

35. Cook, N.H. and Nayak, P.N. "The thermal mechanics of tool wear". Trans. A.S.M.E. 88 (1966) 93.

36. Rabinowitz, E. "Friction and wear of materials". John Wiley and Sons, N.Y. (1965).

37. Rabinowitz, E. "A quantitative study of the wear process". Proc. Phys. Soc. (London), B66 (1953) 929.

38. Kerridge, M. "Metal transfer and the wear process". Proc. Phys. Soc. (London), B68, (1955) 400.

39. Lancaster, J.K. "The formation of surface films at the transition between mild and severe metallic wear". Proc. Roy. Soc. (London), A273 (1963) 466.

40. Whitehead, J.R. "Surface deformation and friction of metals at light loads" Proc. Roy. Soc. (London), A201 (1950) 109.

41. Levik, M. and Solomon, G. "Mechanism of solid friction". Elsevier, N.Y., (1964) 48.

42. Buckley, D.H., Swikert, M. and Johnson, R.L. "Friction, wear and evaporation rates of various materials in vacuum to 10^{-7} mm Hg". Trans. ASLE, 5 (1962) 8.

43. Buckley, D.H. and Johnson, R.L. "Friction and wear of hexagonal metals and alloys as related to crystal structure and lattice parameters in vacuum." Trans. ASLE, 9 (1966) 121.

44. Green, A.P. "Friction between unlubricated metals : A theoretical analysis of the junction model". Proc. Roy. Soc. (London), 228 (1955) 191.

45. Green, A.P. "The plastic yielding of metal junctions due to combined shear and pressure." J. Mech. Phys. Solids, 2 (1954) 197.

46. Green, A.P. "Report of British Iron and Steel Research Association." (1954).

47. Greenwood, J.A. and Tabor, D. "Deformation properties of friction junctions". Proc. Phys. Soc. (London), B68 (1955) 609.

48. Greenwood, J.A. and Tabor D. "Properties of model friction junctions". Proc. Conf. Lubri. and Wear, London, (1957) 314.

49. Shaw, M.C. "Metal cutting principles" M.I.T. Press, (1957)

50. Brockley, C.A. and Fleming, G.K. "A model junction study of severe metallic wear". Wear, 8 (1965) 374.

51. Edward, C.M. and Halling, J. "An analysis of the plastic interaction of surface asperties and its relevance to the coefficient of friction". Mech. Engg. Sci., 10 (1968) 101.

52. Gupta, P.K. and Cook, N.H. "Junction deformation models for asperities in sliding interaction". Wear, 20 (1972) 73.

53. Shewmon, P.G. "Diffusion in solids". McGraw Hill Book Co., Inc. N.Y. (1963).43.

54. Kamenetskaya, D.S., Piletskaya, I.D. and Schiryayev, V.I.Z. "Effect of magnetic field on the plastic deformation of Iron". Sov. Phys. Doklady, 16-8 (1972) 679.

55. Huntington, H.B. "Energy for diffusion by direct interchange". Phy. Rev., 76 (1949) 1728.

56. Zener, C. "Ring diffusion in metals" Acta Cryst., 3-5 (1950) 346.

57. Seeger, A. "The generation of lattice defects by moving dislocations and its application" Phil. Mag., 46 (1955) 1194.

58. Friedel, J. "Dislocations" Addition-Wesley Publishing Co., (1964) 106, 114, 240.

59. Krishthal, M.A. "Diffusion Processes in Iron alloys". Israel programme for scientific translations, Jerusalem (1970).

60. Bugakov, V.Z. Referred to in the above.

61. Hirano, K., Cohen, M., Averbach, B.L. and Ujiiye, N "Self diffusion in Alpha Iron during compressive plastic flow". Trans. A.I.M.E., 227 (1963) 950.

62. Askill, J. "Tracer diffusion data for metals, alloys and simple oxides". IFI Plenum, N.Y. (1970)

63. Loladze, T.N. "Adhesion and diffusion wear in metal-cutting". J. Inst. Engrs. (INDIA) XLIII, ME-2 (1962) 108.

64. Venkatesh, V.C. "Diffusion wear of H.S.S. Tools" Proc. 7th Int. M.T.D.R. Conference, University of Birmingham, Sept. (1966) 401.

65. Bhattacharya, A. and Ghosh, A. "Diffusion wear of cutting tools". Proc. 5th Int. M.T.D.R. Conference, Birmingham, Sept. (1964) 225.

66. Bhattacharya, A. and Ghosh, A. "Diffusion wear of cutting tools". Annals of C.I.R.P., 16 (1968) 369.

67. Kukuchi, K. and Tanaka, Y. "Cutting" Bull. Jap. Soc. Prec. Engg. 82 (1974) 39.

68. Gregory, B. "Surface interaction of cemented carbide tool material and Armco Iron". Brit. J. Appl. Phys., 16 (1965) 693.

69. Svechnikov, A.N. "Diffusion process in metals". Israel programme for scientific translations, Jerusalem (1970)

70. Cook, N.H. and Nayak, P.N. "The thermal mechanics of tool wear". Trans ASME, 88 (1966).

71. Zlatin N. and Merchant M.E. "Distribution of hardness in chips and machined surfaces". Trans. ASME, (1947).

72. Buffington, F.S. and Cohen, M. "Self diffusion in Alpha Iron under uniaxial compressive stress". Trans. ASME, 194 (1952) 859.

73. Lee, C.H. and Maddan, R. "The effect of torsional strains on self-diffusion in silver single crystals". Trans. AIME, 215 (1959) 397.

74. Forestieri, A.F. and Girifalco, L.A. "The effect of plastic deformation on self diffusion in silver". J. Phy. Chem. Sol., 10 (1959) 99.

75. Wazzan, A.R. and Dorn J.E. "Analysis of enhanced diffusivity in Nickel". J. Appl. Phys., 36 (1965) 222.

76. Watanabe, T. and Karashima, S. "On the strain-enhanced diffusion of - iron". Phys. Stat. Sol., 42 (1970) 749.

77. Darby, J.B., Tomizuka, C.T. and Palluffi "Self-duffision in silver during plastic deformation in extension and compression". J. Appl. Phys., 30 (1959) 104.

78. Smithells, C.J. "Metals Reference Book" Butterworths, London, (1967).

79. Cottrell, A.H. "Dislocations and plastic flow in Crystals". Oxford University Press, (1953).

80. Kovacs, I. "Dislocations and plastic deformation". Pergamon Press (1973).

81. Hull, D. "Introduction to dislocations". Pergamon Press, (1965).

82. Mott, N.F. "Theory of work-hardening of metal crystals". Phil. Mag., 43 (1952) 1151.

83. Frank, F.C. "On the equation of motion of crystal dislocations". Proc. Phys. Soc., A62 (1951) 131.

84. Carrington, W., Hale, K.F. and Mclean D. "Arrangement of dislocations in iron". Proc. Roy. Soc., A 259 (1960) 203.

85. Johnston, W.G. and Gilman, J.J. "Dislocation velocities dislocation densities and plastic flow in lithium Fluoride crystals". J. Appl. Phys., 30 (1959) 129.

86. Stein, D.F. and Low, J.R. "Mobility of edge dislocations in Si-Fe crystals". J. Appl. Phys., 31 (1960) 362.

87. Conrad, H. "Thermally activated deformation of metals". J. Metals, 16 (1964) 582.

88. Evans, A.G. and Rawlings, R.O. "Thermally activated deformation of crystalline materials" Phys. Stat. Sol., 34 (1969) 9.

89. Watanabe, T. and Karashima, S. "An analysis of high temperature creep in Alpha iron, based on super jog mechanism". Trans. Japan Inst. Metals, 11 (1970) 159.

90. Blum, W. and Reppich, B. "On the stress dependence of the stationary deformation" Acta. Met., 17 (1969) 959.

91. Jonas, J.J., Sellars, C.M. and Tegart W.J. Mig. "Strength and structure under hot working conditions". Metals and Materials Review 130. (1961) 1.

92. Mcqueen, H.J. "Deformation Mechanism in hot working". J. Metals, (1968) 1

93. Wong, W.A. and Jones, J.J. "Aluminium extrusion as a thermally activated process". Trans. AIME, 242 (1968) 2.

94. Stroh, A.N. "Formation of cracks in plastic flow - II". Proc. Roy. Soc. (London), 232A. (1958) 5.

95. Eshelby, J.D., Frank, F.C. and Nabarro, F.R.N. "The equilibrium of linear arrays of dislocations". Phil. Mag., 42 (1951) 351.

96. Stroh, A.N. "Formation of cracks as a result of plastic flow". Proc. Roy. Soc., 223A (1954) 484.

97. Brown, A.F. "Slip bands and hardening process in aluminium". J. Inst. Metals, 80 (1951) 115.

98. Head, A.K. "The interaction of dislocations and boundaries". Phil. Mag., 44 (Jan 1953) 92.

99. Conners, G.H. "The interaction of a dislocation with a coated plane boundary". Int. J. Engg. Sci., 5 (1967) 25.

100. Warren, W.E. "Interaction of dislocations with surface notches and protrusions". Int. J. Engg. Sci., 8 (1970) 545.

101. Chikazumi, S. "Physics of Magnetism". John Wiley and Sons, N.Y. (1964).

102. Weiss, P. "Hypothesis of the molecular field and ferromagnetic properties." J. Phys., 6 (1907) 661.

103. Heisemberg, W. "On the theory of ferromagnetism" Z. Physik, 49 (1928) 619.

104. Berkhausen, H. "Two Phenomenae uncovered with the help of the new amplifiers". Z. Physik, 20 (1919) 401.

105. Sixtus, K.J. and Tonks, L. "Propagation of large Barkhausen discontinuities". Phys. Rev., 37 (1931) 930.

106. Bitter, F. "On inhomogeneities in the magnetisation of ferromagnetic materials". Phy. Rev., 38 (1931) 1903.

107. Landau, L. and Lifshitz, E. "The theory of dispersion of magnetic permeability in ferromagnetic bodies". Physik, Z. Sowjet Union, 8 (1935) 153.

108. Bloch, F. "Theory of exchange problems and of residual ferromagnetis" Z. Physik, 74 (1932) 295.

109. Stewart, K.H. "Ferromagnetic domains" University Press, Cambridge (1954).

110. Bozoroth, R.M. "Ferromagnetism". D. Van-Nostrand Co., Inc., Princeton (1951) 632.

111. Trauble, H.. "Magnetism and Metallurgy" Edited by Berkowitz, A. and Kneller, E., Academic Press, N.Y. (1969) 622 - 631.

112. Gemperle, R. "The ferromagnetic domain structure of thin single-crystal Fe platelets in an external field". Phy. Stat. Sol., 14 (1966) 121.

113. Bourret, A. and Dantreppe, D. "Observation des domaines en rubans dans les lames mines de fer pur par microscopic electro technique". Phy. Stat. Sol., 13 (1966) 559.

114. Chebotkevich, L.A., Urusovskaya, A.A., Veter, V.V. and Ershov, A.D. "Interaction of Bloch walls with dislocations in weak fields". Sov. Phys. - Solid State, 9-4 (1967) 854.

115. Hayashi, S. "Direct observations of the dislocation motion in ferromagnetic crystals under alternating magnetic fields". Jap. J. Appl. Phys., 12 (1973) 182.

116. Nabarro, F.R.N. "Theory of Crystal dislocations" Clarendon Press, (1967) 659, 663.

117. Conard, H. "The athermal components of the flow stress in crystalline solids". Mat. Sci. Engg., 6 (1970) 265.

118. Hayashi, S. "Magneto-plastic effect in nickel single crystals". J. Phy. Soc. Japan, 30 (1971) 381.

119. Dieter, G.E. Jr. "Mechanical Metallurgy" Mcgraw-Hill Book Co., Inc., (1961) 121.

120 Saada, G. "Sur le Durcissement $D\bar{U}\ \bar{A}$ LA Recombinaison des dislocations". Acta Met., 8 (1960) 841.

121. Li, C.M. "Stress dependence of dislocation velocity inferred from strain-rate sensitivity". Acta. Met., 11 (1963) 317.

122. Cuddy, and Ralay "The effect of internal stress on the activation parameters for creep of Fe-Ni alloys" Acta. Met.,21(1973) 427.

APPENDIX

Figure A.1 shows a pin of radius r_p rubbing against a cylinder of radius r_c in the manner employed in the experiments described in section 5.2.5. At any instant after the rubbing has started the dimensions of the elliptical wear scar would be d_o, d_i, where d_o is the major axis and d_i the minor axis of the wear scar. This is shown in Figure A.3. From Figure A.1 it can be seen that,

$$\frac{d_o}{2} = r_c \sin\psi_o \qquad (A.1)$$

Also, from Figure A.4

$$(A\,E)^2 = C\,E \times E\,D = C\,E\,(CD - CE)$$

$$\therefore \left(\frac{d_i}{2}\right)^2 = \left[r_c\,(1 - \cos\psi_o)\right]\left[(2\,r_p - r_c(1 - \cos\psi_o)\right] \qquad (A.2)$$

$$\text{or } d_i^2 = 4\left[2\,r_c\,r_p\,(1 - \cos\psi_o) - r_c^2\,(1 - \cos\psi_o)^2\right]$$

For small values of ψ_o,

$$\cos\psi_o \simeq 1 - \frac{\psi_o^2}{2} \qquad (A.3)$$

and $\sin\psi_o \simeq \psi_o$

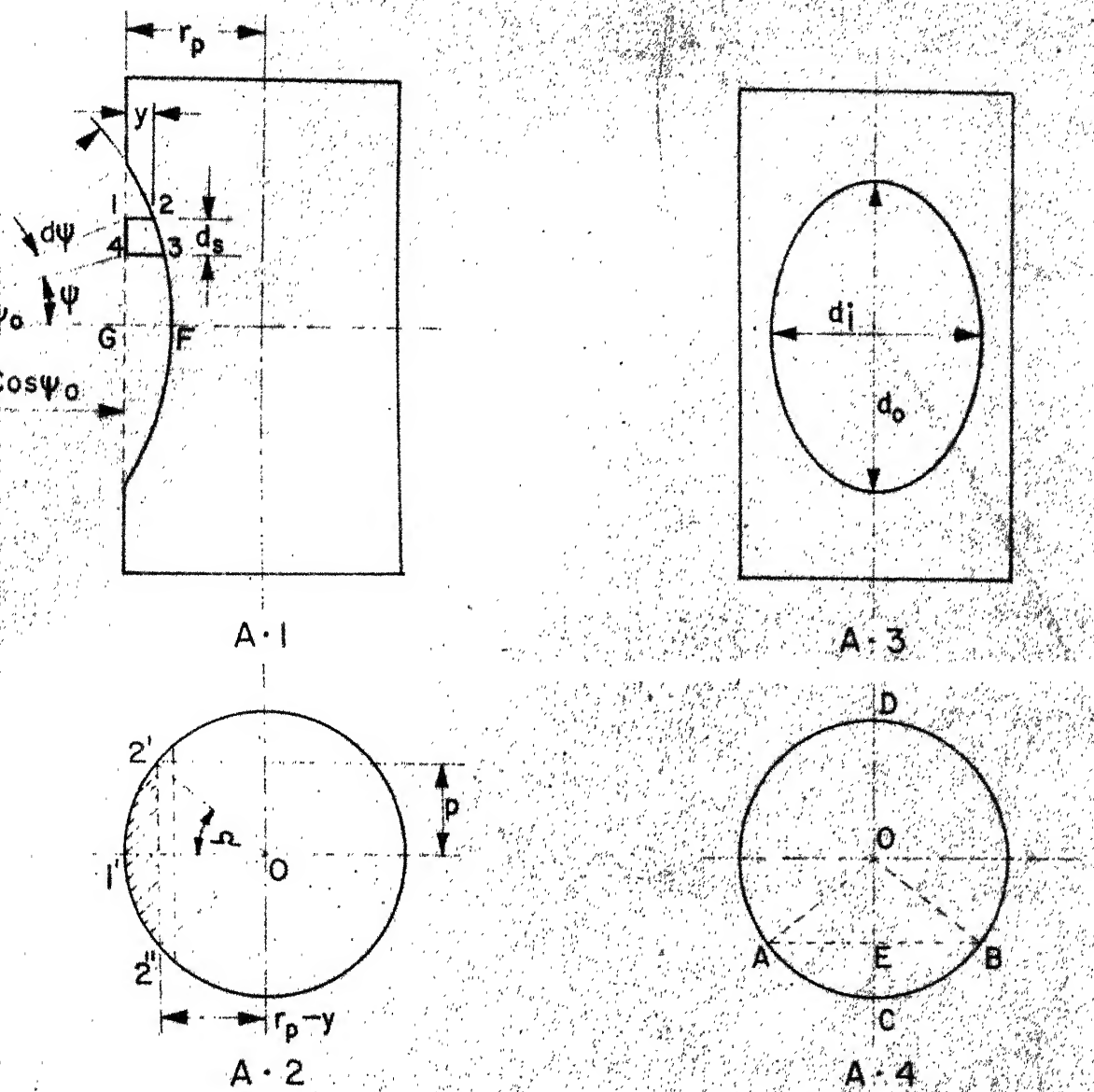

Fig. A. Geometrical Configuration Of a Wear Scar Of a Pin Rubbing Against a Cylinder.

$$\therefore \quad d_i^2 = 4\left[\left\{2\, r_c\, r_p \left(\frac{\psi_o}{2}\right)^2 - r_c^2 \left(\frac{\psi_o}{2}\right)^2\right\}\right]$$

$$4\, r_c\, r_p\, \psi_o^2 \text{ , (ignoring the higher powers or } \psi_o^2 \text{)}$$

$$\therefore \quad \frac{d_i}{2} = \psi_o \sqrt{r_c\, r_p} \qquad (A.4)$$

$$\text{and} \quad d_o \simeq 2\, r_c\, \psi_o \qquad (A.5)$$

$$(A.6)$$

Now, volume $d\omega$ of a small element 1 - 2 - 3 - 4 is equal to the product of its thickness (equal to time element ds) and its projected area dA_s in the plan shown as the shaded region 1' - 2' - 2" in Figure A.2.

$$\therefore \quad d\omega = ds \times d\, A_s \qquad (A.7)$$

From Figure A.1, it can also be seen that

$$(\tan(\psi + d\psi) - \tan\psi) = \left(\frac{ds}{r_c \cos\psi_o}\right) \qquad (A.8)$$

Expanding $\tan(\psi + d\psi)$ and $\tan\psi$, it can be seen that

$$ds = \left(\frac{r_c \cos\psi_o}{\cos^2\psi}\right) . d\psi \qquad (A.9)$$

The shaded area $d\, A_s$ (1' - 2' - 2") is estimated as follows

$d\, A_s$ = area of the sector (0 - 2' - 1' - 2"), $d\, A_1$, minus the area of triangle 0 - 2' - 2", $d\, A_2$.

Area of the sector 0 - 2' - 1' - 2" is

$$dA_1 = \left(\frac{\pi r_p^2}{2\pi} \; 2\Lambda \right)$$

$$= r_p^2 \Lambda \qquad (A.10)$$

Area of the triangle 0 - 2' - 2" is

$$dA_2 = \frac{2p}{2} (r_p - y) = p (r_p - y) \qquad (A.11)$$

From, Figure A.2, $\quad \sin\Lambda = \frac{p}{r_p} \qquad (A.12)$

For small values of Λ , $\Lambda \simeq \frac{p}{r_p} \qquad (A.13)$

lso, $\quad p^2 = y (2 r_p - y)$

$$\simeq 2 r_p y \qquad (y << r_p) \qquad (A.14)$$

Since Λ is small

$$\Lambda \simeq \sqrt{\frac{2 r_p y}{r_p^2}} = \sqrt{\frac{2y}{r_p}} \qquad (A.15)$$

Substituting the Equations A.14 and A.15 into Equations A.10 and A.11, the area dA_s can be calculated to be

$$dA_s = r_p^2 \sqrt{(\frac{2y}{r_p})} - (r_p - y) \sqrt{2 r_p y} \qquad (A.16)$$

$$= \sqrt{2 y r_p^3} - \sqrt{2 r_p^3 y} + \sqrt{2 r_p y^3} \qquad (A.17)$$

$$= \sqrt{2} \sqrt{r_p y^3} \qquad (A.18)$$

Substituting value of dA_s and ds into equation A.7 the volume $d\omega \simeq dA_s \times ds$ reduces to

$$d\omega = \sqrt{2}\ \sqrt{r_p\, y^3}\ \frac{r_c \cos\psi_o}{\cos^2\psi}\, d\psi \qquad (A.19)$$

Now, the value y may be obtained in terms of r_c, ψ and ψ_o as follows.

From Figure A.1, magnitude of y is given by

$$y = \sqrt{r_c^2 - L_1 \tan^2\psi} \qquad (A.20)$$

where $L_1 = r_c \cos\psi_o$ (A.21)

$$\therefore\ y = r_c \sqrt{(1 - \cos^2\psi_o \tan^2\psi)} - r_c \cos\psi_o$$

$$\simeq r_c \left[1 - \tfrac{1}{2}\cos^2\psi_o \tan^2\psi - \cos\psi_o\right] \qquad (A.22)$$

and, $$y^{3/2} = r_c^{3/2}\left[1 - \cos\psi_o - \frac{\cos^2\psi_o \tan^2\psi}{2}\right]^{3/2} \qquad (A.23)$$

Now, $1 - \cos\psi_o - \dfrac{\cos^2\psi_o \tan^2\psi}{2}$ may be further simplified to be

$$= 1 - (1 - \frac{\psi_o^2}{2}) - \frac{1}{2}(1 - \frac{\psi_o^2}{2})^2 \frac{\sin^2\psi}{\cos^2\psi}$$

$$\simeq \frac{\psi_o^2}{2} - \frac{1}{2}(1 - \psi_o^2 + \frac{\psi_o^4}{4}) \frac{\psi^2}{(1 - \psi^2/2)}$$

$$\simeq \frac{\psi_o^2}{2} - \frac{1}{2}(1 - \psi_o^2) \times \psi^2(1 + \frac{\psi^2}{2}),$$

neglecting higher powers of ψ_o^2.

$$\simeq \frac{\psi_o^2}{2} - \frac{(1 - \psi_o^2)(\psi^2)}{2},$$ neglecting higher powers of ψ_o^2.

$$\simeq \frac{\psi_o^2}{2} - \frac{\psi^2 - \psi^2 \psi_o^2}{2} \qquad (A.24)$$

Again, since ψ and ψ_o both are small the product $\psi^2 \psi_o^2$ can be neglected in comparison to ψ^2.

So, $$(1 - \cos\psi_o \quad \frac{\cos^2\psi_o \tan^2\psi}{2})^{3/2} \simeq (\frac{\psi_o^2 - \psi^2}{2})^{3/2} \qquad (A.25)$$

and, $$y^{3/2} = r_c^{3/2} (\frac{\psi_o^2 - \psi^2}{2})^{3/2} \qquad (A.26)$$

Substituting the above value of $y^{3/2}$ in Equation A.19 the value of the elemental volume $d\omega$ comes out to be,

$$d\omega \simeq \sqrt{2}\ r_p^{1/2}\ r_c^{3/2} (\frac{\psi_o^2 - \psi^2}{2})^{3/2} r_c \frac{\cos\psi_o}{\cos^2\psi} d\psi$$

$$\simeq \sqrt{2}\ r_p^{1/2}\ r_c^{5/2} (\frac{\psi_o^2 - \psi^2}{2})^{3/2} \frac{\cos\psi_o}{\cos^2\psi} d\psi \qquad (A.27)$$

The volume of wear associated with the entire shaded sector 0 - 2' - 1' - 2" is therefore,

$$W = 2 \int_{\psi=0}^{\psi_o} d\omega = (\frac{2\sqrt{2}}{\sqrt{8}})\ r_p^{1/2}\ r_c^{5/2} \cos\psi_o \int_{\psi=0}^{\psi_o} \frac{(\psi_o^2 - \psi^2)^{3/2}}{\cos^2\psi} d\psi$$

$$= r_p^{1/2}\ r_c^{5/2} \cos\psi_o \int_{\psi=0}^{\psi_o} \frac{(\psi_o^2 - \psi^2)}{(1 - \psi^2)} d\psi \qquad (A.28)$$

Since $\psi^2 << 1$, Equation A.28 reduces to

$$W = r_p^{1/2}\ r_c^{5/2} \cos\psi_o \int_{\psi=0}^{\psi_o} (\psi_o^2 - \psi^2)^{3/2} d\psi \qquad (A.29)$$

The integral $\int_{\psi=0}^{\psi_0} (\psi_0^2 - \psi^2)^{3/2} \, d\psi$ is evaluated as follows:

By substituting $\psi = \psi_0 \sin \acute{x}$

$$(\psi_0^2 - \psi^2)^{3/2} = (\psi_0^2 - \sin^2 \acute{x} \, \psi_0^2)^{3/2} = \psi_0^3 \cos^3 \acute{x} \qquad (A.30)$$

Also, $d\psi = \psi_0 \cos \acute{x} \, d\acute{x}$ (A.31)

when, $\psi = 0$, $\acute{x} = 0$

and when $\psi = \psi_0$, $\acute{x} = \pi/2$

$$\therefore \int_{\psi=0}^{\psi_0} (\psi_0^2 - \psi^2)^{3/2} \, d\psi = \int_0^{\pi/2} \psi_0^4 \cos^4 \acute{x} \, d\acute{x} \qquad (A.32)$$

Again, $\cos^4 \acute{x} = \cos 4\acute{x} + 2 \cos 3\acute{x} + 6 \cos \acute{x} + 1$ (A.33)

and $\int_{\psi=0}^{\psi_0=\pi/2} 8 \cos^4 \acute{x} \, d\acute{x} = 8.47$

or $\int_0^{\pi/2} \cos^4 \acute{x} \, d\acute{x} = 1.06$

$$\therefore W = r_p^{1/2} \, r_c^{5/2} \cos \psi_0 \quad \psi_0^4 \times 1.06 \qquad (A.34)$$

From equation A.6; $d_o = 2 r_c \psi_o$

$$\therefore W \simeq \sqrt{r_p \, r_c^5} \, (1.06) \left(\frac{d_o}{2 r_c} \right)^4$$

$$\simeq 1.06 \, r_p^{1/2} \, r_c^{5/2-4} \, \frac{d_o^4}{16}$$

$$\simeq \frac{1}{16} \, r_p^{1/2} \, \frac{d_o^4}{r_c^{3/2}} \simeq \frac{1}{16} (d_o^4) \sqrt{\frac{r_p}{r_c^3}} \qquad (A.35)$$

For the same r_p and r_c, the volume of wear of pin with and without magnetic field may therefore be written as

$$W_I^H = \text{const.}\ d_{o,H}^4 \qquad (A.36)$$

and, $$W_I^o = \text{const.}\ d_{o,o}^4 \qquad (A.37)$$

where constant $= \frac{1}{16}\sqrt{\frac{r_p}{r_c^3}}$

and W_I^H = volume of wear of pin (body I) in presence of magnetic field.

W_I^o = volume of wear of pin (body I) in absence of magnetic field.

Therefore, the gain factor G_I in this case is calculated as

$$G_I = \frac{d_{o,o}^4 - d_{o,H}^4}{d_{o,o}^4} \qquad (A.38)$$

where,

$d_{o,o}$ = major axis, d_o, of the wear scar when no magnetic field is applied to the pin

$d_{o,H}$ = major axis, d_o, of the wear scar when magnetic field is applied to the wear scar.